Supplementary information

Green synthesis of a large series of bimetallic MIL-100(Fe,M) MOFs

Timothy Steenhaut, Sophie Hermans* and Yaroslav Filinchuk**

Institute of Condensed Matter and Nanosciences, Place Louis Pasteur 1/L4.01.03, 1348 Louvain-la-Neuve, Belgium
E-mail: timothy.steenhaut@uclouvain.be; sophie.hermans@uclouvain.be; yaroslav.filinchuk@uclouvain.be

A. Procedure for the isolation of the $Fe_3BTC_2{\cdot}12H_2O$ and $Co_3BTC_2{\cdot}12H_2O$ intermediates.

Figure S1. Nitrogen sorption isotherms (77K) and BJH transform plots of MIL-100(Fe) obtained in acidic and basic medium.

Figure S2. Laboratory measured PXRD patterns of MIL-100(Fe) obtained in acidic and basic conditions.

Figure S3. Synchrotron PXRD patterns of the as-synthesized MIL-100(Fe,Co) samples, using different Co/Fe ratios for the synthesis.

Figure S4. ATR-IR spectra of the as-synthesized MIL-100(Fe,Co) samples, using different Co/Fe ratios for the synthesis.

Figure S5. PXRD patterns of the obtained $Fe_3BTC_2{\cdot}nH_2O$ and $Co_3BTC_2{\cdot}nH_2O$ intermediates.

B. Post-synthetic exchange of Co^{2+} starting from pure MIL-100(Fe).

Figure S6. Synchrotron PXRD patterns of MIL-100(Fe,M) materials obtained using different doping metals (sample temperature 200°C).

Figure S7. ATR-IR spectra of as-synthesized and activated MIL-100(Fe,M) materials.

Table S1. Doping metal content determined by ICP-OES and surface content determined by XPS for samples obtained using 20 mol% doping metal for synthesis.

Figure S8. Nitrogen adsorption-desorption isotherms (77K) for the different MIL-100(Fe,M) materials, calculated BET surface areas and BJH transform plots.

Figure S9. Temperature-dependent synchrotron PXRD of MIL-100(Fe,Ln) and MIL-100(Fe,Y) to evidence the secondary phase observed at low temperature in solvated samples.

Figure S10. Survey of XPS spectra of some of the MIL-100(Fe,Ln) compounds, indicating the presence of Na on the surface of the samples.

Figure S11. TGA plots of the MIL-100(Fe,M) materials under nitrogen and air.

Figure S12. XPS regions around the doping metals for the MIL-100(Fe,M) samples.

Figure S13. PXRD patterns of the calcined MIL-100(Fe,M) samples and PXRD-based metal quantification.

Table S2. Quantities of reagents for the syntheses of MIL-100(Fe,M), pH of the reaction mixtures and colours observed during the reactions.

A. Procedure for the isolation of the $Fe_3BTC_2{\cdot}12H_2O$ and $Co_3BTC_2{\cdot}12H_2O$ intermediates

The $Fe_3BTC_2{\cdot}12H_2O$ salt was synthesized according to the same procedure as for the synthesis of MIL-100(Fe) in acidic conditions, except that the water was degassed before making the solutions and that the reaction was performed under inert atmosphere. In brief, a degassed aqueous solution of Na_3BTC was added to a degassed aqueous solution of $FeSO_4$ under stirring. To facilitate the filtration, that was performed after about 30 minutes of reaction once the intermediate precipitated, the reaction was performed in Schlenk flasks equipped with a fritted disk (see upper picture below). The solid was then filtered and washed with degassed ethanol followed by degassed diethylether. The yellow powder was then dried under vacuum prior to analysis. Capillaries for PXRD were sealed with grease in an argon-filled glove box to avoid oxidation of the Fe^{II} compound. The $Co_3BTC_2{\cdot}12H_2O$ salt was synthesized by a similar procedure, by replacing the $FeSO_4$ solution by a $CoSO_4$ aqueous solution. A pink powder that becomes blue upon heating was obtained (see lower figure below).

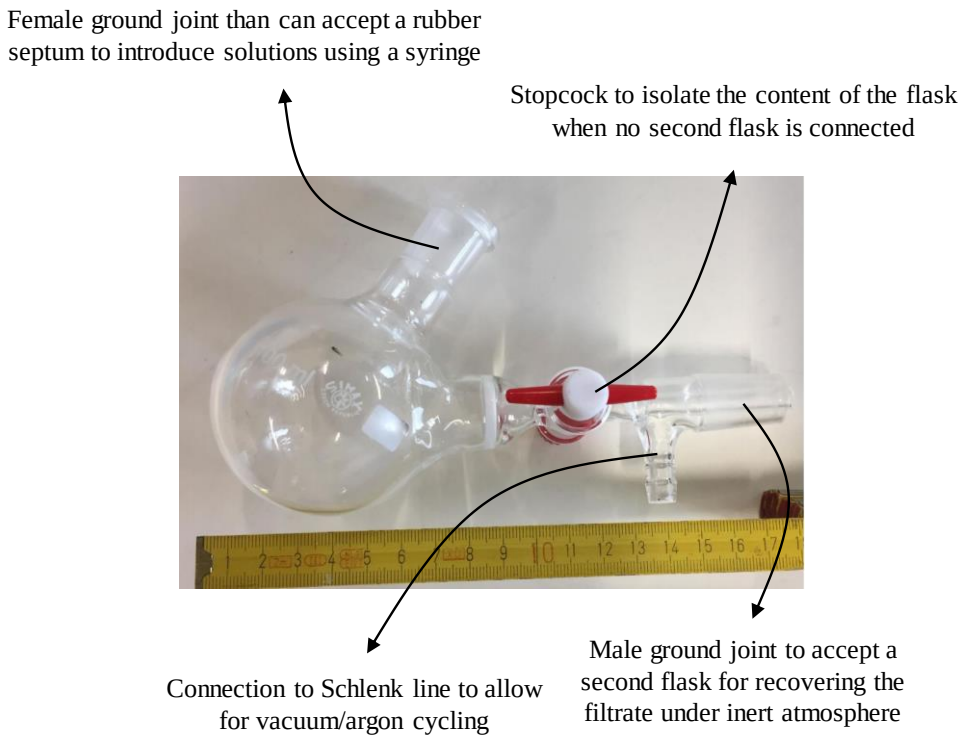

Figure S1. Nitrogen sorption isotherms (77K) (top) and BJH transform plots (bottom) of MIL-100(Fe) obtained in acidic (red curve) and basic medium (blue curve). BET calculated surface areas are 2012 m²/g and 1542 m²/g respectively.

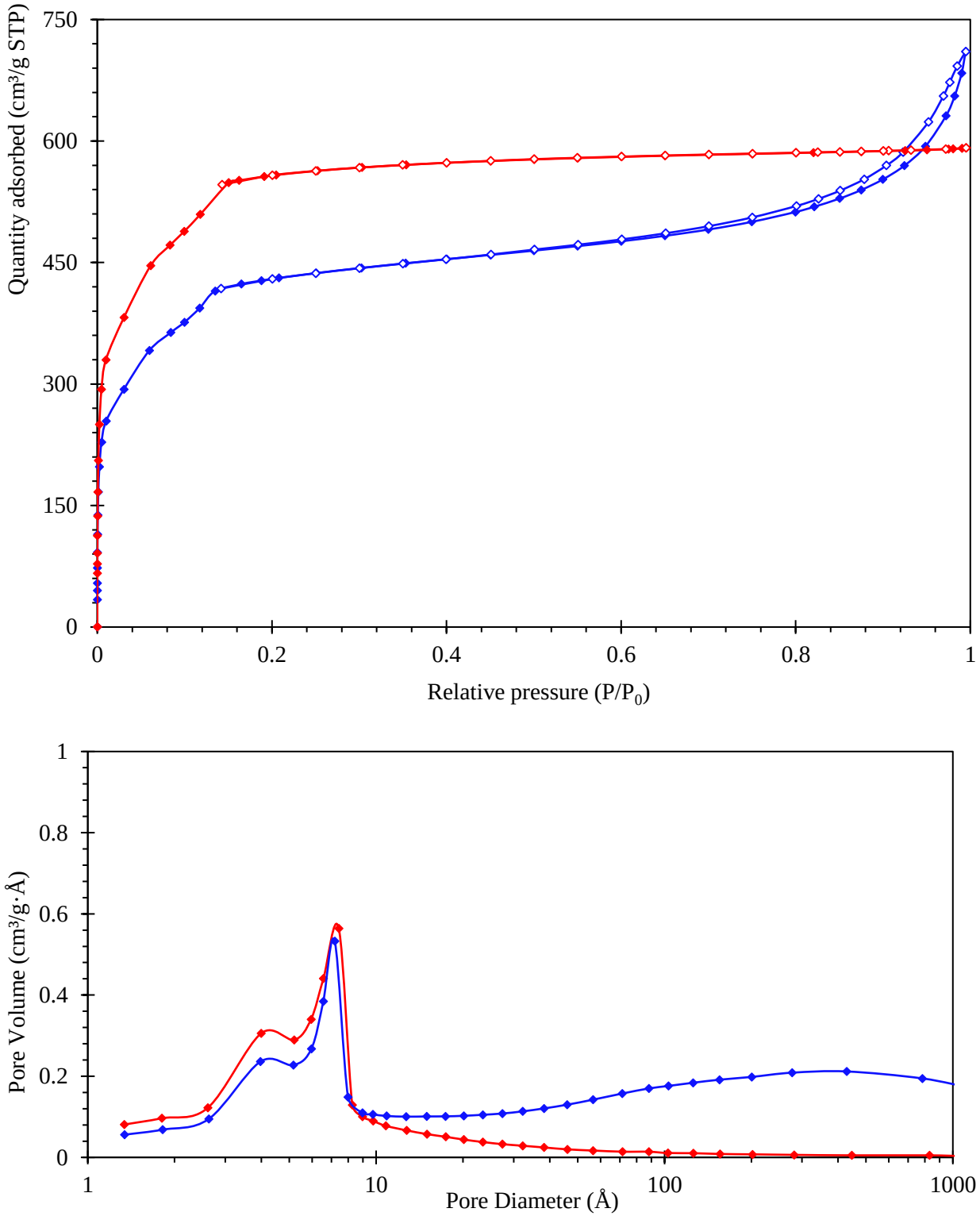

- Figure S1 -

Figure S2. Laboratory measured PXRD patterns of MIL-100(Fe) obtained in acidic and basic conditions.

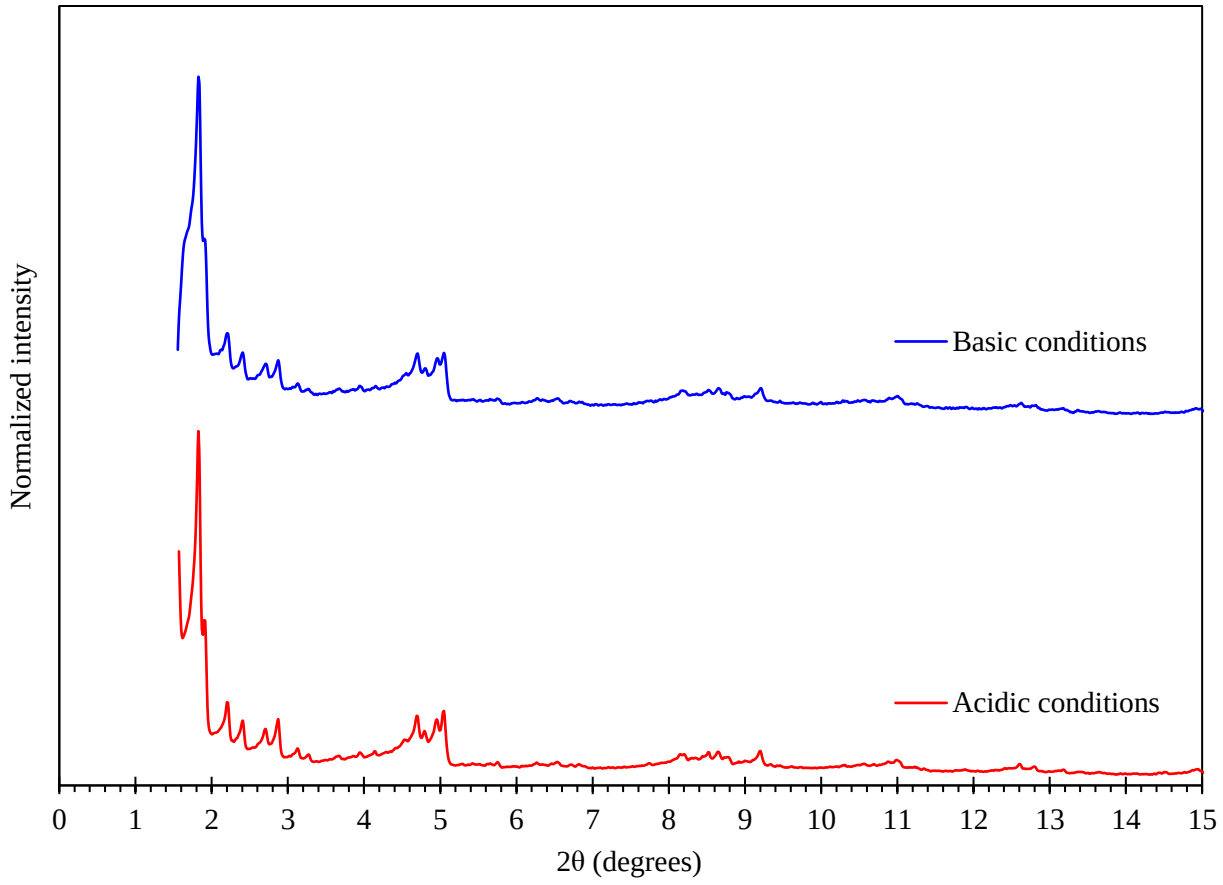

Figure S3. Synchrotron PXRD patterns of the as-synthesized MIL-100(Fe,Co) samples, using different Co/Fe ratios in the synthesis (indicated percentages correspond to mol%).

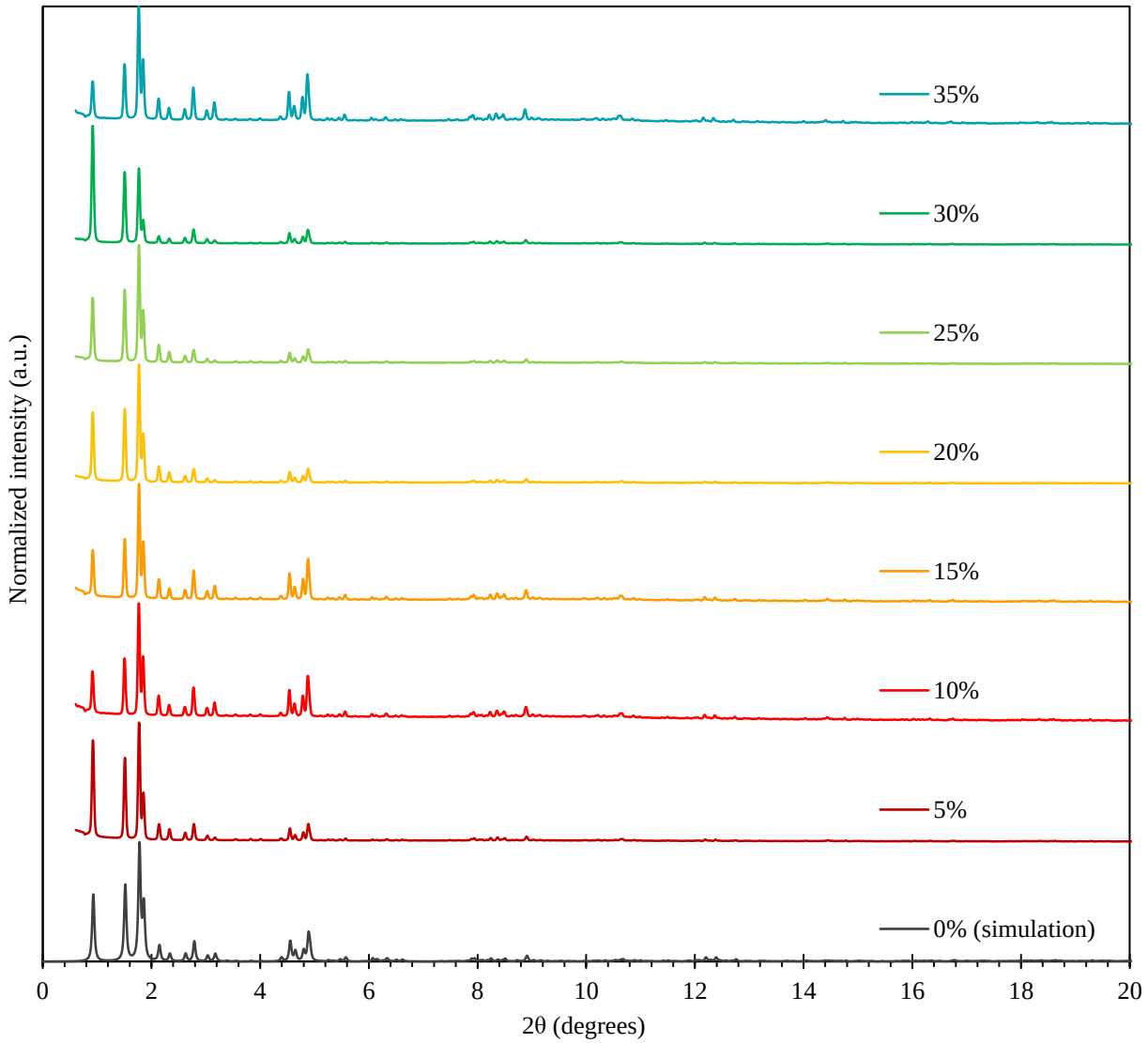

Figure S4. ATR-IR spectra of the as-synthesized MIL-100(Fe,Co) samples, using different Co/Fe ratios in the synthesis (indicated percentages correspond to mol%).

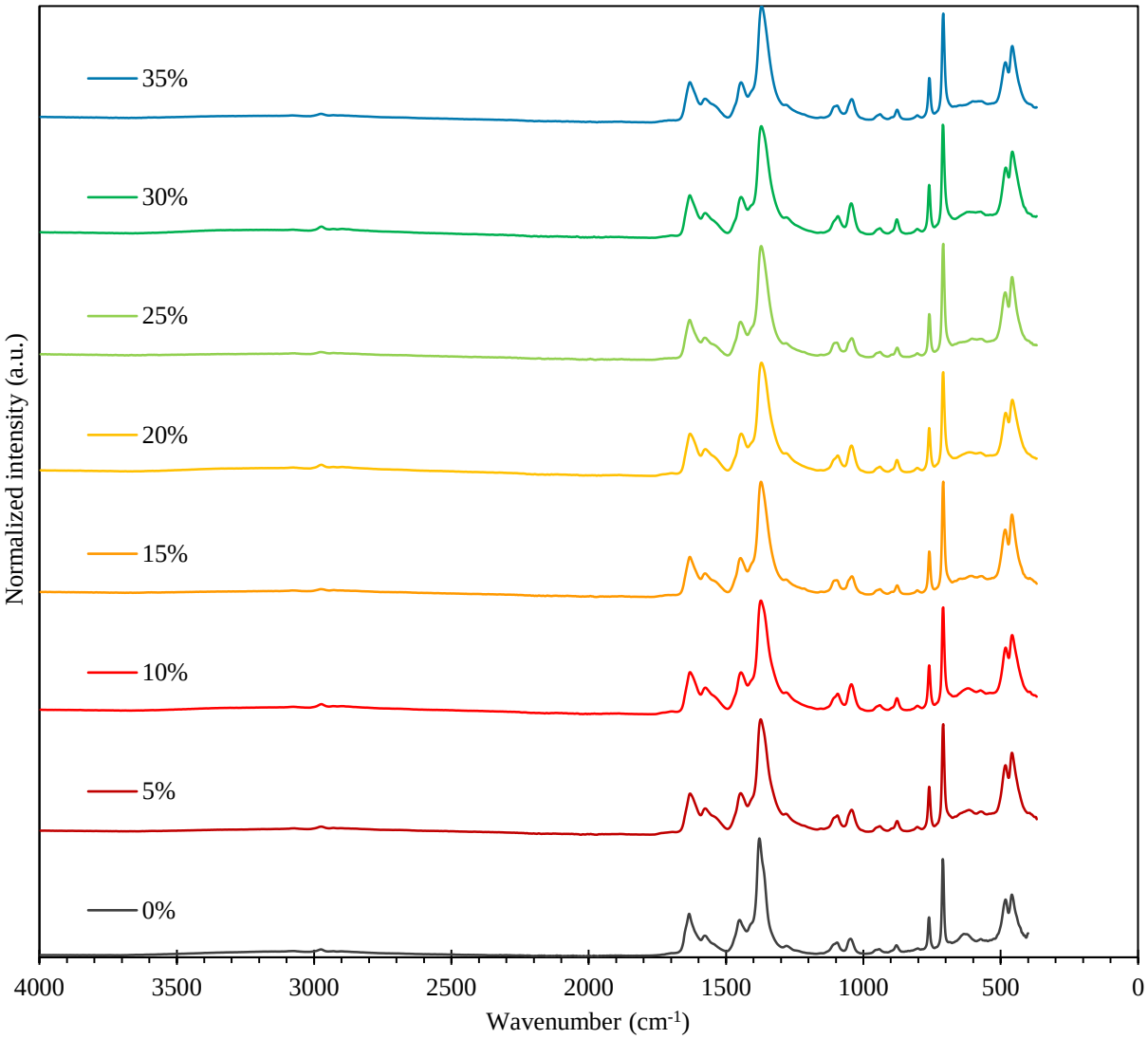

Fig. S5 A. Experimental synchrotron PXRD pattern and simulated pattern of the obtained $Fe_3BTC_2 \cdot 12H_2O$ intermediate.

$(C_{18}H_{30}Fe_3O_{24})_n$: $Fe_3BTC_2 \cdot 12H_2O$

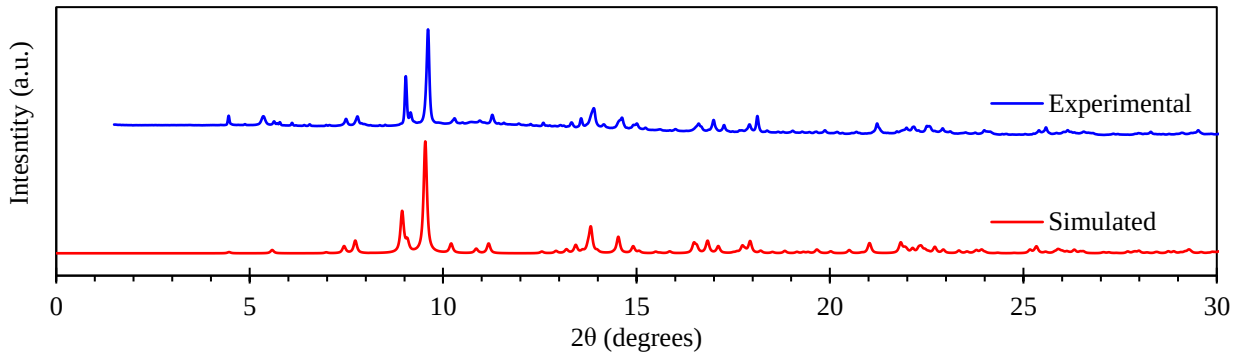

The simulated pattern was obtained using the Mercury software. The data for the simulation was obtained from the CCDC database [Refcode (entry ID): XIZHAP]. Wavelength: 0.79800 Å.

Fig. S5 B. Experimental synchrotron PXRD pattern and simulated pattern of the obtained $Co_3BTC_2 \cdot 12H_2O$ intermediate.

$(C_{18}H_{30}Co_3O_{24})_n$: $Co_3BTC_2 \cdot 12H_2O$

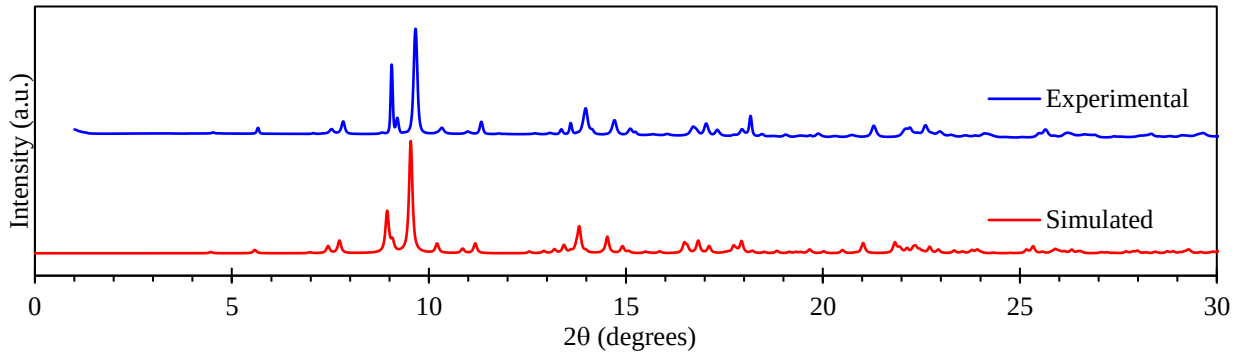

The simulated pattern was obtained using the Mercury software. The data for the simulation was obtained from the CCDC database [Refcode (entry ID): TOPMIU]. Wavelength: 0.79800 Å.

- Figure S5 -

B. Post-synthetic exchange of Co^{2+} starting from pure MIL-100(Fe).

For comparison with our direct synthesis strategy, 100 mg of a sample of pure MIL-100(Fe) was incubated in 100 ml of a 1 M aqueous solution of $CoSO_4 \cdot 7H_2O$ (28.1 g) for 24 h at room-temperature to allow post-synthetic exchange to proceed with the iron present in MIL-100(Fe). This was followed by three washings with water and three washings with ethanol. The sample was then dried under vacuum. ICP analysis revealed a bulk doping metal content of 3.3 mol% Co, which is less than in all the samples of MIL-100(Fe,Co) obtained by direct synthesis, except the one using 5 mol% Co/M_{tot} for the synthesis. The starting Co/Fe ratio was about 1100/1 for the post-synthetic exchange compared to only 0.05/1 for the direct synthesis to yield comparative doping percentage. Direct synthesis is thus a much more economical way to achieve Co incorporation into MIL-100(Fe).

Figure S6. Synchrotron PXRD patterns of MIL-100(Fe,M) materials obtained using different doping metals (sample temperature 200°C).

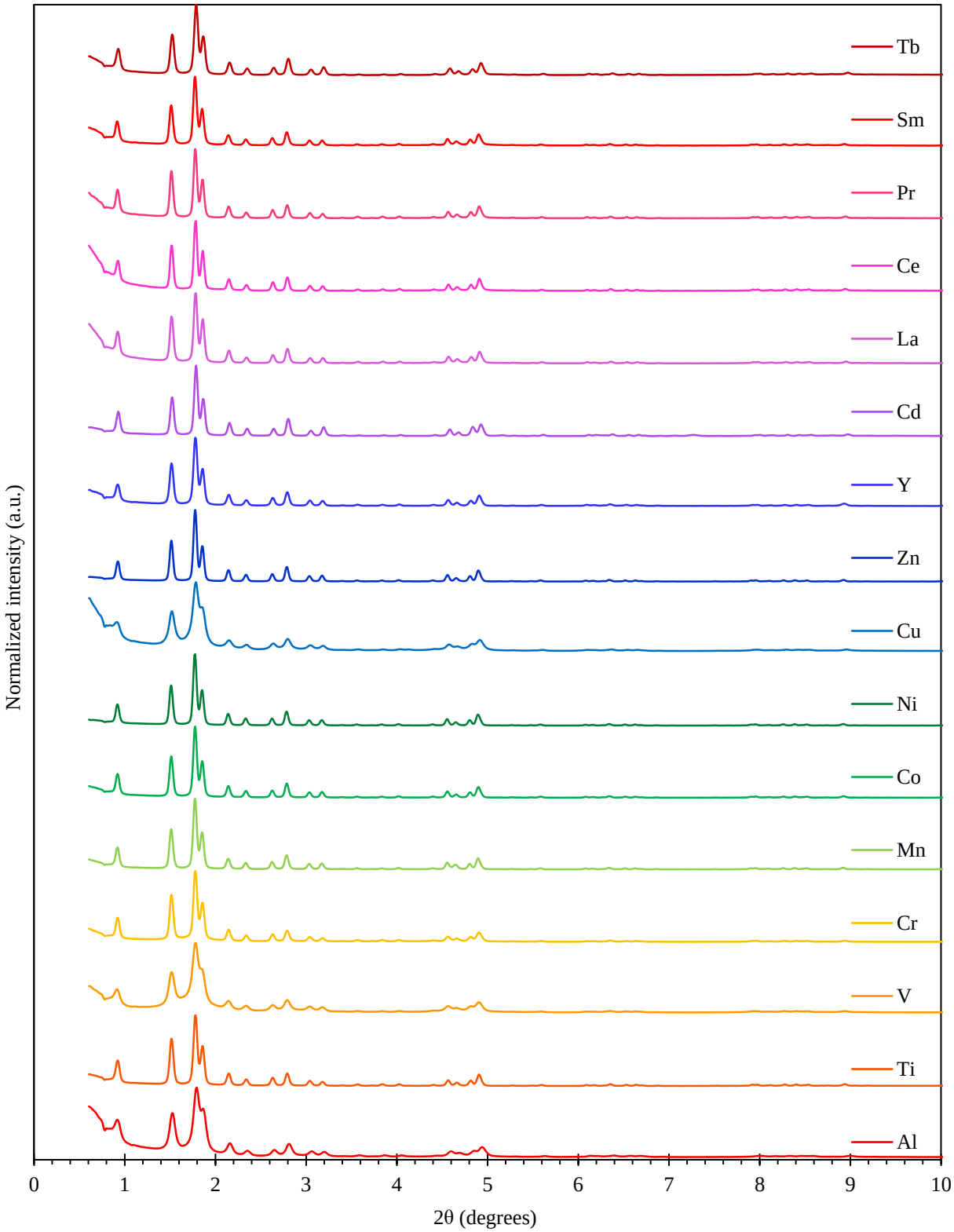

- Figure S6 -

Figure S7. ATR-IR spectra of as-synthesized MIL-100(Fe,M) materials.

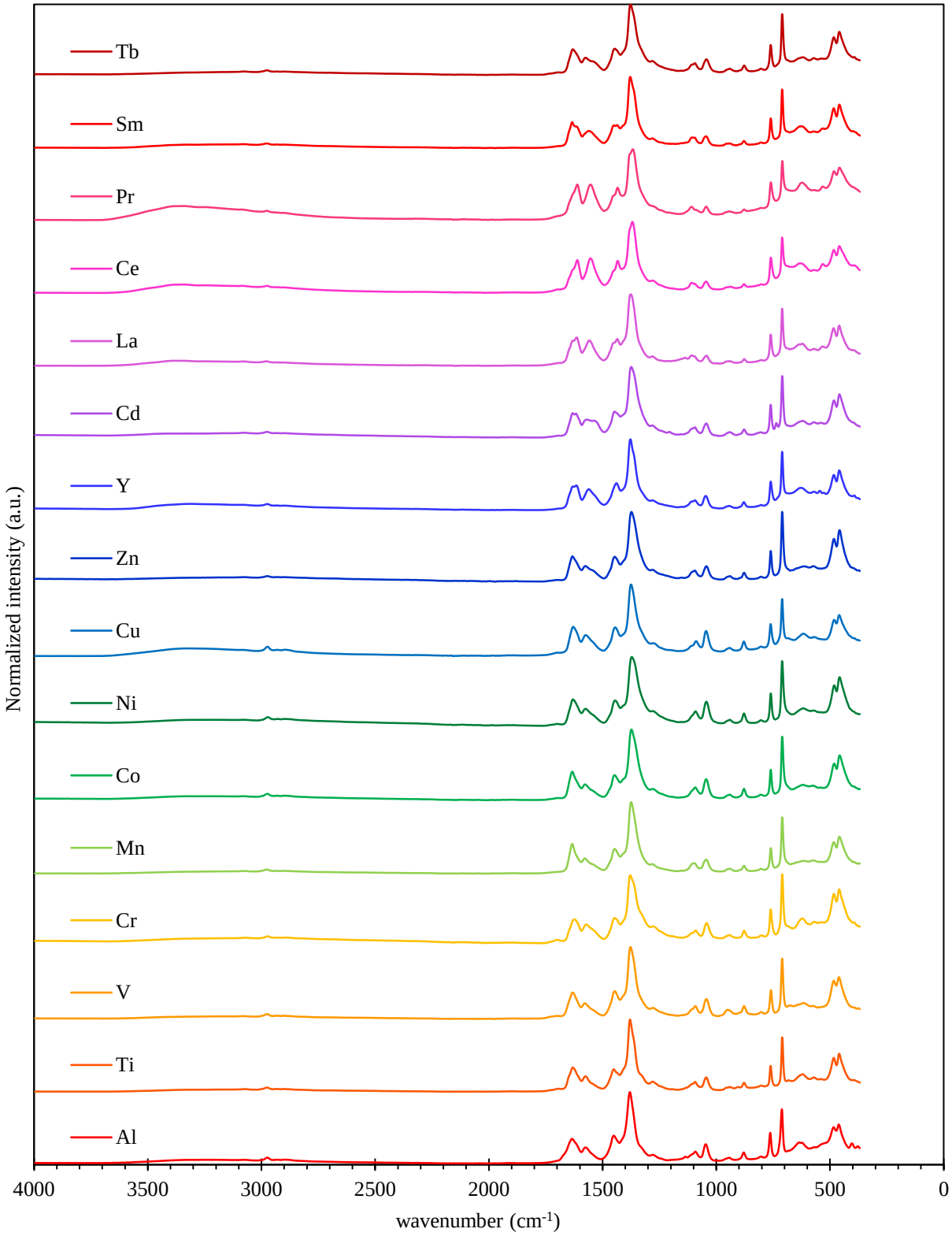

Table S1. Doping metal content determined by ICP-OES and surface content determined by XPS for samples obtained using 20 mol% doping metal during synthesis. The reported values correspond to the results of the following formula:

$$\text{Doping metal content} = \frac{\%_{at}\ \text{doping metal}}{\%_{at}\ \text{Fe} + \%_{at}\ \text{doping metal}} \times 100$$

NB: The values obtained from ICP measurements (in wt. %) were converted to at. % prior to applying the above formula.

Doping metal	Bulk doping metal content (ICP)	Surface doping metal content (XPS)
Al	21.5 mol%	14.1 mol%
Ti	15.6 mol%	12.0 mol%
V	14.7 mol%	6.5 mol%
Cr	21.6 mol%	7.6 mol%
Mn	10.5 mol%	9.5 mol%
Co	11.0 mol%	11.7 mol%
Ni	7.5 mol%	15.6 mol%
Cu	19.9 mol%	17.9 mol%
Zn	9.7 mol%	12.3 mol%
Y	25.7 mol%	9.8 mol%
Cd	20.1 mol%	27.4 mol%
La	21.0 mol%	17.1 mol%
Ce	29.9 mol%	34.1 mol%
Pr	24.5 mol%	13.7 mol%
Sm	24.5 mol%	3.0 mol%
Tb	21.2 mol%	5.1 mol%

Figure S8. Nitrogen adsorption-desorption isotherms (77K) for the different MIL-100(Fe,M) materials. Calculated BET surface areas are given in the insets. BJH transform plots are represented to highlight the presence of micropores and intergrain spaces in the Al, Cu and V-doped materials.

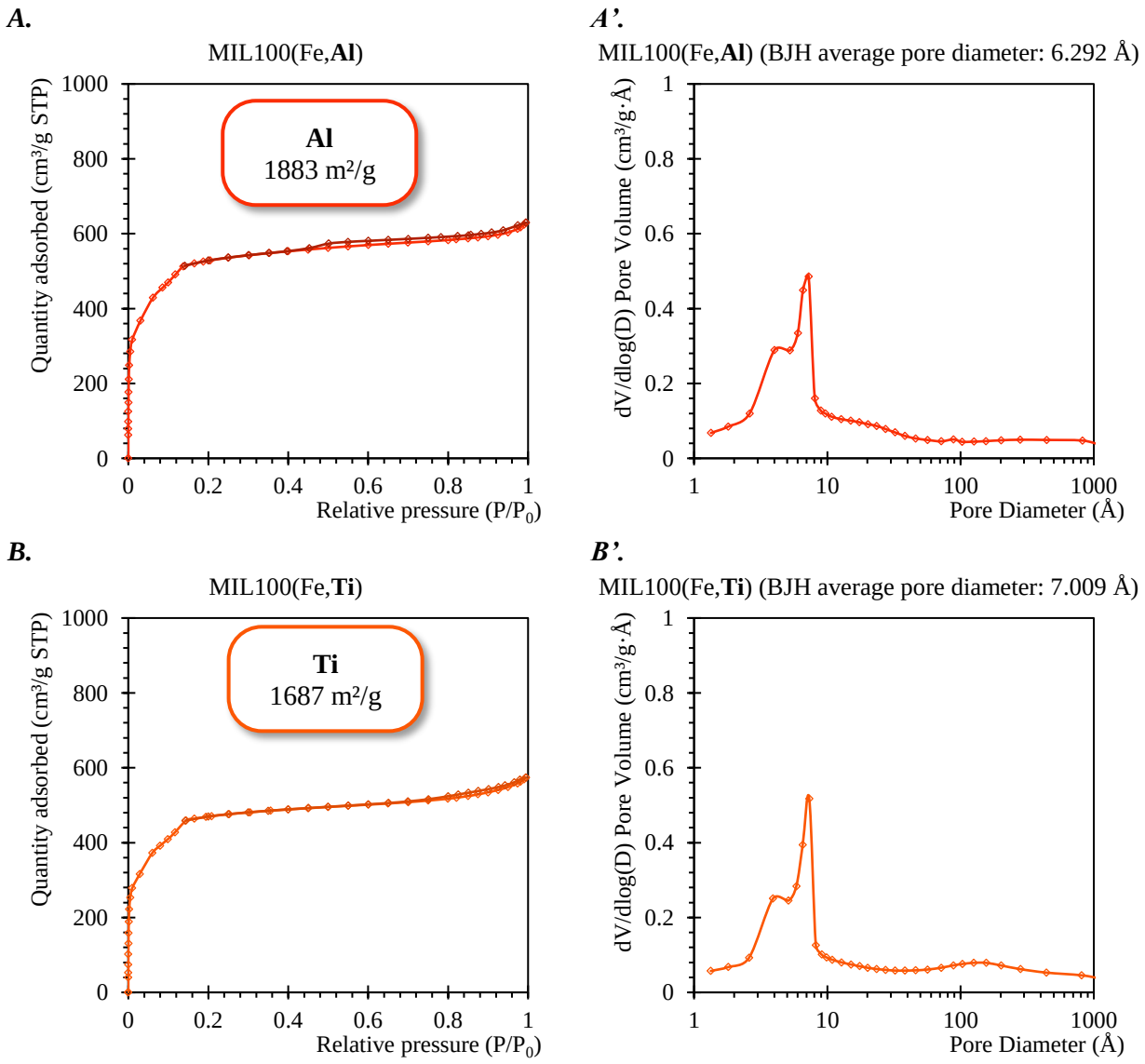

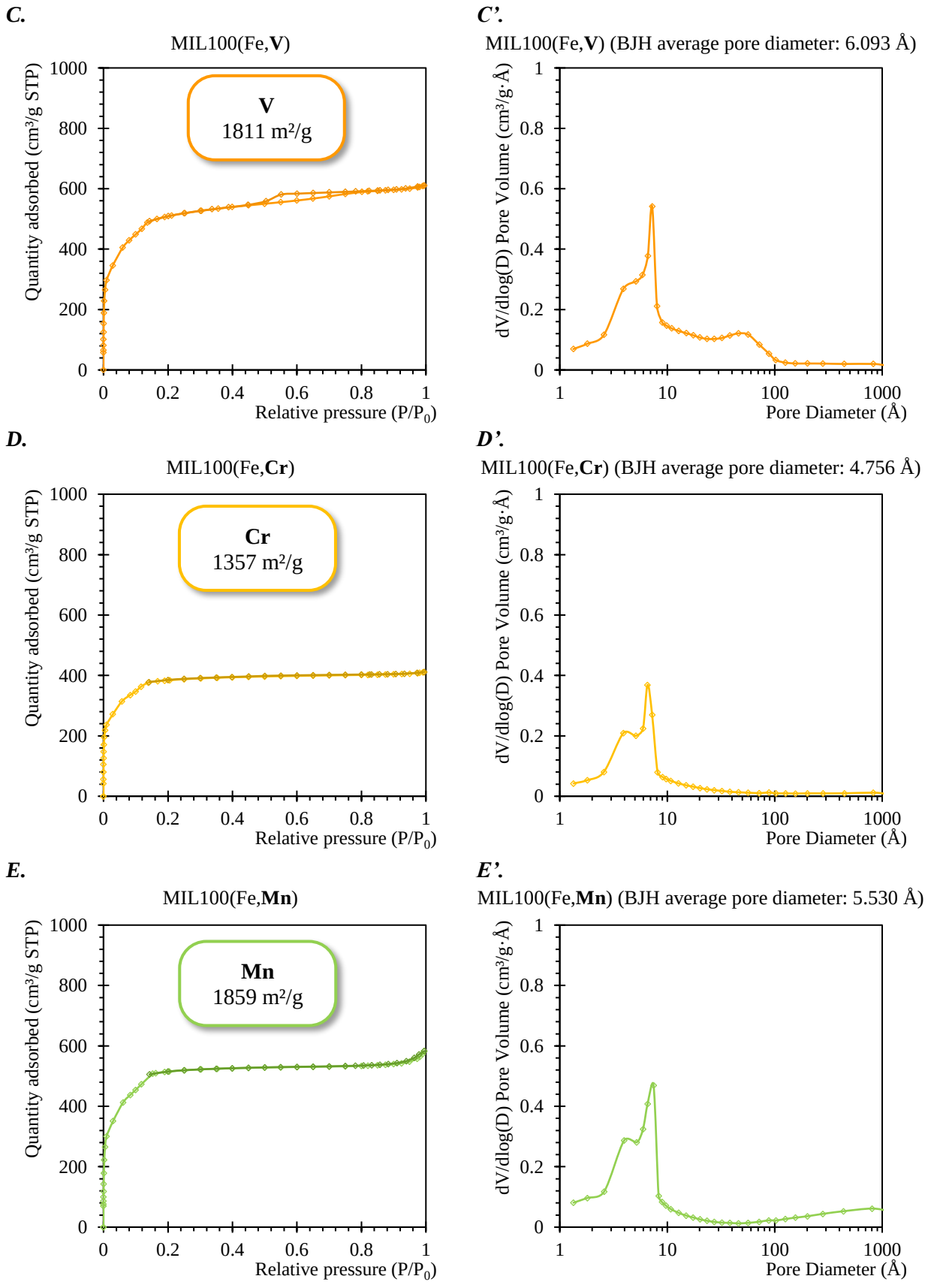
C.
MIL100(Fe,V)
V
1811 m²/g
Quantity adsorbed (cm³/g STP)
Relative pressure (P/P0)
C'.
MIL100(Fe,V) (BJH average pore diameter: 6.093 Å)
dV/dlog(D) Pore Volume (cm³/g·Å)
Pore Diameter (Å)
D.
MIL100(Fe,Cr)
Cr
1357 m²/g
Quantity adsorbed (cm³/g STP)
Relative pressure (P/P0)
D'.
MIL100(Fe,Cr) (BJH average pore diameter: 4.756 Å)
dV/dlog(D) Pore Volume (cm³/g·Å)
Pore Diameter (Å)
E.
MIL100(Fe,Mn)
Mn
1859 m²/g
Quantity adsorbed (cm³/g STP)
Relative pressure (P/P0)
E'.
MIL100(Fe,Mn) (BJH average pore diameter: 5.530 Å)
dV/dlog(D) Pore Volume (cm³/g·Å)
Pore Diameter (Å)

- Figure S8 -

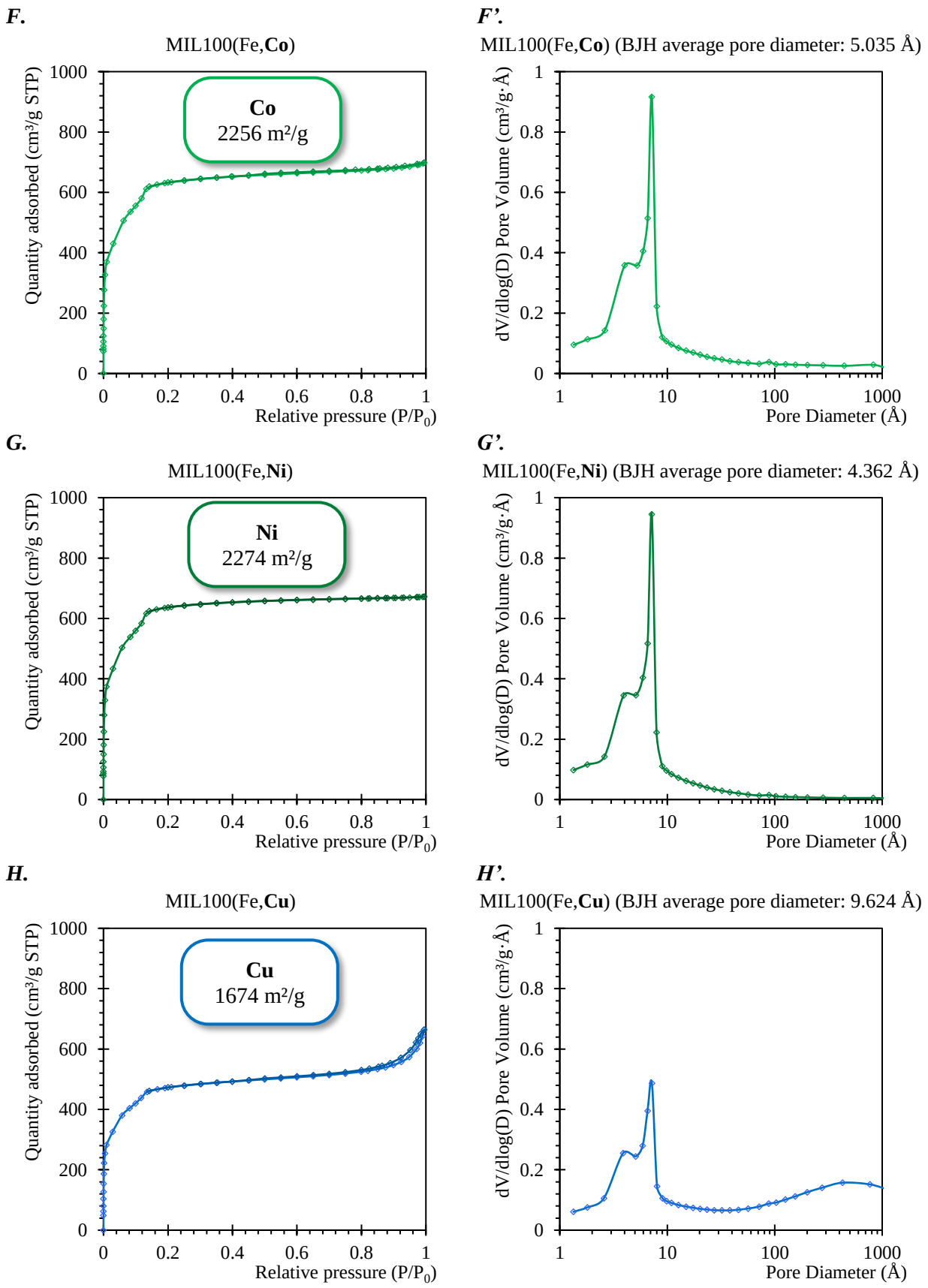
F.
MIL100(Fe,Co)
Co
2256 m²/g
Quantity adsorbed (cm³/g STP)
Relative pressure (P/P0)
F'.
MIL100(Fe,Co) (BJH average pore diameter: 5.035 Å)
dV/dlog(D) Pore Volume (cm³/g·Å)
Pore Diameter (Å)
G.
MIL100(Fe,Ni)
Ni
2274 m²/g
Quantity adsorbed (cm³/g STP)
Relative pressure (P/P0)
G'.
MIL100(Fe,Ni) (BJH average pore diameter: 4.362 Å)
dV/dlog(D) Pore Volume (cm³/g·Å)
Pore Diameter (Å)
H.
MIL100(Fe,Cu)
Cu
1674 m²/g
Quantity adsorbed (cm³/g STP)
Relative pressure (P/P0)
H'.
MIL100(Fe,Cu) (BJH average pore diameter: 9.624 Å)
dV/dlog(D) Pore Volume (cm³/g·Å)
Pore Diameter (Å)

- Figure S8 -

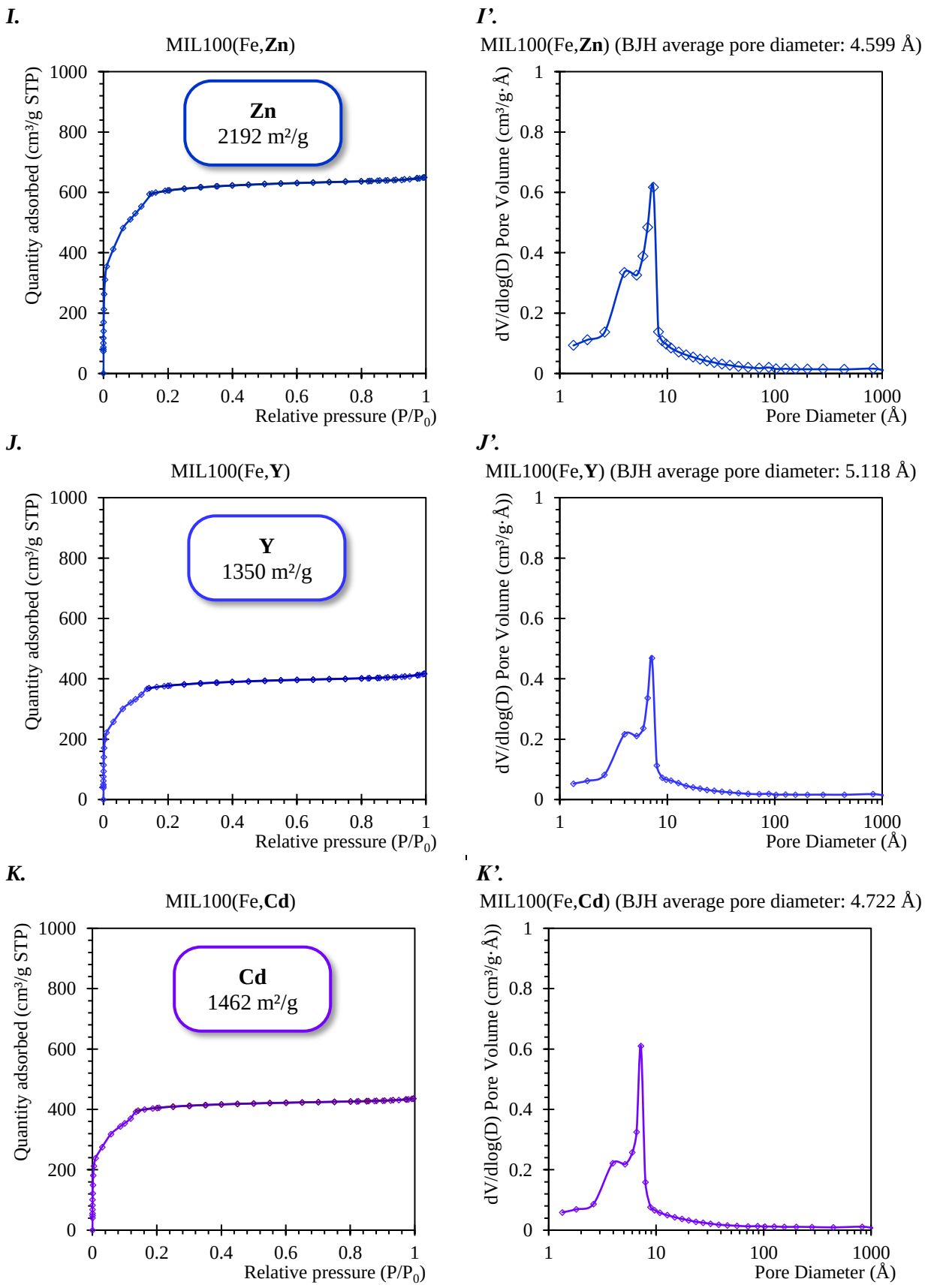
I.
MIL100(Fe,Zn)
Zn
2192 m²/g
Quantity adsorbed (cm³/g STP)
Relative pressure (P/P0)
I'.
MIL100(Fe,Zn) (BJH average pore diameter: 4.599 Å)
dV/dlog(D) Pore Volume (cm³/g·Å)
Pore Diameter (Å)
J.
MIL100(Fe,Y)
Y
1350 m²/g
Quantity adsorbed (cm³/g STP)
Relative pressure (P/P0)
J'.
MIL100(Fe,Y) (BJH average pore diameter: 5.118 Å)
dV/dlog(D) Pore Volume (cm³/g·Å))
Pore Diameter (Å)
K.
MIL100(Fe,Cd)
Cd
1462 m²/g
Quantity adsorbed (cm³/g STP)
Relative pressure (P/P0)
K'.
MIL100(Fe,Cd) (BJH average pore diameter: 4.722 Å)
dV/dlog(D) Pore Volume (cm³/g·Å))
Pore Diameter (Å)

- Figure S8 -

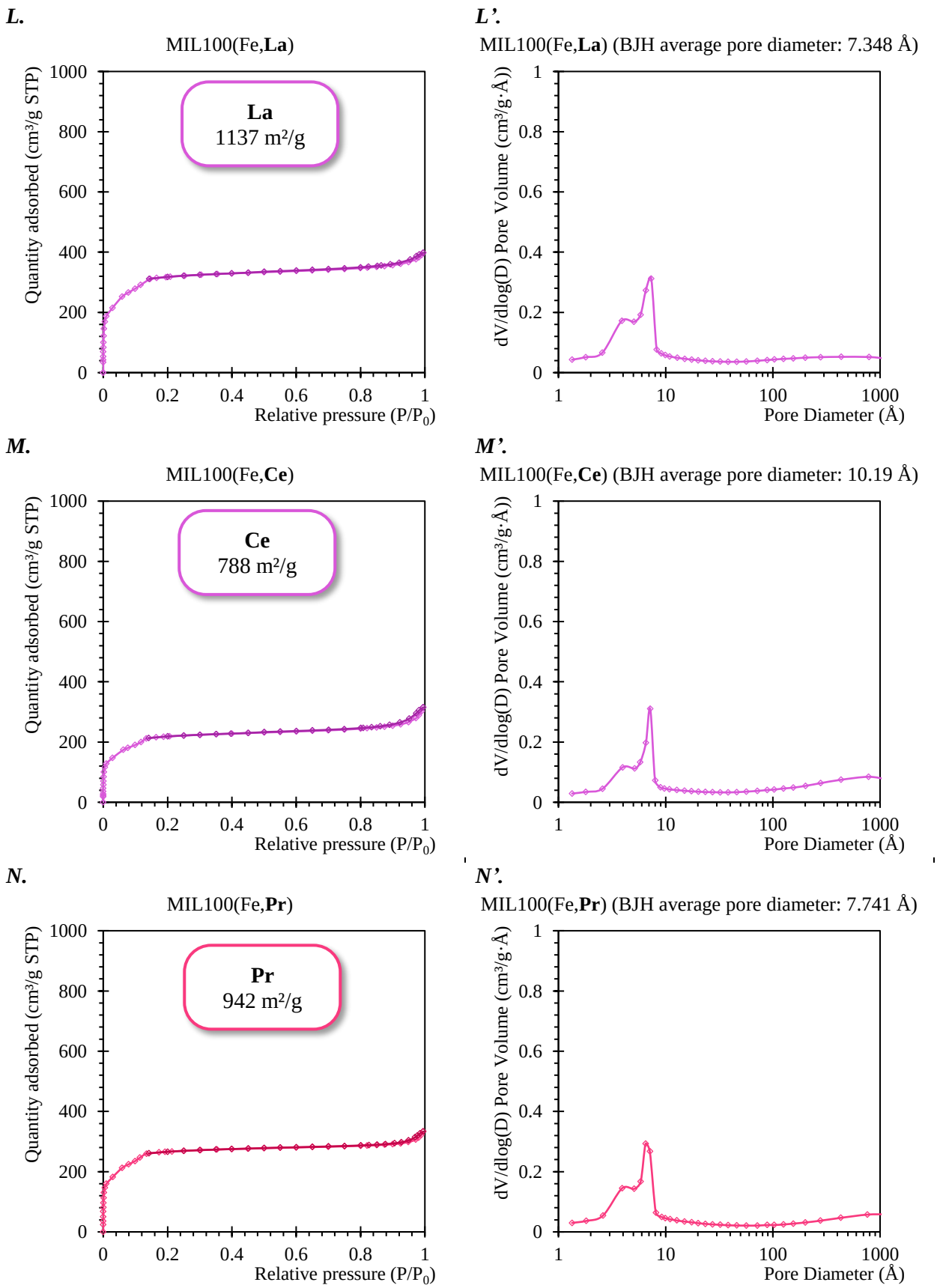
L.
MIL100(Fe,La)
La
1137 m²/g
Quantity adsorbed (cm³/g STP)
Relative pressure (P/P0)
L'.
MIL100(Fe,La) (BJH average pore diameter: 7.348 Å)
dV/dlog(D) Pore Volume (cm³/g·Å))
Pore Diameter (Å)
M.
MIL100(Fe,Ce)
Ce
788 m²/g
Quantity adsorbed (cm³/g STP)
Relative pressure (P/P0)
M'.
MIL100(Fe,Ce) (BJH average pore diameter: 10.19 Å)
dV/dlog(D) Pore Volume (cm³/g·Å))
Pore Diameter (Å)
N.
MIL100(Fe,Pr)
Pr
942 m²/g
Quantity adsorbed (cm³/g STP)
Relative pressure (P/P0)
N'.
MIL100(Fe,Pr) (BJH average pore diameter: 7.741 Å)
dV/dlog(D) Pore Volume (cm³/g·Å))
Pore Diameter (Å)

- Figure S8 -

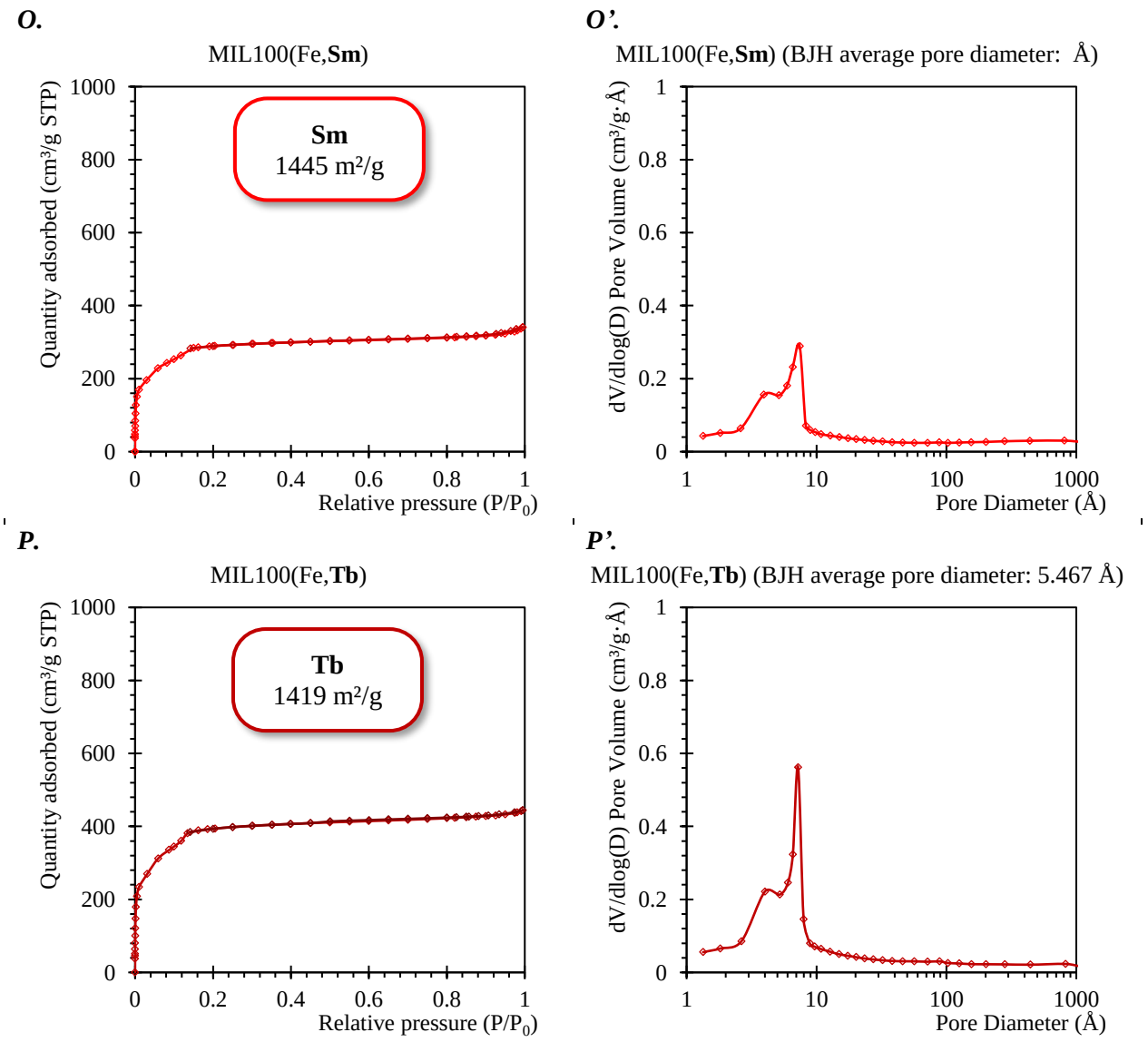
O.
MIL100(Fe,Sm)
Sm
1445 m²/g
Quantity adsorbed (cm³/g STP)
Relative pressure (P/P0)
O'.
MIL100(Fe,Sm) (BJH average pore diameter: Å)
dV/dlog(D) Pore Volume (cm³/g·Å)
Pore Diameter (Å)
P.
MIL100(Fe,Tb)
Tb
1419 m²/g
Quantity adsorbed (cm³/g STP)
Relative pressure (P/P0)
P'.
MIL100(Fe,Tb) (BJH average pore diameter: 5.467 Å)
dV/dlog(D) Pore Volume (cm³/g·Å)
Pore Diameter (Å)

- Figure S8 -

Figure S9 A. Ionic radii of the lanthanide ions used for the synthesis of MIL-100(Fe,Ln) and temperature at which the secondary crystalline phase disappears.

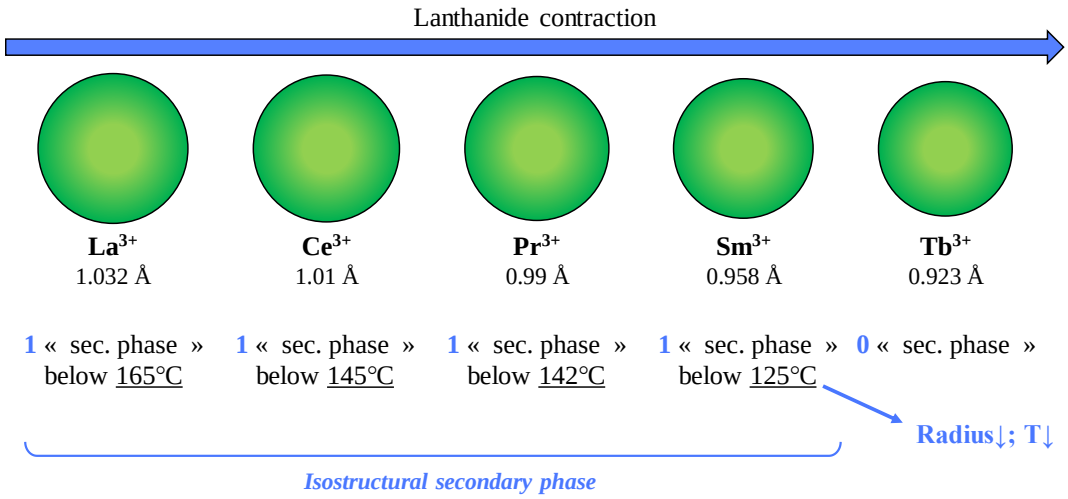

Figure S9 B. *In-situ* temperature-dependent synchrotron PXRD patterns of MIL-100(Fe,Ln) materials obtained after synthesis.

MIL-100(Fe,La)

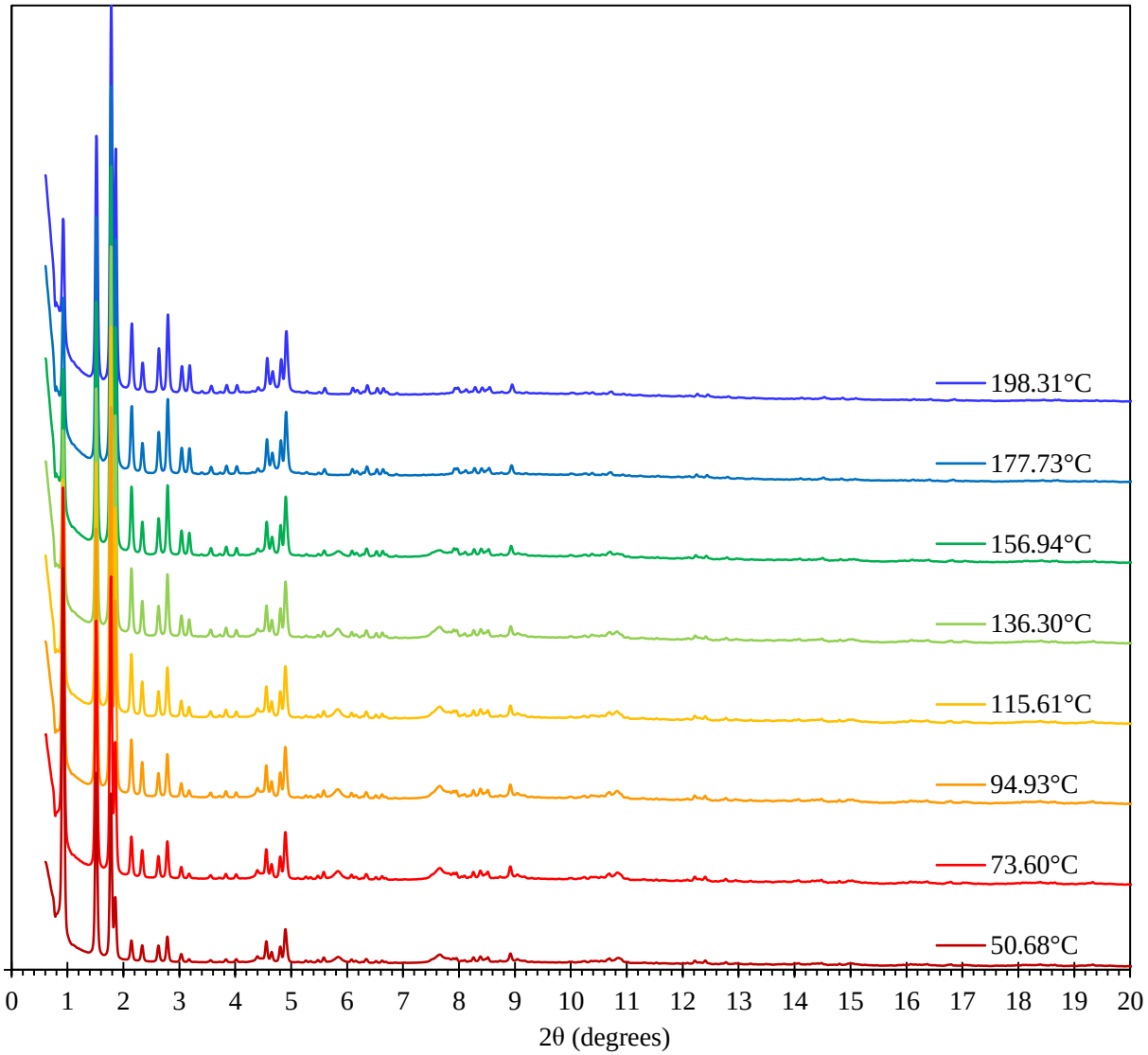

- Figure S9 -

MIL-100(Fe,Ce)

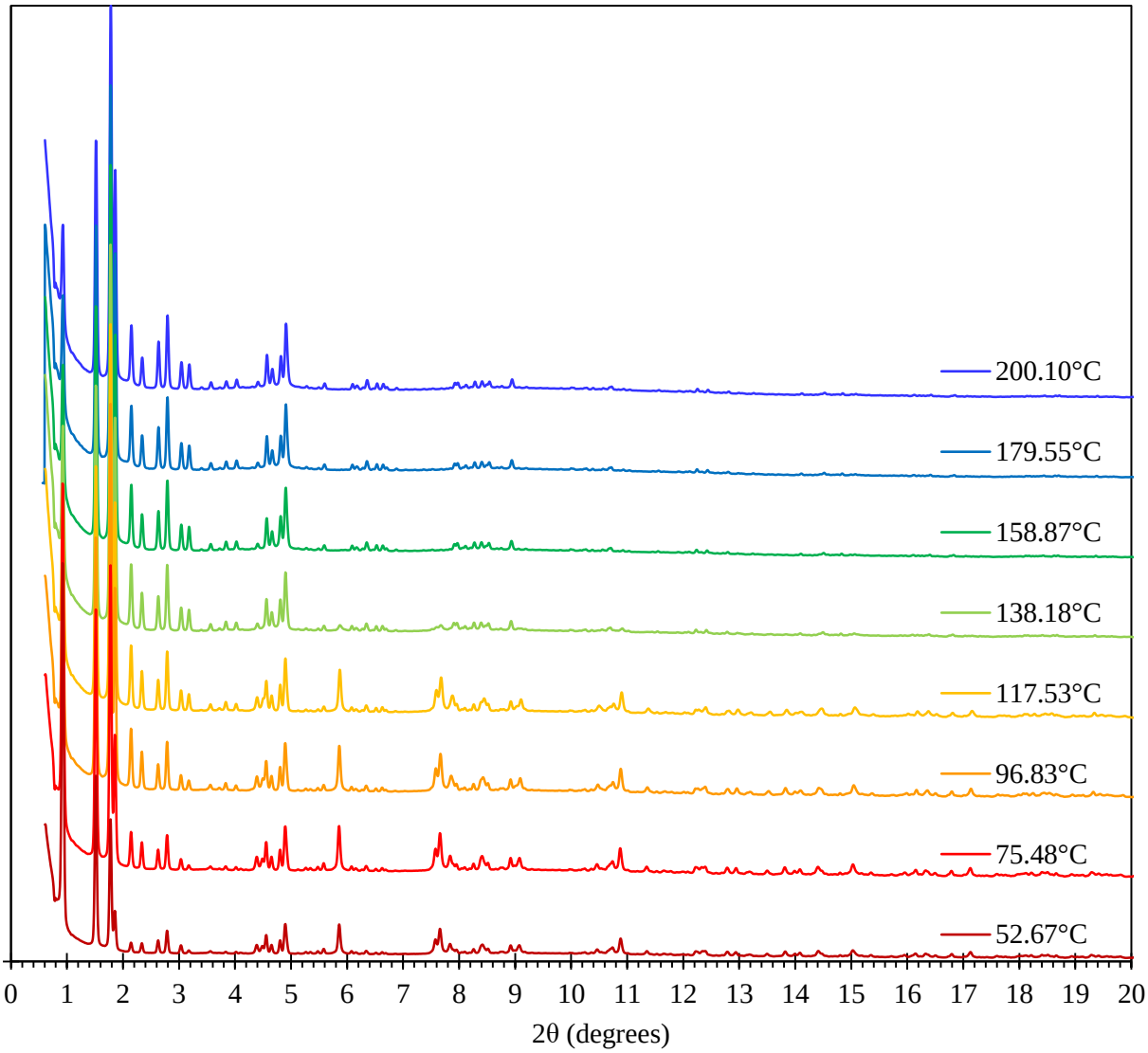

- Figure S9 -

MIL-100(Fe,Pr)

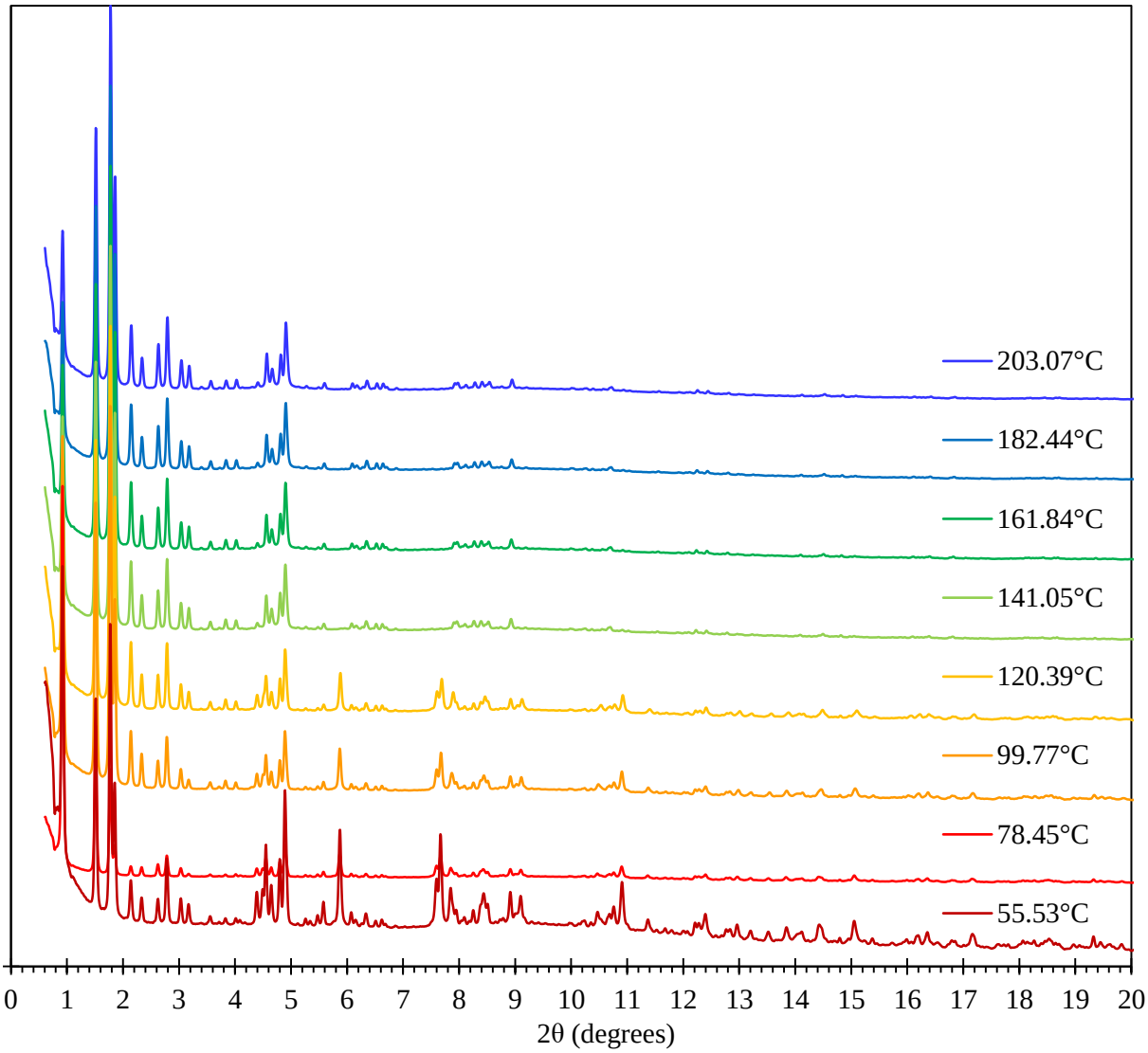

- Figure S9 -

MIL-100(Fe,Sm)

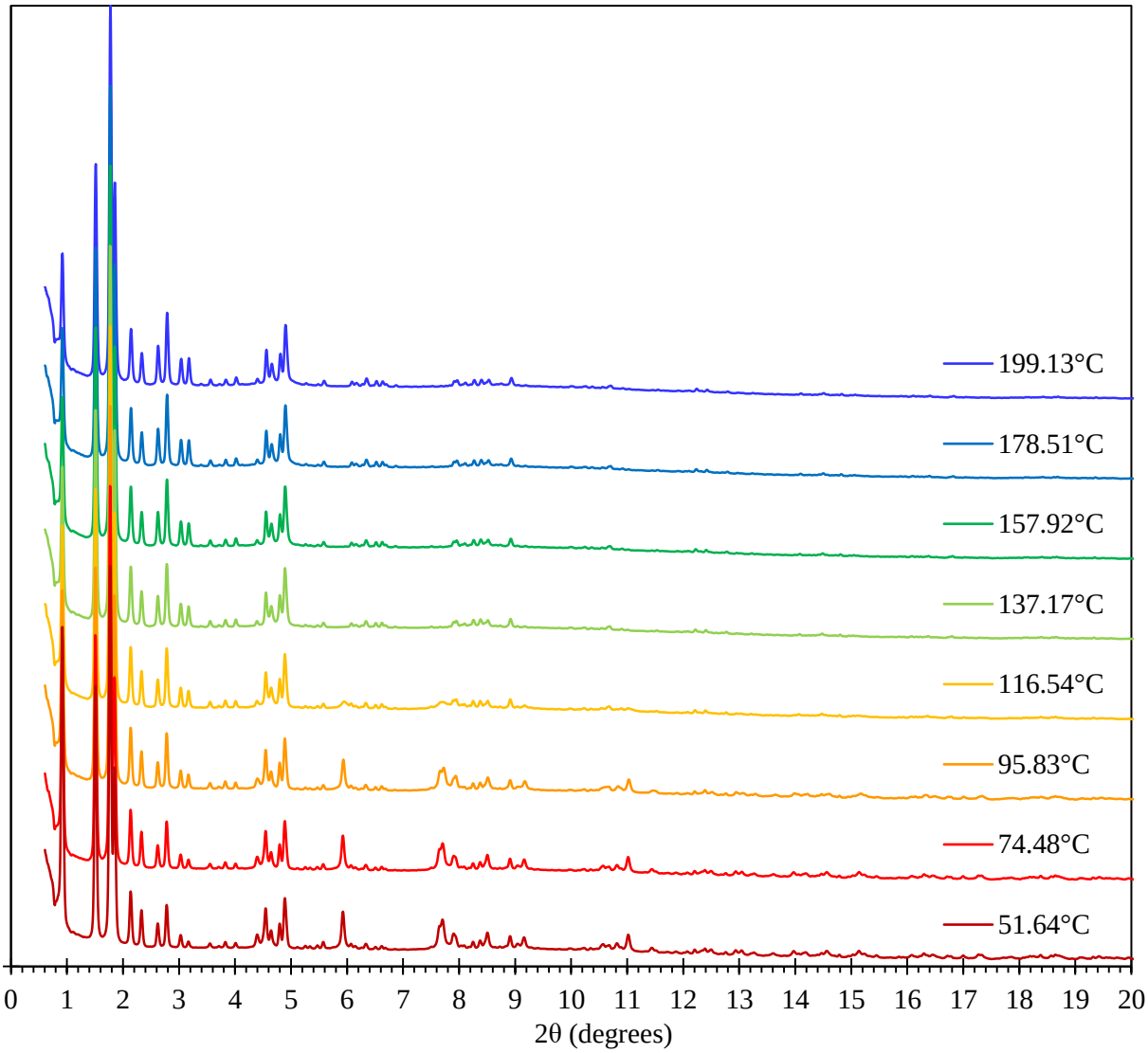

- Figure S9 -

Figure S9 C. *In-situ* temperature-dependent synchrotron PXRD patterns of MIL-100(Fe,Y) obtained after synthesis.

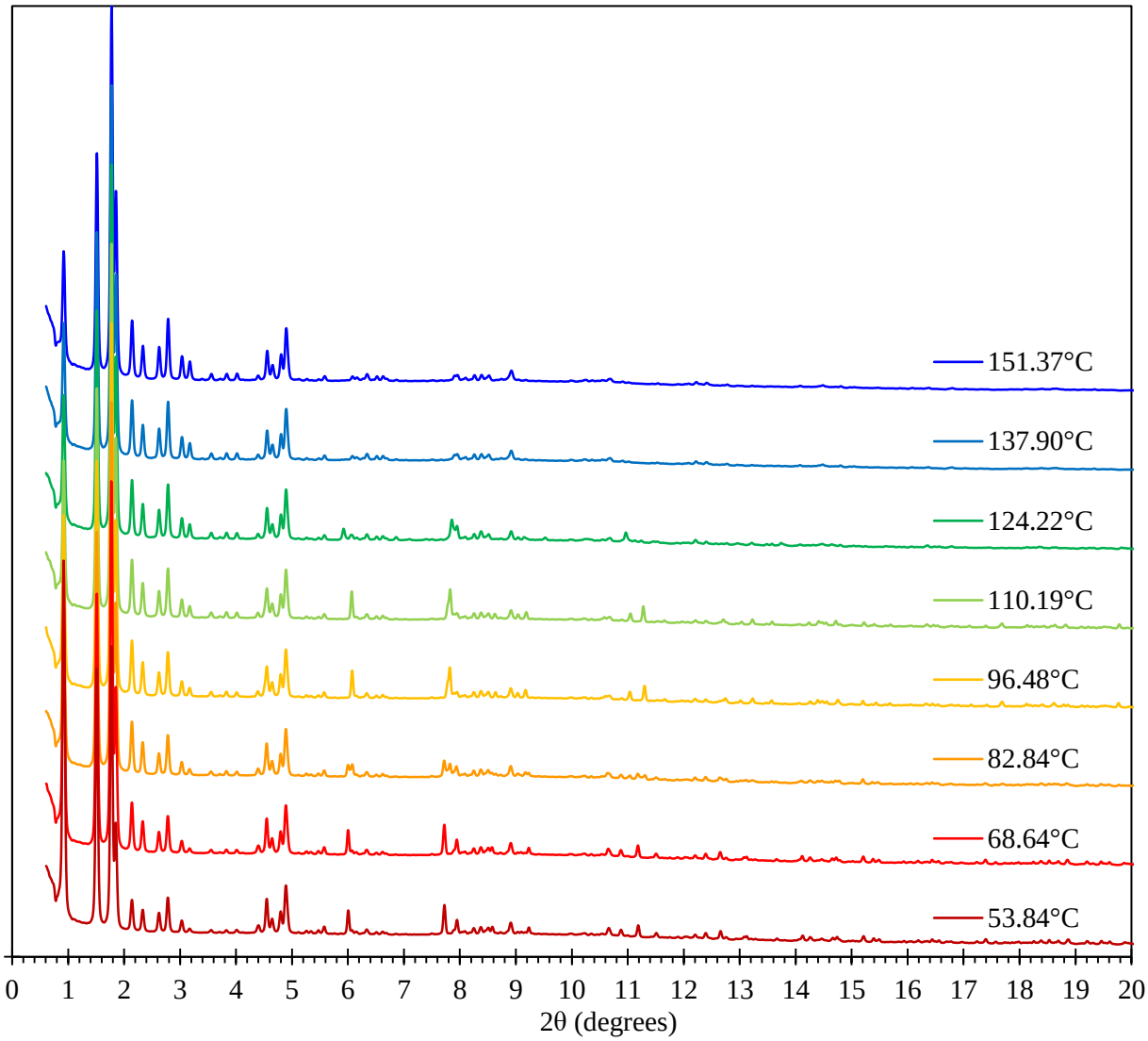

Figure S9 D. Laboratory PXRD patterns of MIL-100(Fe,Pr) obtained after synthesis, cooled sample after heating *ex-situ* under vacuum at 200°C and same sample that underwent a second washing procedure with water and ethanol

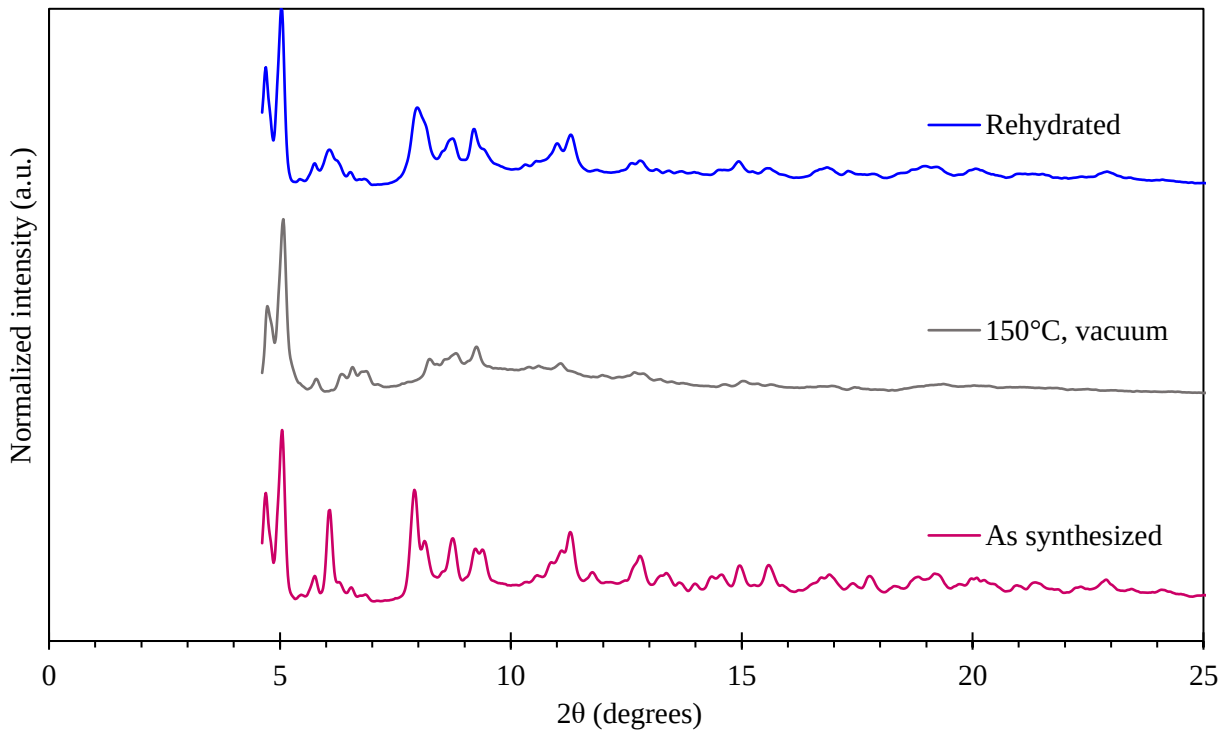

Figure S10. XPS survey scan of some of the MIL-100(Fe,Ln) compounds, indicating the presence of Na on the surface of the samples (the binding energy of Na1s is 1071 eV (see arrows), Na contamination is particularly visible on the MIL-100(Fe,M) samples with M = La, Pr and Sm). The XPS survey scan of MIL-100(Fe) is also shown for comparison purposes.

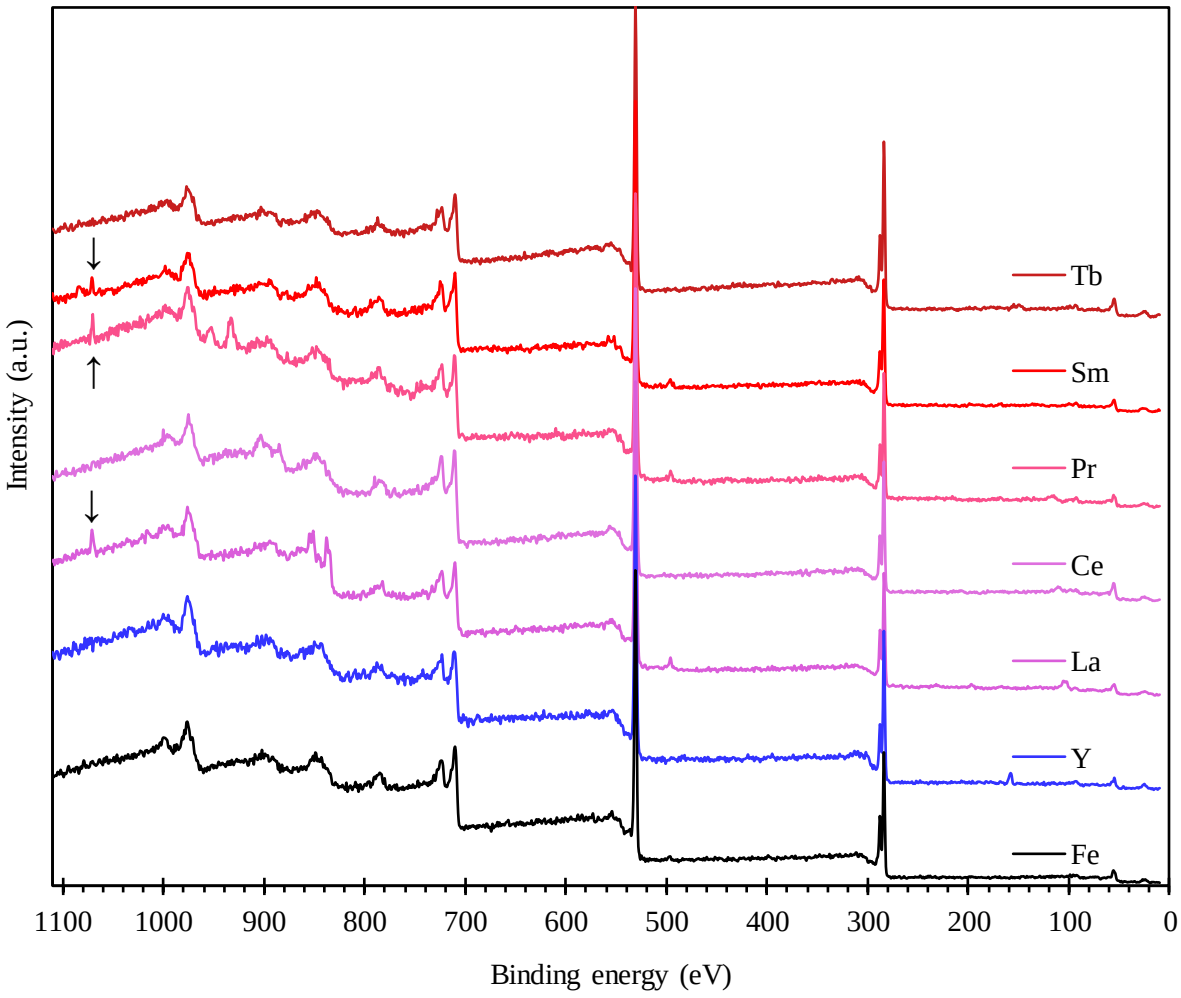

Concentrations of sodium detected by ICP analysis in the bulk of the materials for each doping metal:

Weight percent: Y < 0.1% ; La 1.6% ; Pr 1.2% ; Sm 1.0% ; Ce 0.2%

Comparison of the Na/M_{tot} content in the bulk and on the surface of the materials, showing homogeneous distribution of Na on the surface and in the bulk:

Na/(Na+Fe+M) at.%, **ICP**: La 15.8 % ; Pr 12.7 % ; Sm 10.8 % ; Ce 2.8 %

Na/(Na+Fe+M) at.%, **XPS** : La 20.0 % ; Pr 15.5 % ; Sm 10.6 % ; Ce 0.4 %

Figure S11 A. TGA plots of the MIL-100(Fe,M) materials under nitrogen.

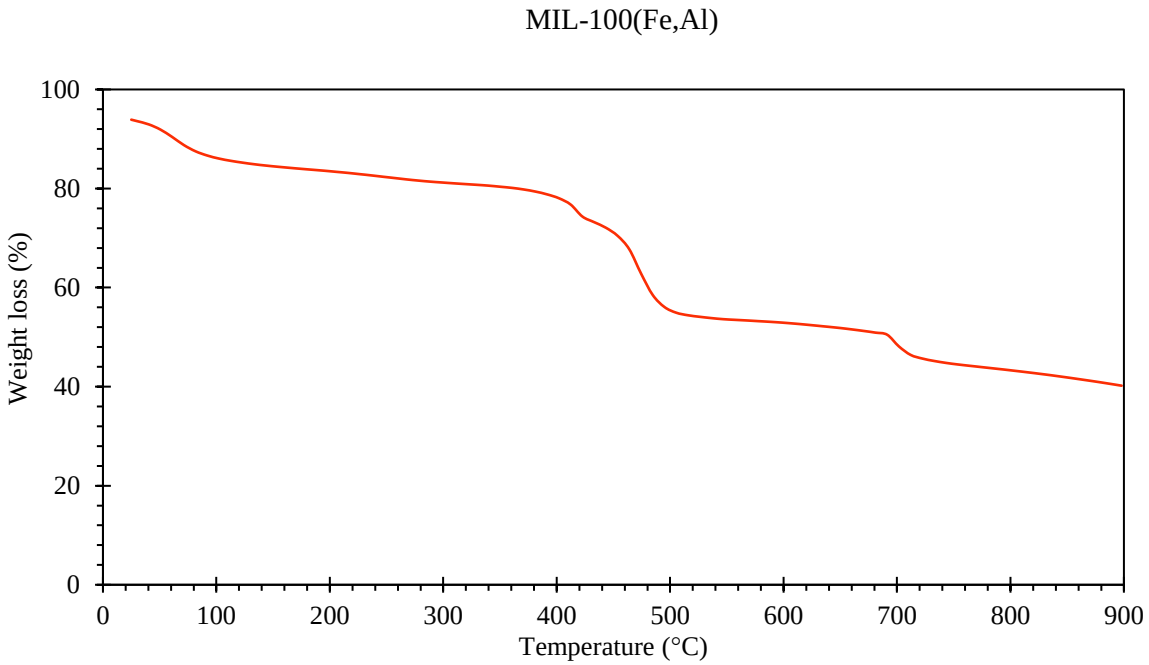

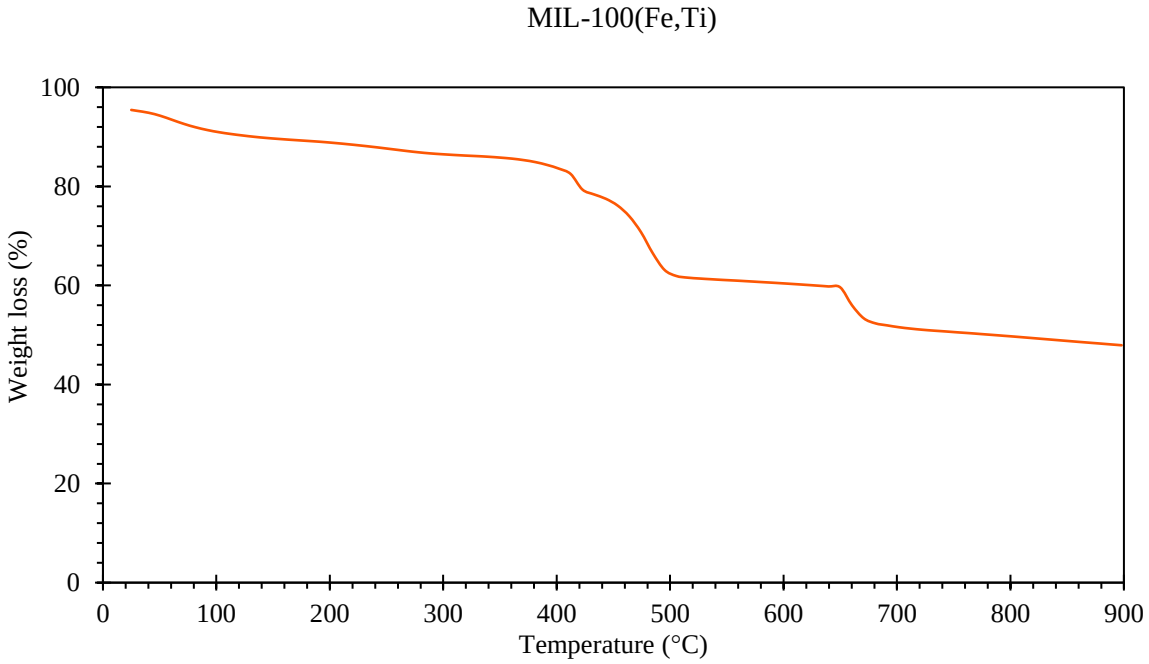

- Figure S11 -

MIL-100(Fe,V)

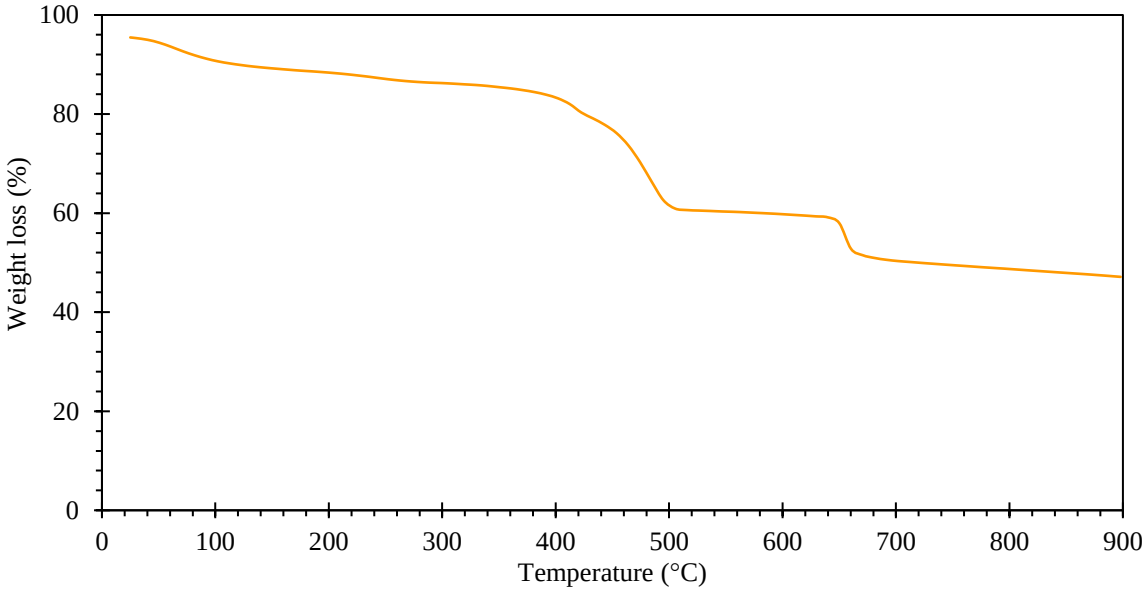

MIL-100(Fe,Cr)

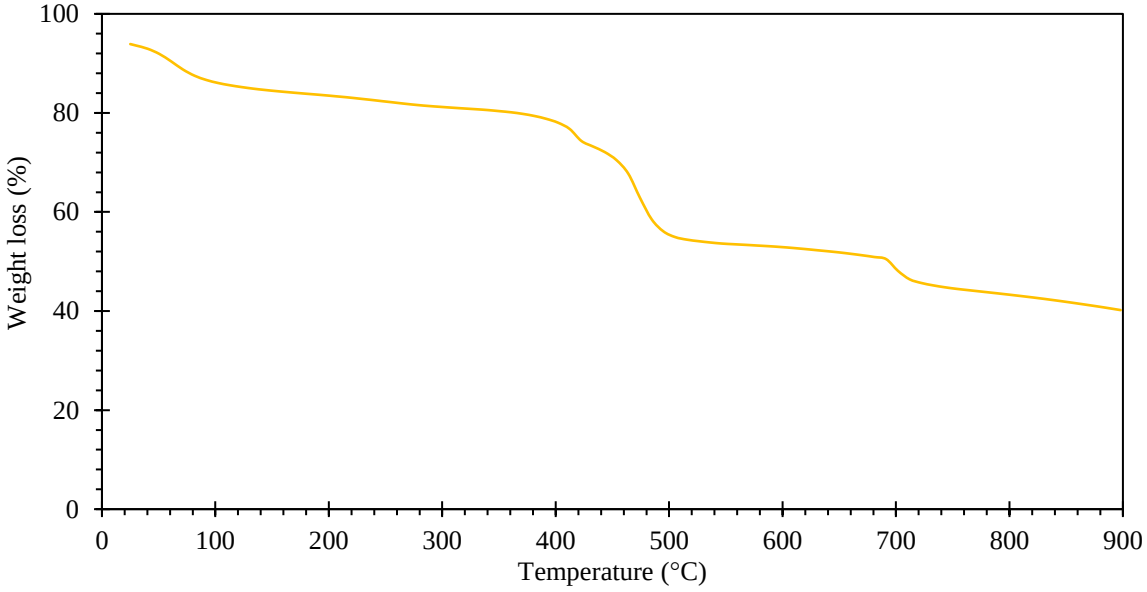

- Figure S11 -

MIL-100(Fe,Mn)

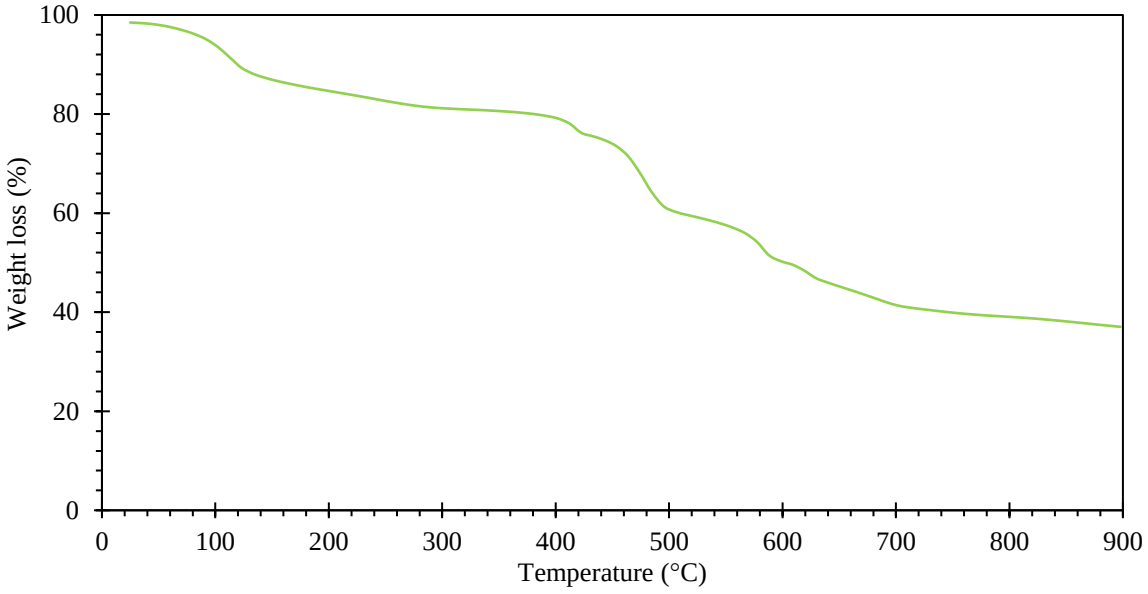

MIL-100(Fe,Co)

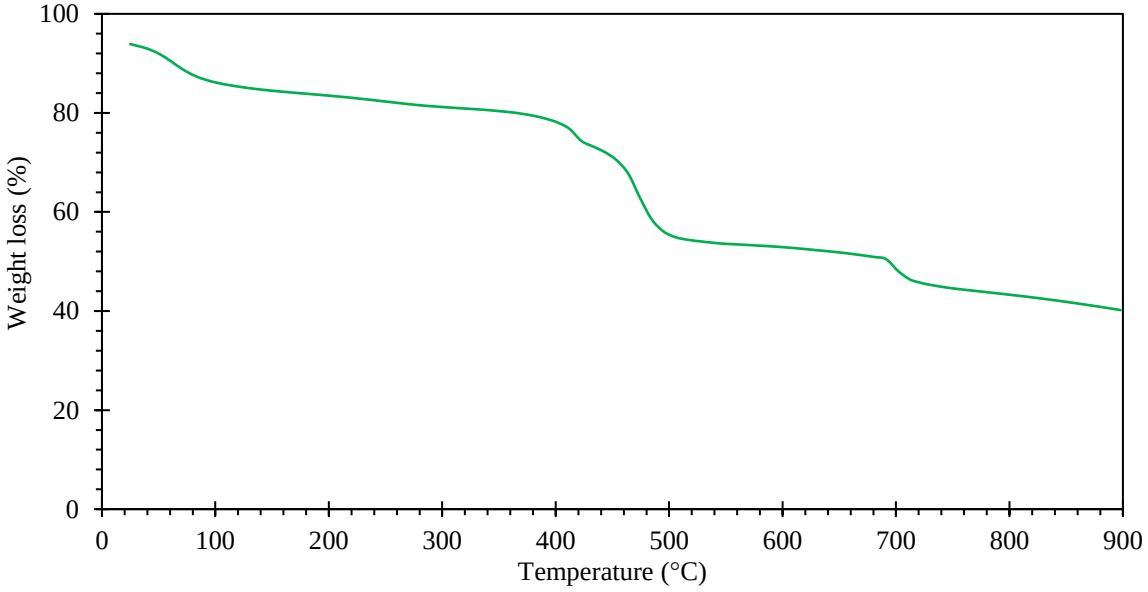

- Figure S11 -

MIL-100(Fe,Ni)

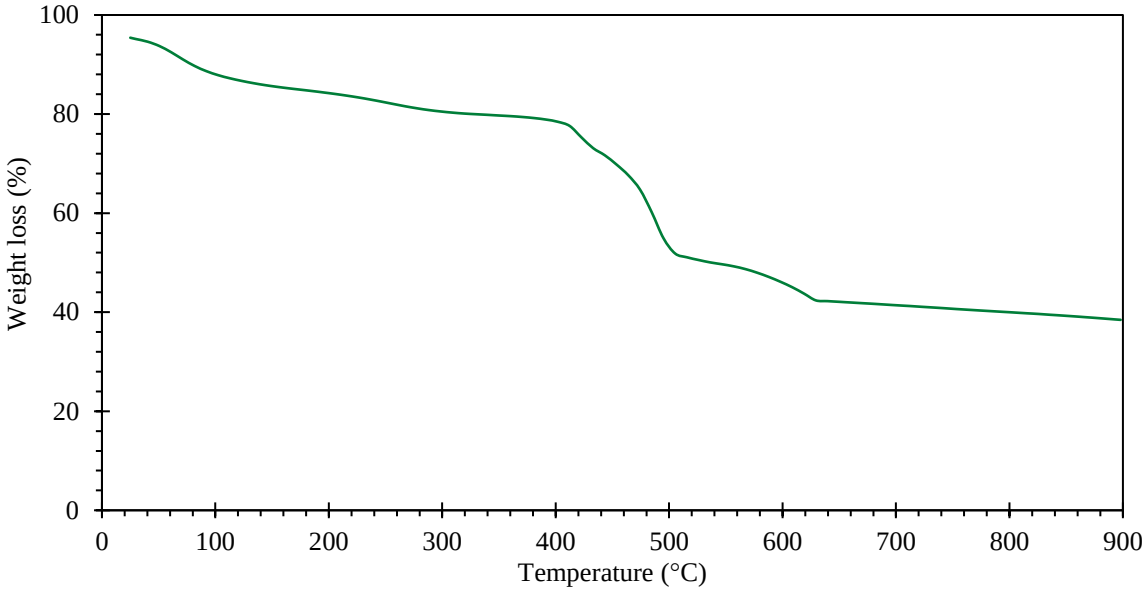

MIL-100(Fe,Cu)

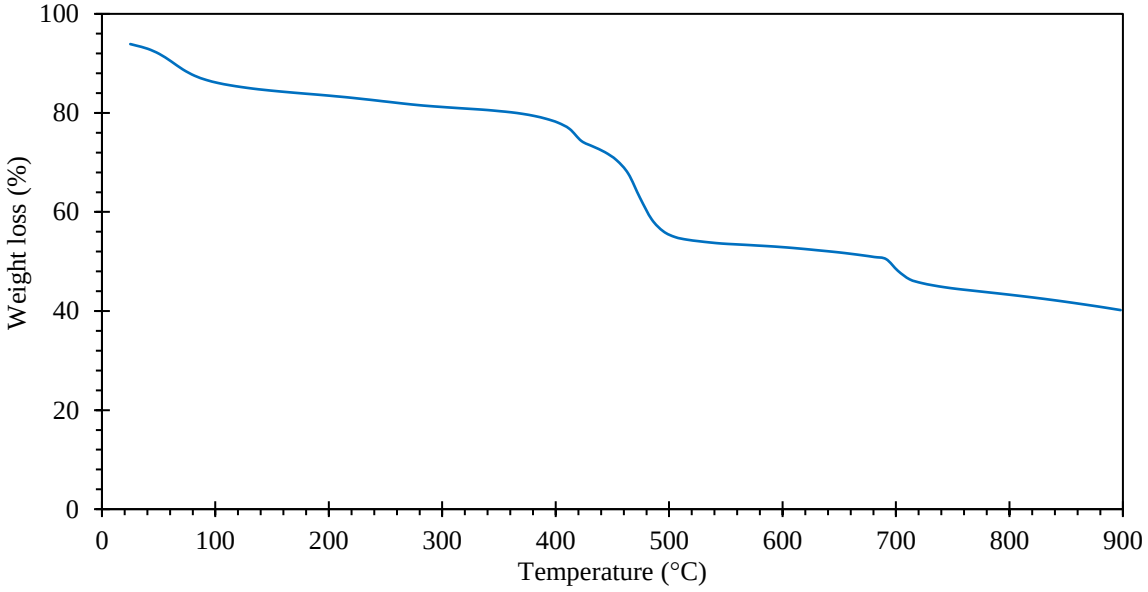

- Figure S11 -

MIL-100(Fe,Zn)

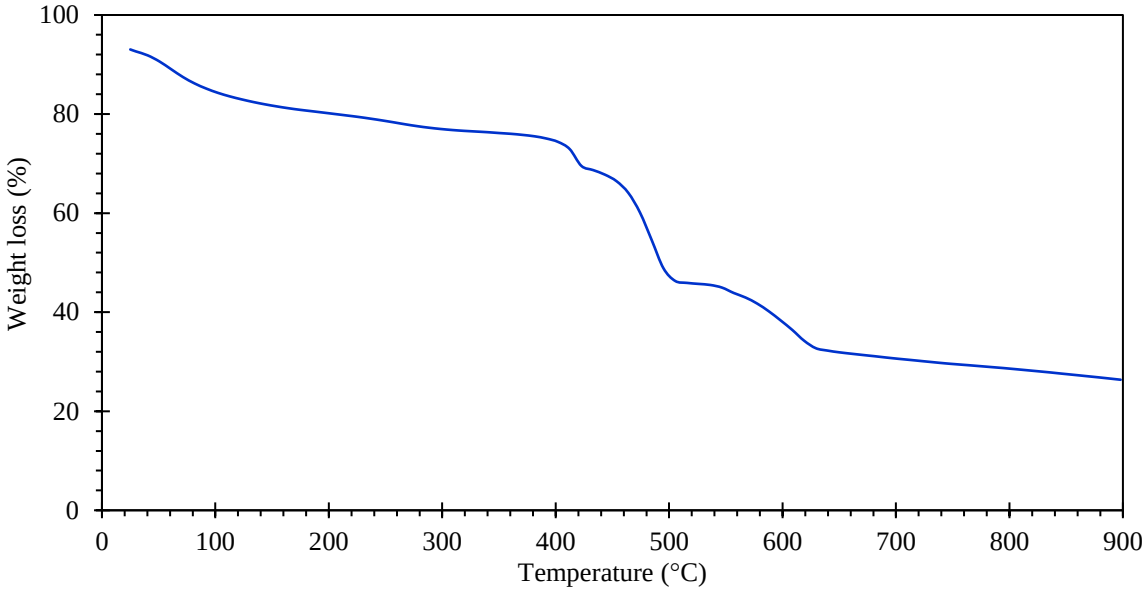

MIL-100(Fe,Y)

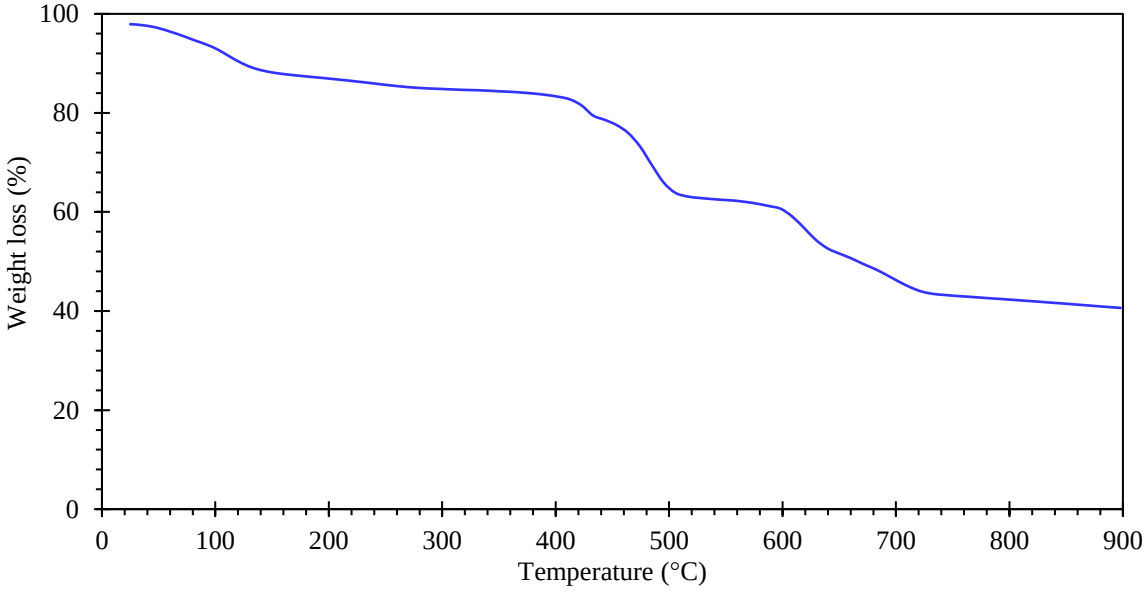

- Figure S11 -

MIL-100(Fe,Cd)

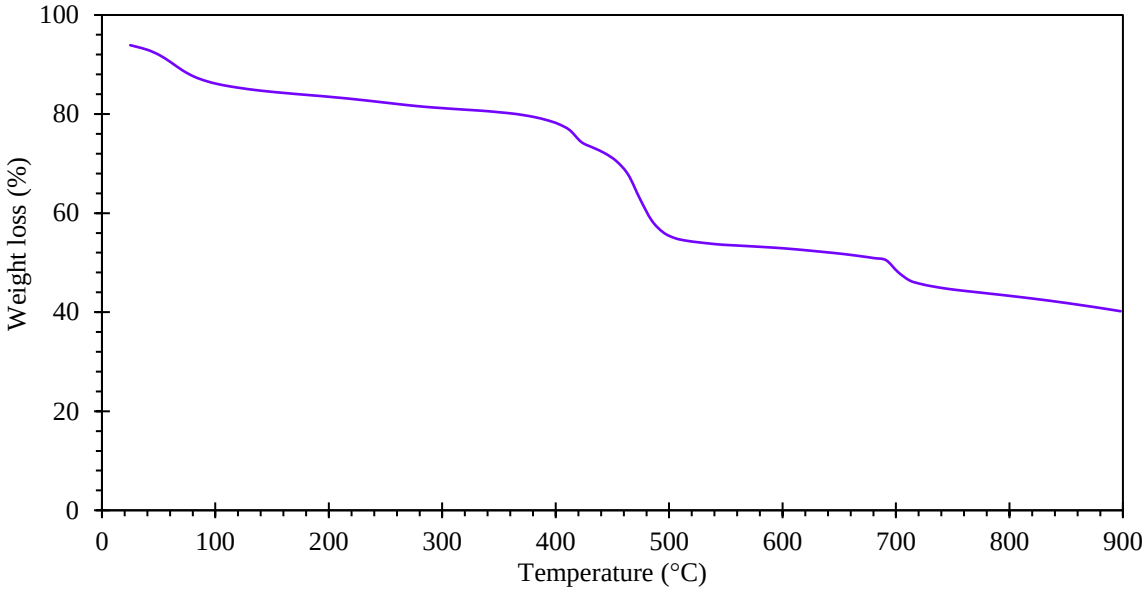

MIL-100(Fe,La)

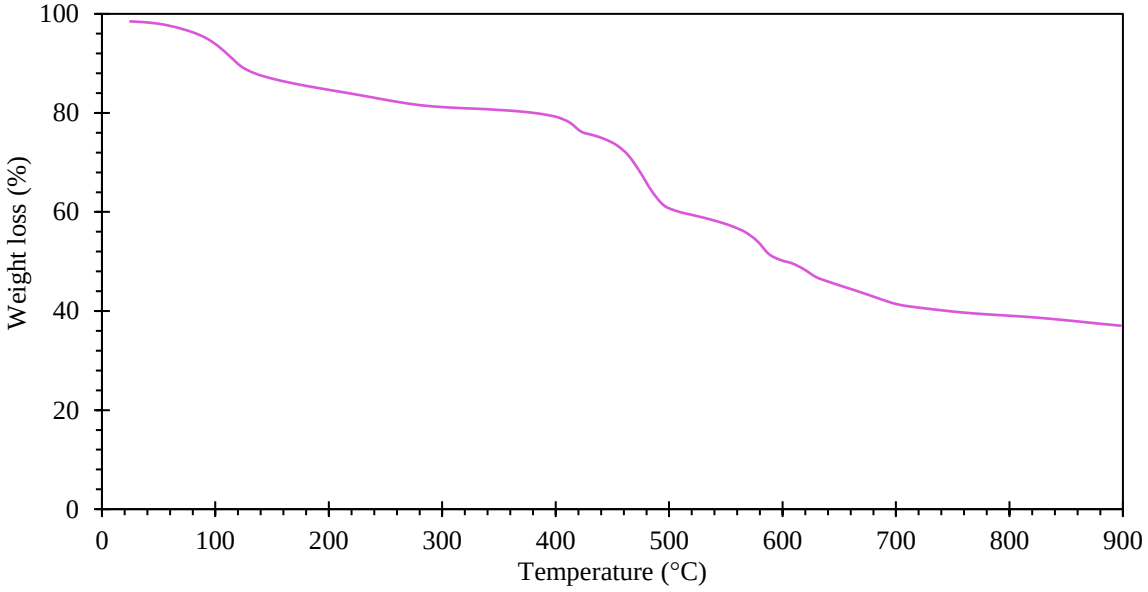

- Figure S11 -

MIL-100(Fe,Ce)

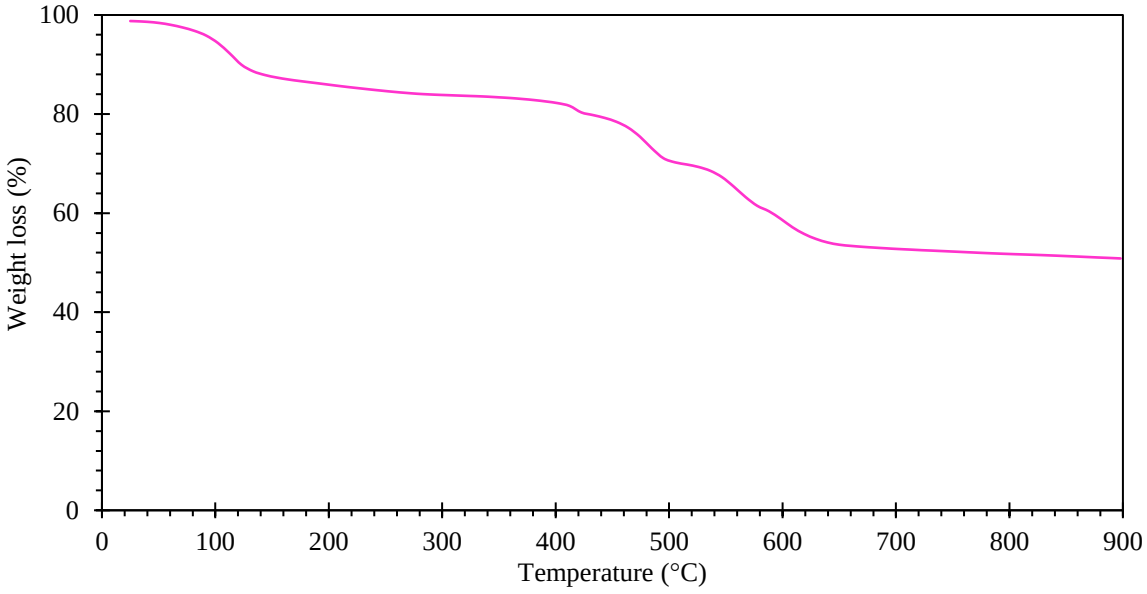

MIL-100(Fe,Pr)

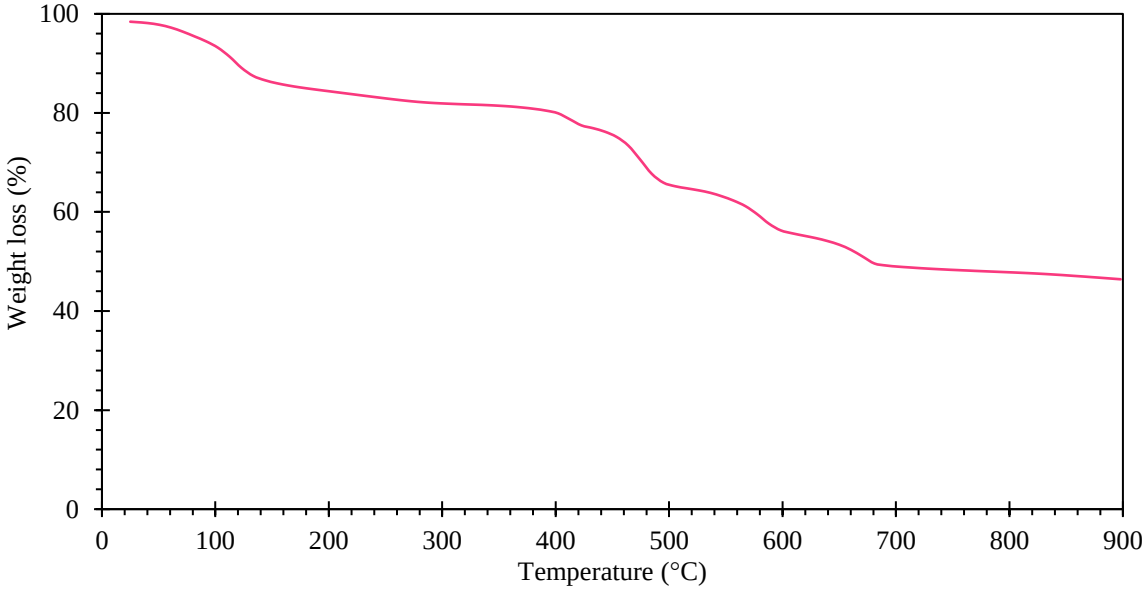

- Figure S11 -

MIL-100(Fe,Sm)

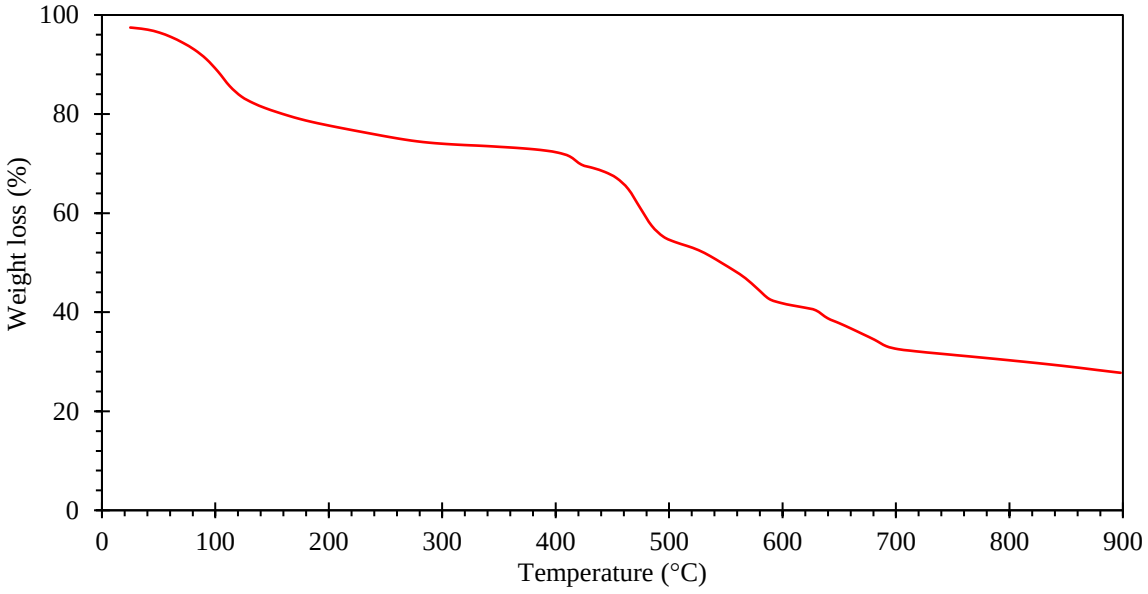

MIL-100(Fe,Tb)

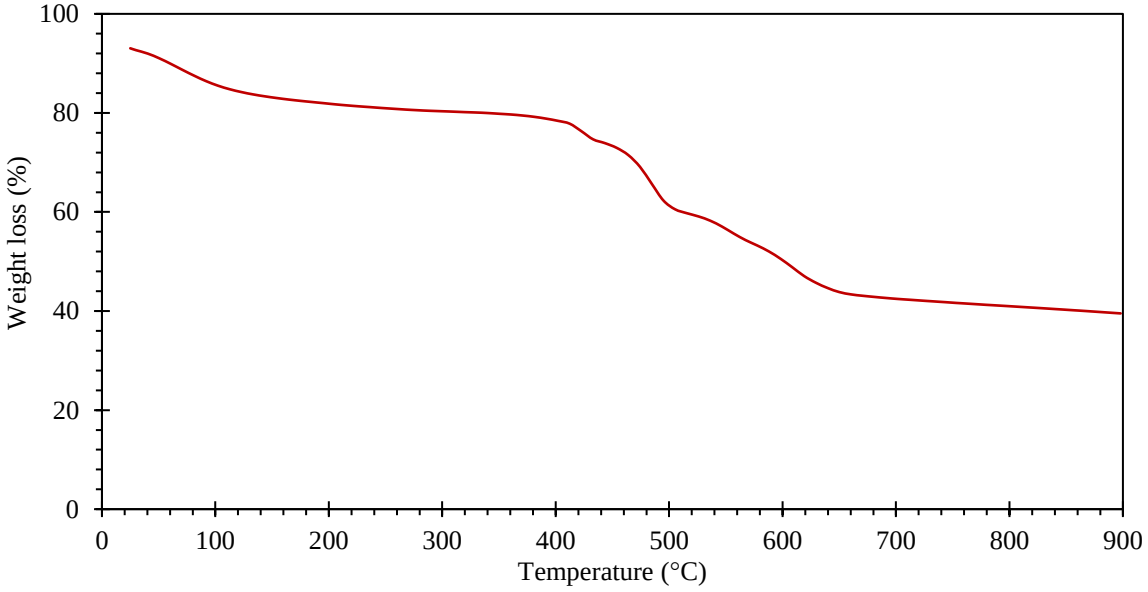

- Figure S11 -

Figure S11 B. TGA plots of the MIL-100(Fe,M) materials under air (first derivatives are indicated in dashed lines).

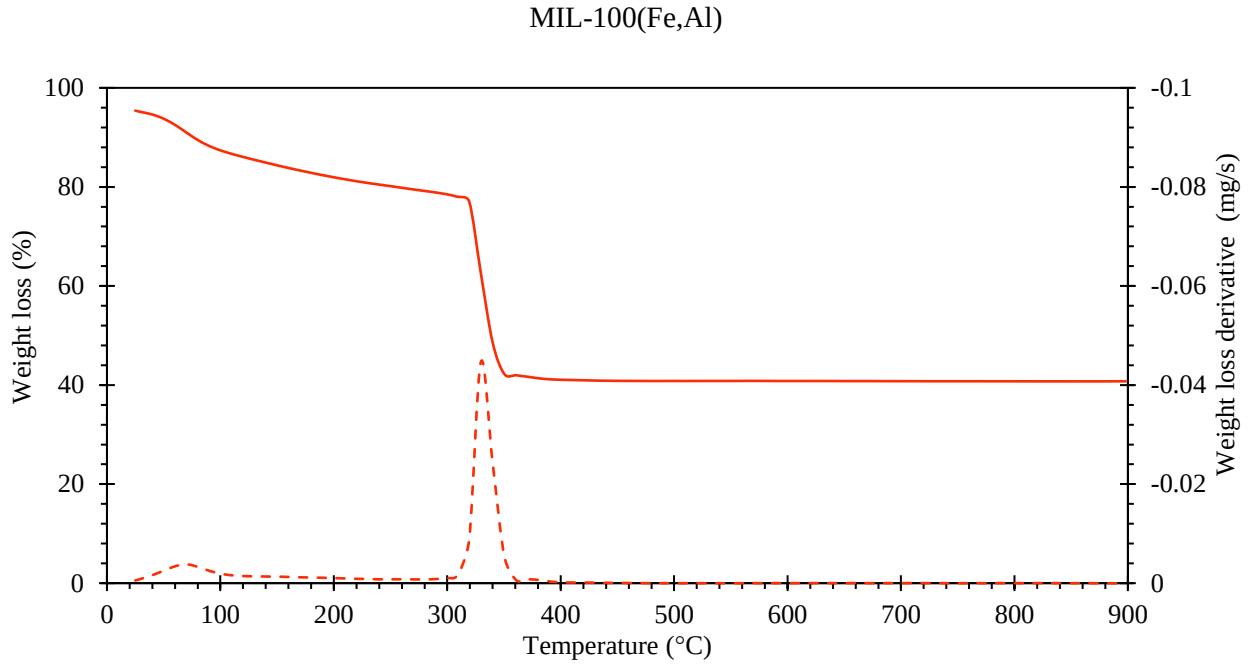

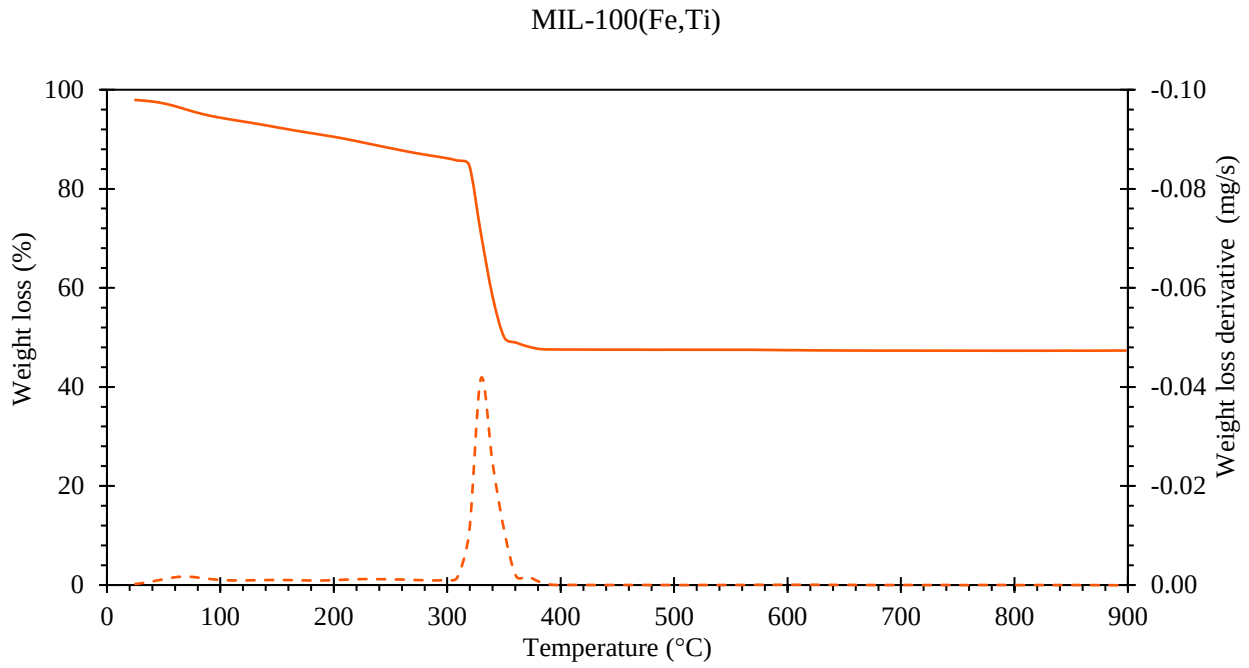

- Figure S11 -

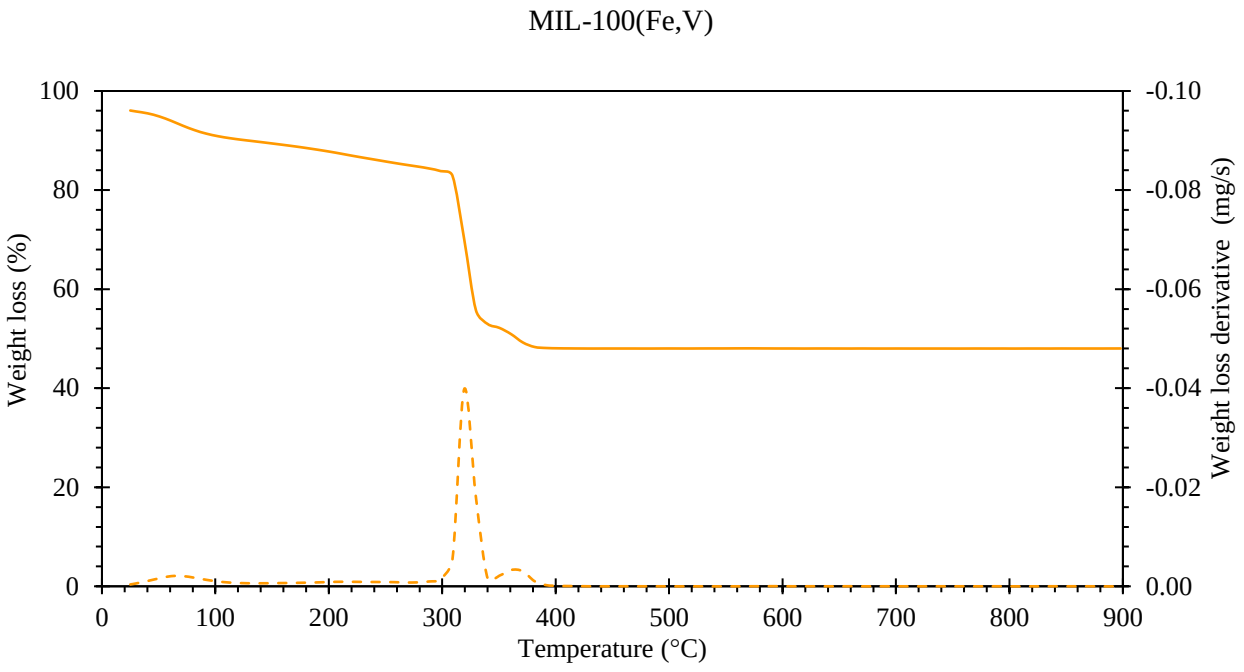
MIL-100(Fe,V)
Weight loss (%)
Weight loss derivative (mg/s)
Temperature (°C)
100
80
60
40
20
0
-0.10
-0.08
-0.06
-0.04
-0.02
0.00
0
100
200
300
400
500
600
700
800
900

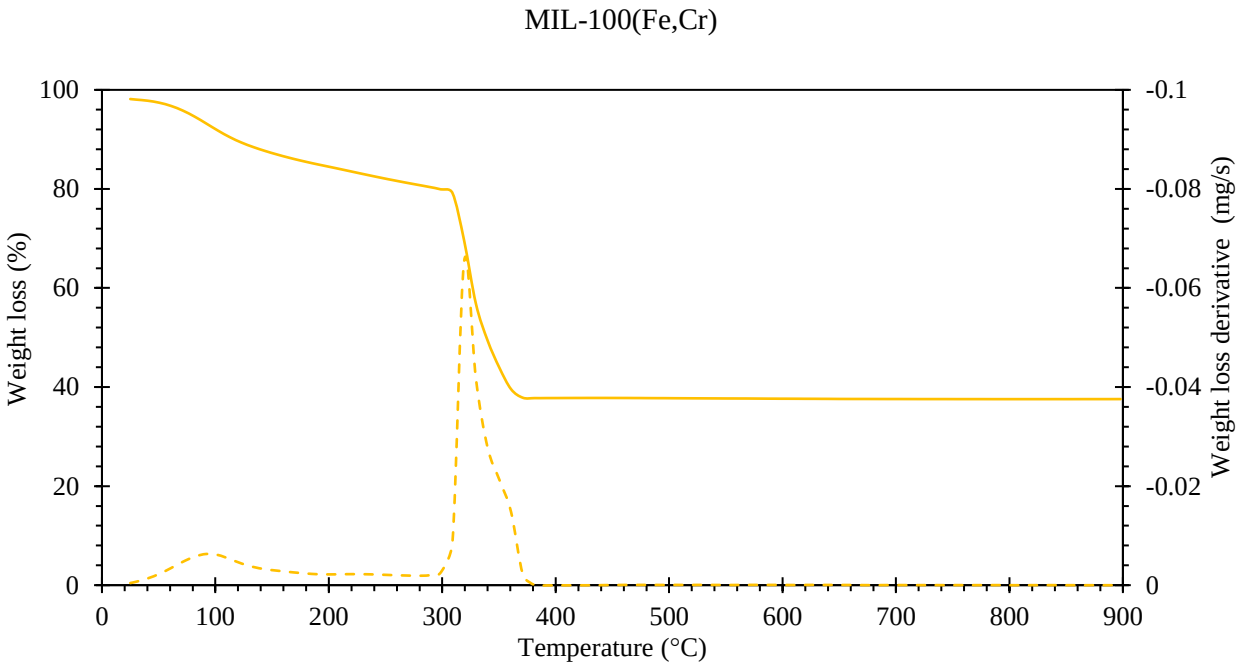
MIL-100(Fe,Cr)
Weight loss (%)
Weight loss derivative (mg/s)
Temperature (°C)
100
80
60
40
20
0
-0.1
-0.08
-0.06
-0.04
-0.02
0
0
100
200
300
400
500
600
700
800
900

- Figure S11 -

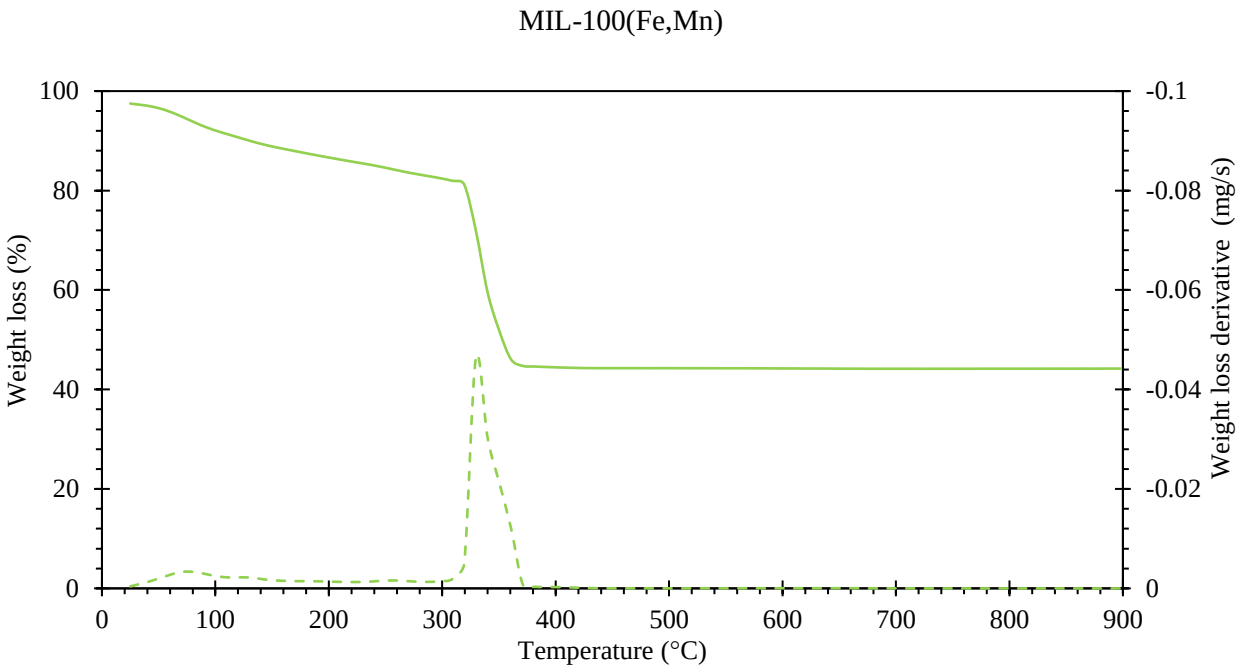
MIL-100(Fe,Mn)
Weight loss (%)
Weight loss derivative (mg/s)
Temperature (°C)
100
80
60
40
20
0
-0.1
-0.08
-0.06
-0.04
-0.02
0
0
100
200
300
400
500
600
700
800
900

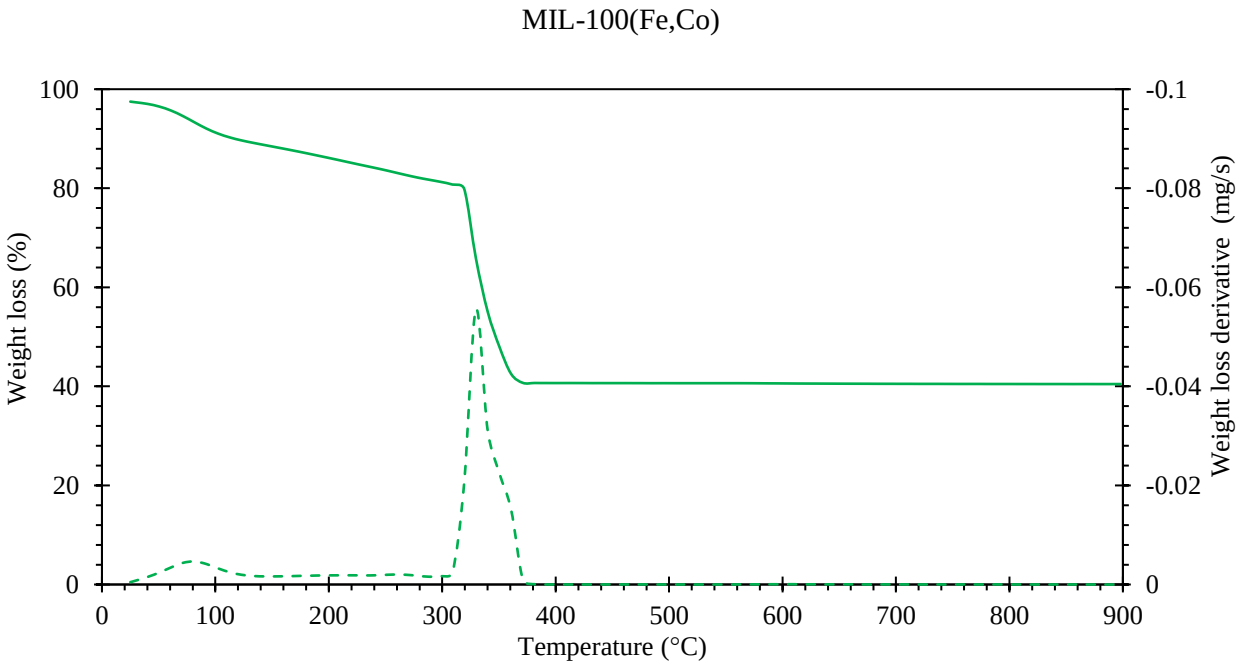
MIL-100(Fe,Co)
Weight loss (%)
Weight loss derivative (mg/s)
Temperature (°C)
100
80
60
40
20
0
-0.1
-0.08
-0.06
-0.04
-0.02
0
0
100
200
300
400
500
600
700
800
900

- Figure S11 -

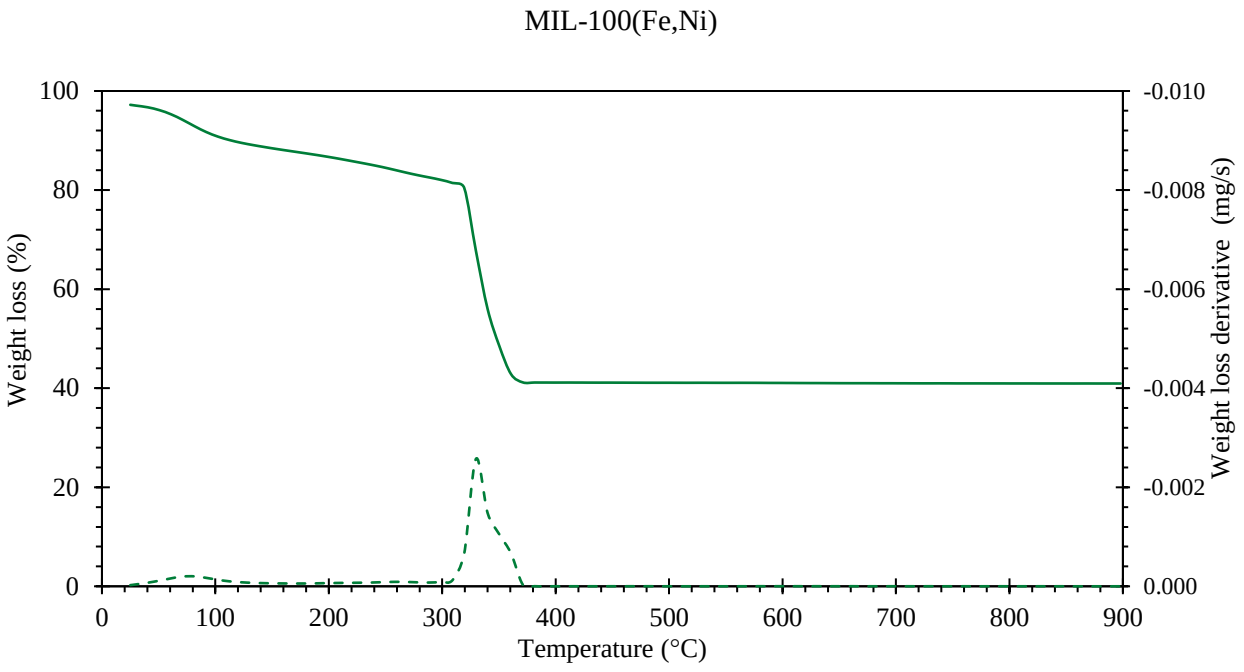
MIL-100(Fe,Ni)
Weight loss (%)
Weight loss derivative (mg/s)
Temperature (°C)
100
80
60
40
20
0
-0.010
-0.008
-0.006
-0.004
-0.002
0.000
0
100
200
300
400
500
600
700
800
900

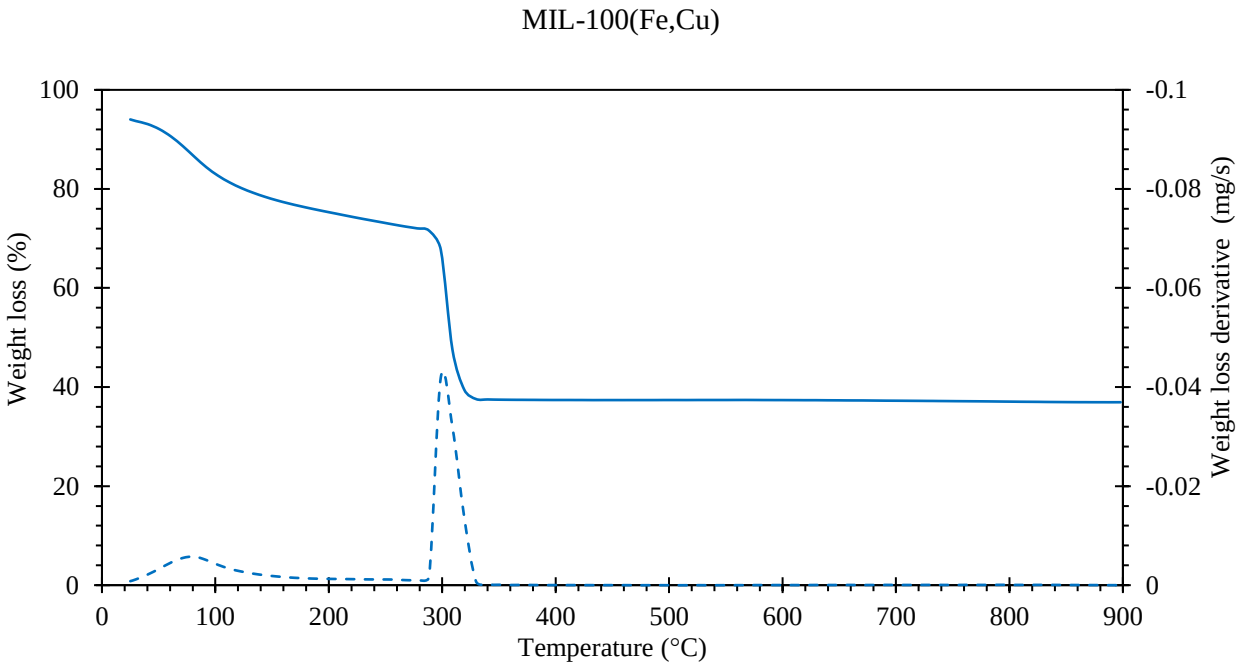
MIL-100(Fe,Cu)
Weight loss (%)
Weight loss derivative (mg/s)
Temperature (°C)
100
80
60
40
20
0
-0.1
-0.08
-0.06
-0.04
-0.02
0
0
100
200
300
400
500
600
700
800
900

- Figure S11 -

MIL-100(Fe,Zn)

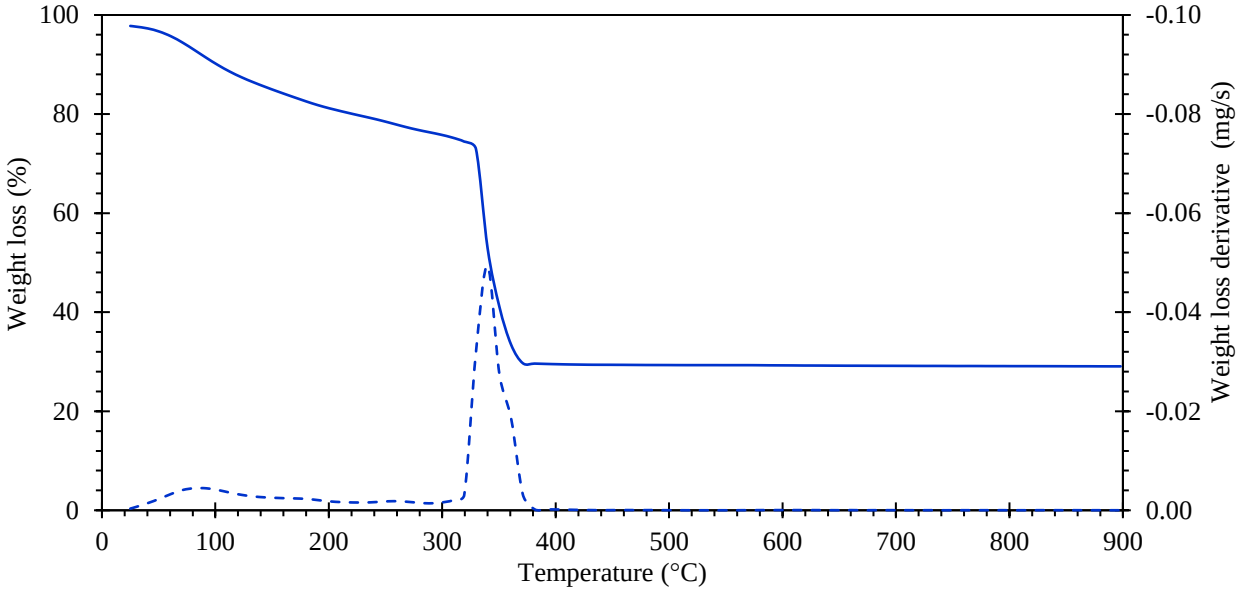

MIL-100(Fe,Y)

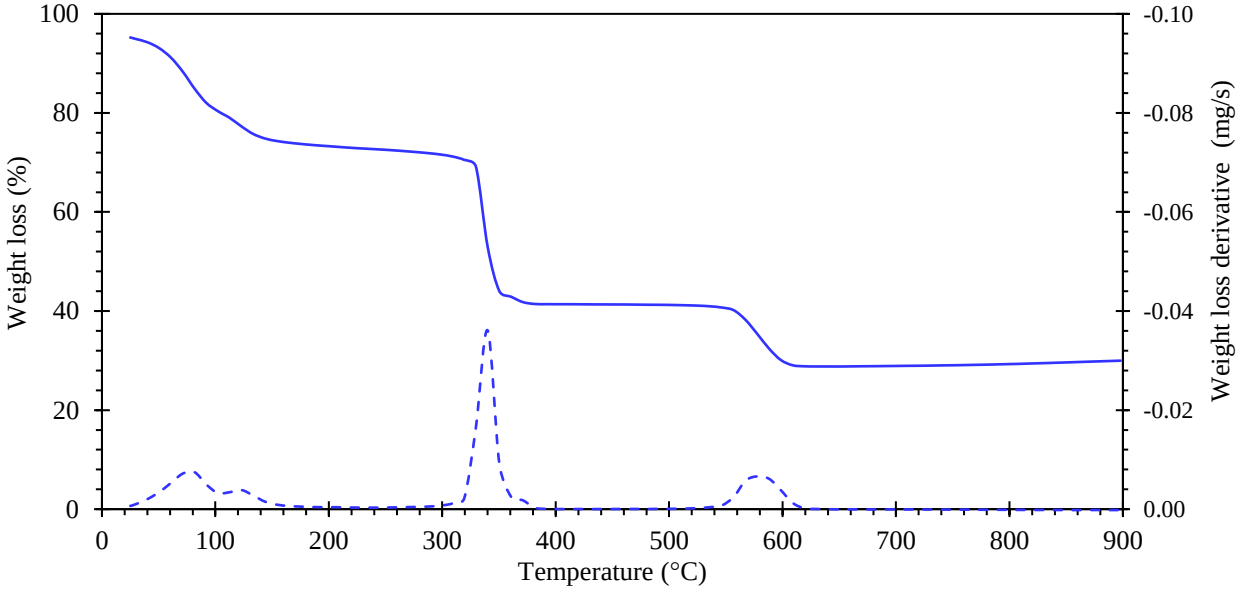

- Figure S11 -

MIL-100(Fe,Cd)

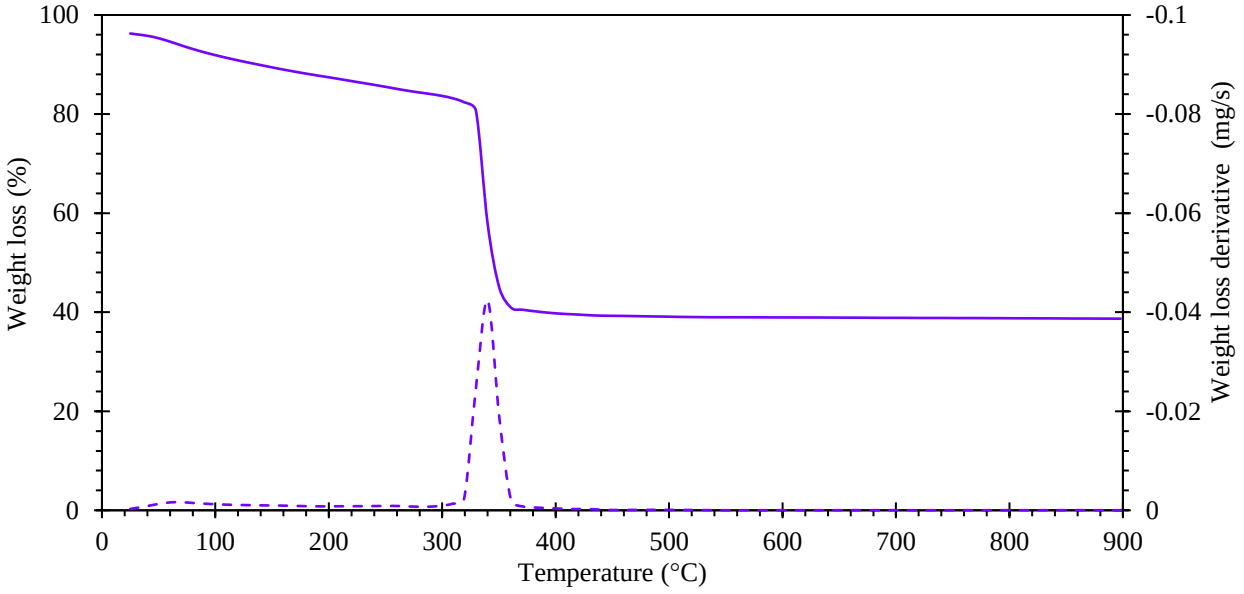

MIL-100(Fe,La)

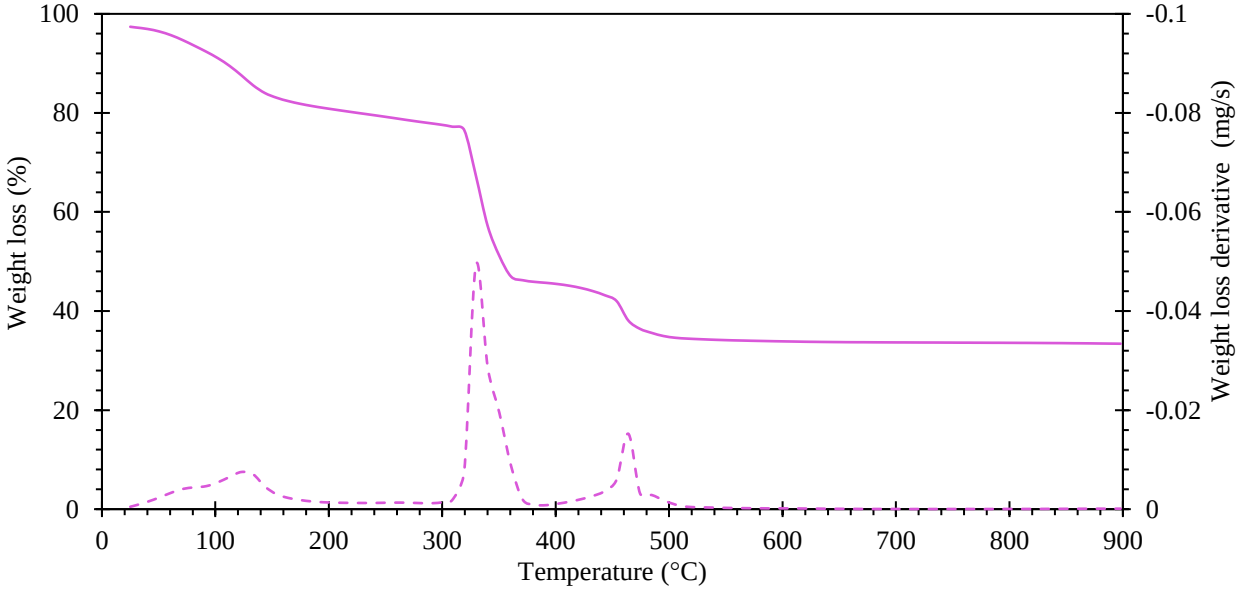

- Figure S11 -

MIL-100(Fe,Ce)

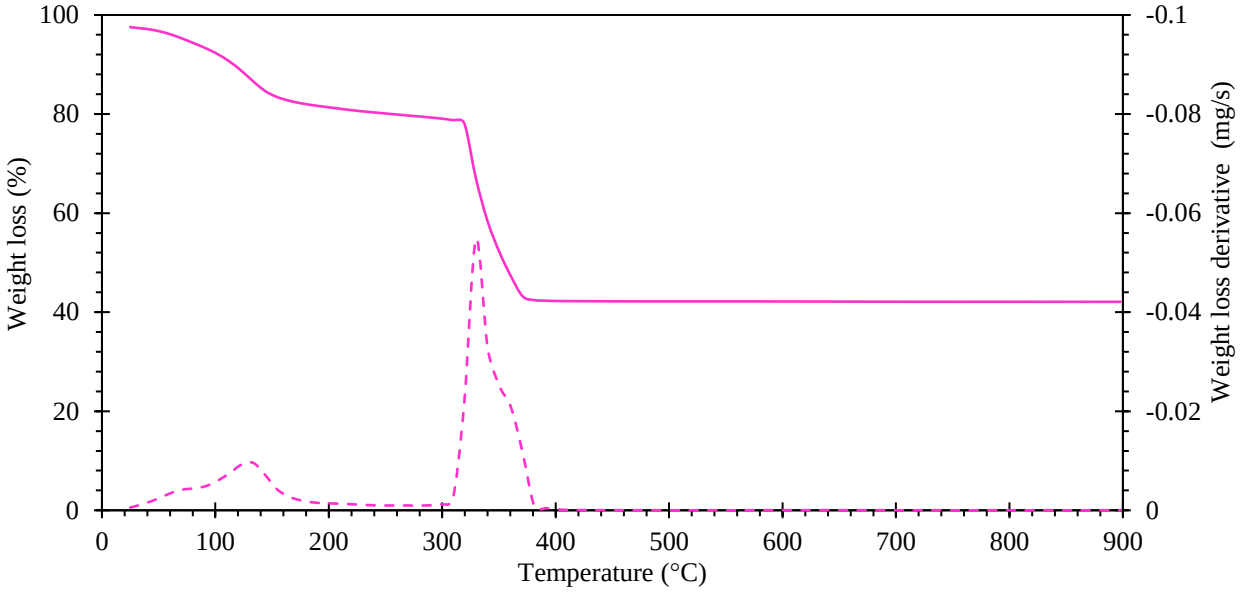

MIL-100(Fe,Pr)

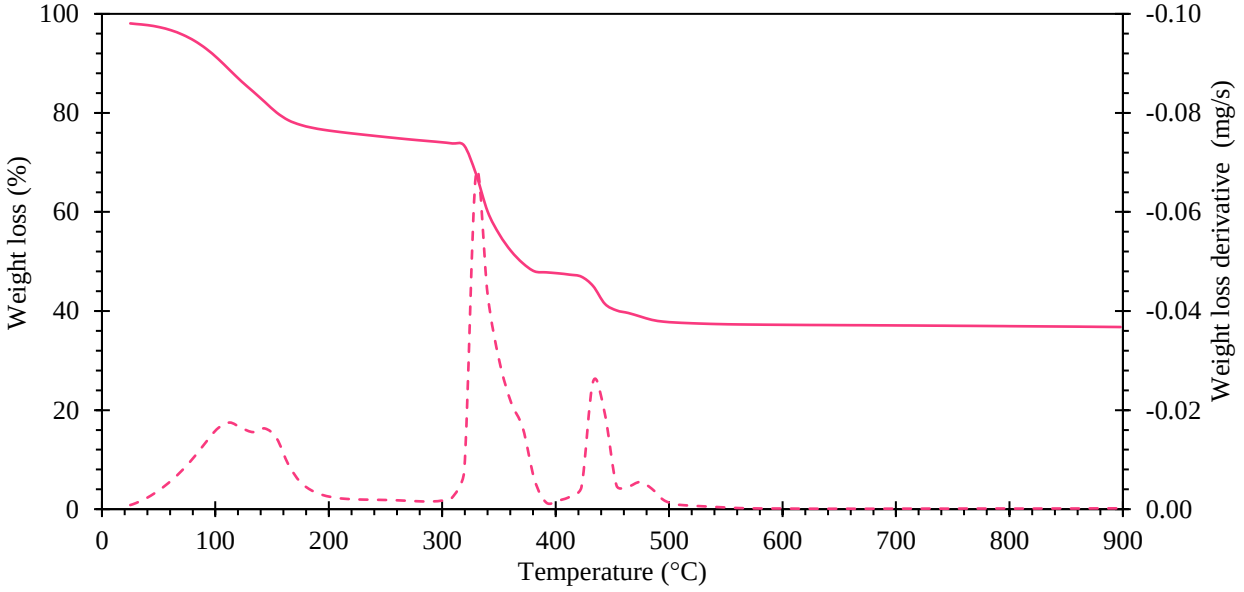

- Figure S11 -

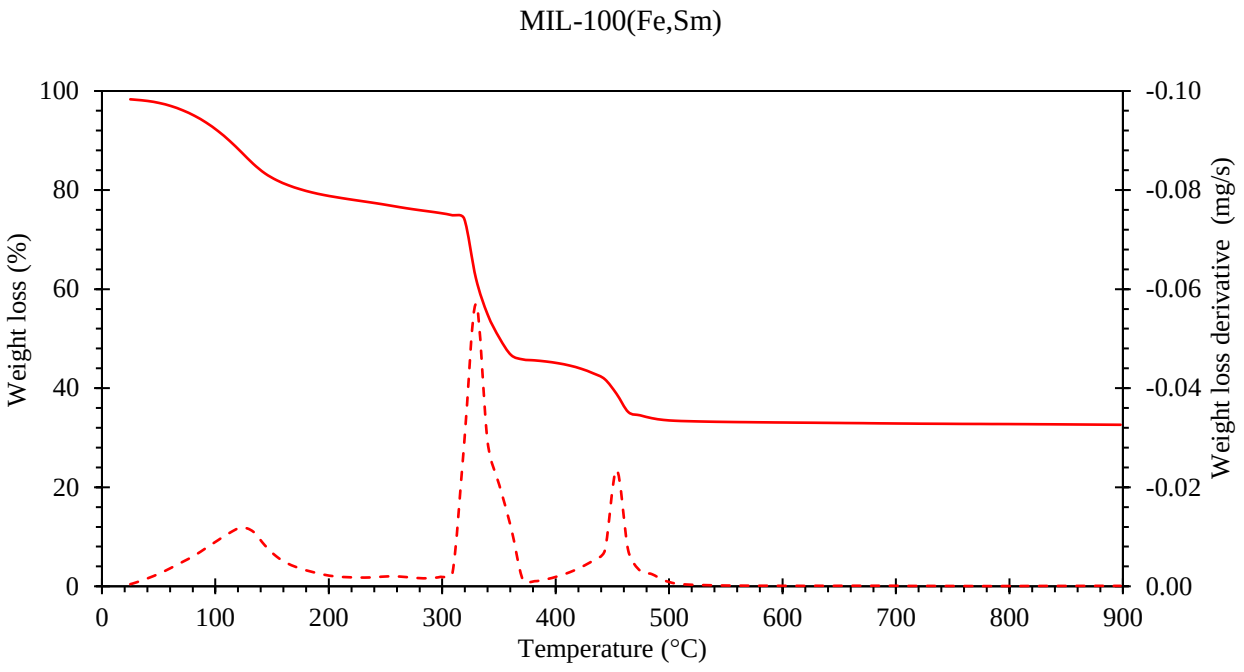
MIL-100(Fe,Sm)
Weight loss (%)
Weight loss derivative (mg/s)
Temperature (°C)
100
80
60
40
20
0
-0.10
-0.08
-0.06
-0.04
-0.02
0.00
0
100
200
300
400
500
600
700
800
900

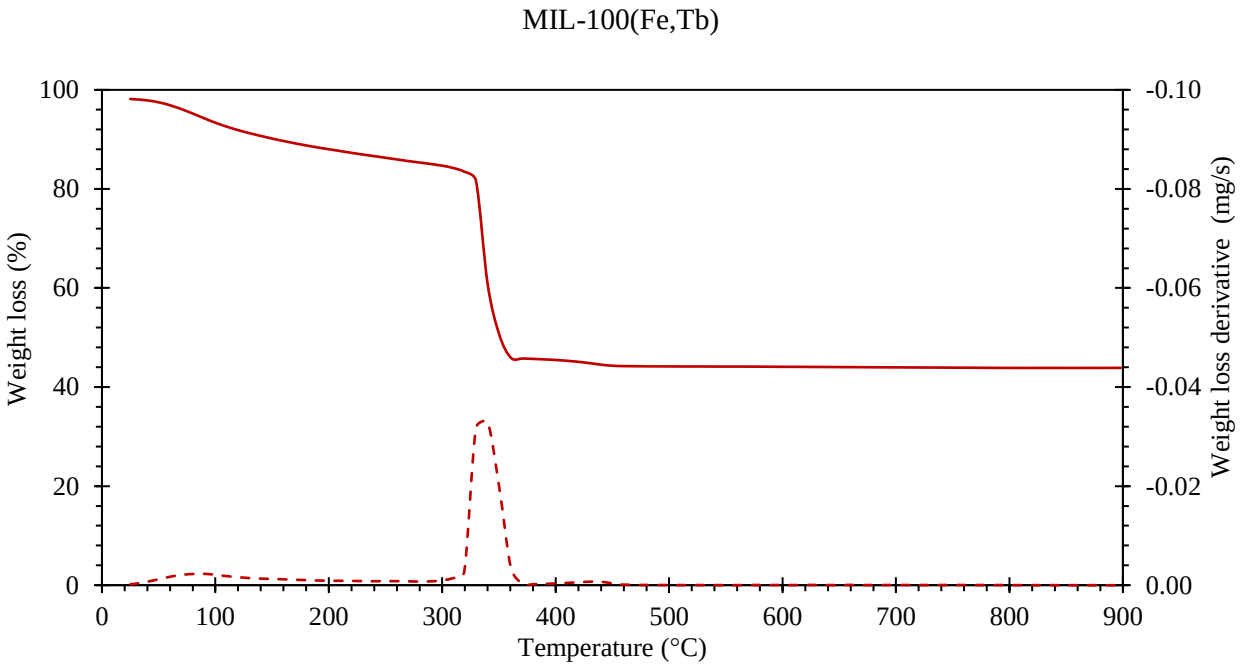
MIL-100(Fe,Tb)
Weight loss (%)
Weight loss derivative (mg/s)
Temperature (°C)
100
80
60
40
20
0
-0.10
-0.08
-0.06
-0.04
-0.02
0.00
0
100
200
300
400
500
600
700
800
900

- Figure S11 -

Figure S12. XPS regions in the energy range of the doping metals for the MIL-100(Fe,M) samples.

MIL-100(Fe,Al)

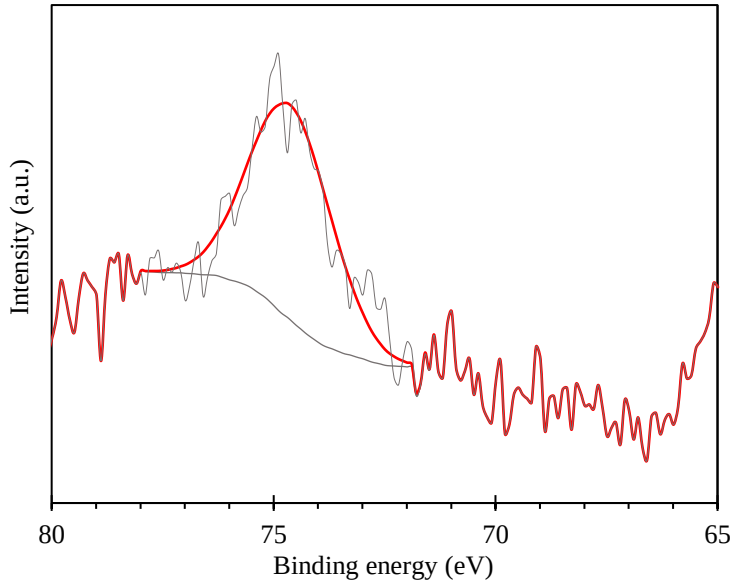

Al2p region of the XPS spectrum

Identified oxidation state:

Al^{3+}

Position of peak:

Al2p: 74.6eV

Note: the position of the peak corresponds to what is expected for Al(III) (Al2p of Al_2O_3 is located at 74.6 eV).[1]

MIL-100(Fe,Ti)

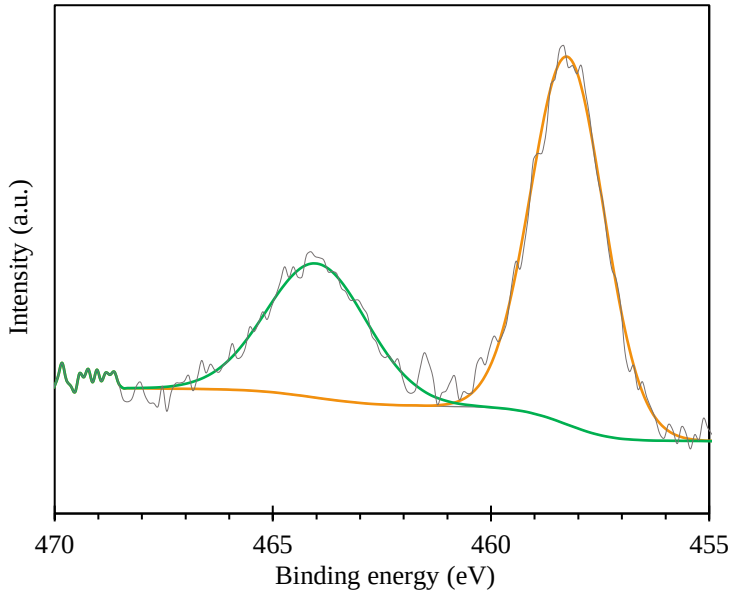

Ti2p region of the XPS spectrum

Identified oxidation state:

Ti^{4+}

Attribution of the deconvolution peaks:

$Ti2p_{3/2}$: 458.3 eV
$Ti2p_{1/2}$: 464.0 eV

Note: the position of the $Ti2p_{3/2}$ is close to what is expected for TiO_2 (458.5 eV),[2] suggesting that Ti is in the +IV oxidation state. ΔE is equal to 5.7 eV, which is the value expected for Ti(IV) species like TiO_2.[3]

[1] https://xpssimplified.com/elements/aluminum.php
[2] https://xpssimplified.com/elements/titanium.php
[3] http://www.xpsfitting.com/search/label/Titanium

MIL-100(Fe,V)

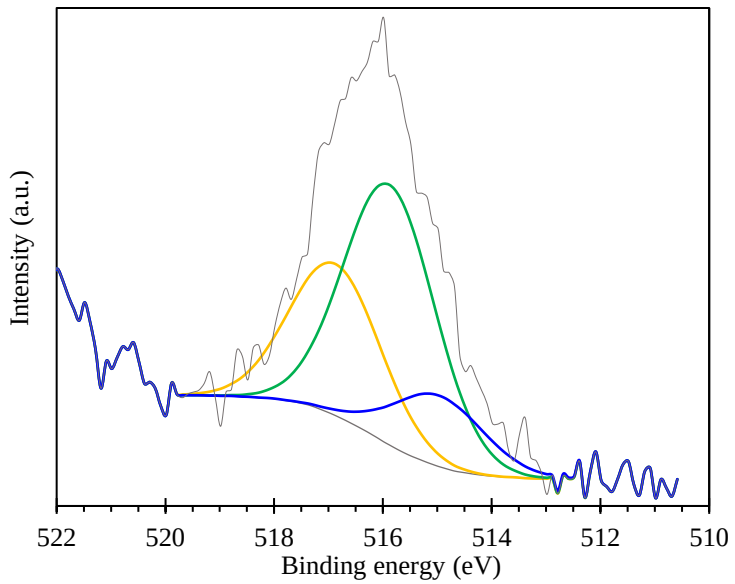

V2p region of the XPS spectrum

Identified oxidation states:

V^{5+}, V^{4+} and V^{3+}

Attribution of the deconvolution peaks:

V(V): 516.9 eV
V(IV): 515.9 eV
V(III): 515.0 eV

Note: the deconvolution of the peaks was realized according to an oxide model.[4]

MIL-100(Fe,Cr)

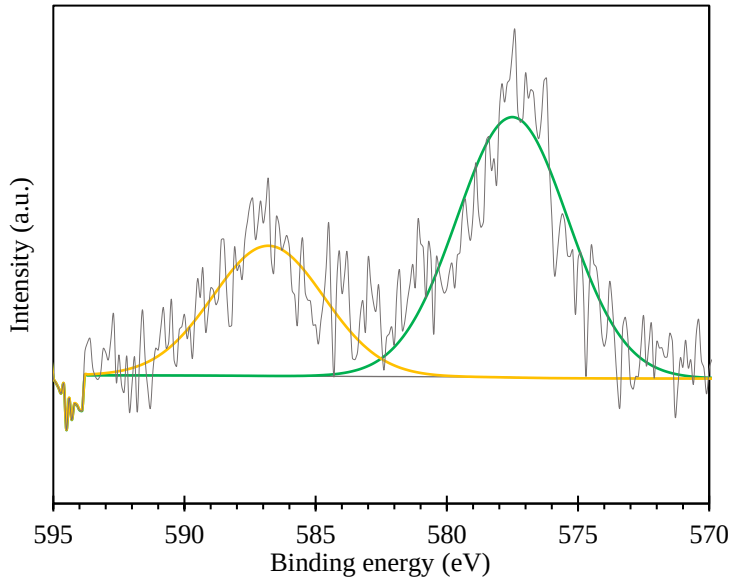

Cr2p region of the XPS spectrum

Identified oxidation state:

Cr^{3+}

Attribution of the deconvolution peaks:

$Cr2p_{3/2}$: 577.5 eV
$Cr2p_{1/2}$: 586.8 eV

The binding energy of the main peak (577.8 eV) corresponds to what is expected for Cr(III) species like Cr_2O_3 (576 eV)[5] or $Cr(OH)_3$ (577.3 eV).[6]

[4] http://www.xpsfitting.com/2008/09/vanadium.html
[5] https://xpssimplified.com/elements/chromium.php
[6] http://www.xpsfitting.com/search/label/Chromium

- Figure S12 -

MIL-100(Fe,Mn)

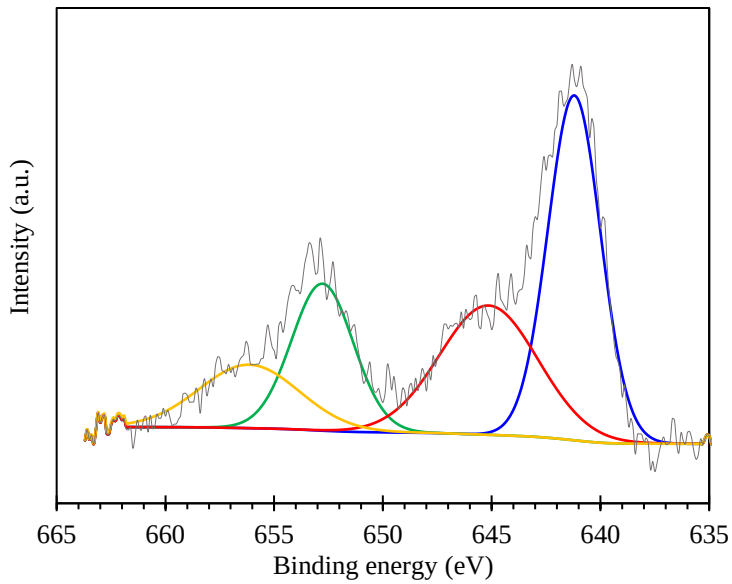

Mn2p region of the XPS spectrum

Identified oxidation states:

Mn^{2+}, impossible to exclude the presence of Mn^{3+} and/or Mn^{4+} by the measurement of Mn2p region only.

Attribution of the deconvolution peaks:

$Mn2p_{3/2}$: 641.2 eV
$Mn2p_{3/2}$ sat.: 645.1 eV
$Mn2p_{1/2}$: 652.8 eV
$Mn2p_{1/2}$ sat.: 656.2 eV

The presence of Mn^{2+} is deduced from the satellite peaks, which are present in MnO but not for either Mn_2O_3 or MnO_2.[7]

MIL-100(Fe,Co)

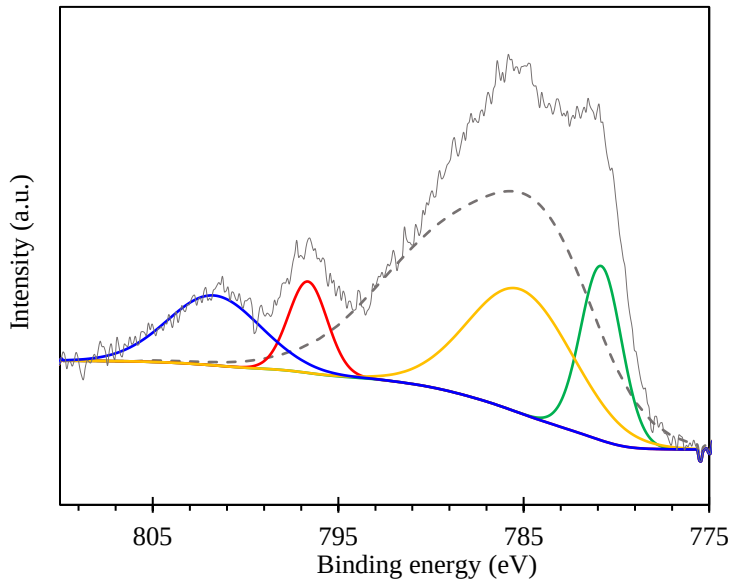

Co2p region of the XPS spectrum

Identified oxidation state:

Co^{2+}

Dashed curve: Fe auger

Attribution of the deconvolution peaks:

$Co2p_{3/2}$: 780.8 eV
$Co2p_{3/2}$ sat.: 785.2 eV
$Co2p_{1/2}$: 796.6 eV
$Co2p_{1/2}$ sat.: 801.7 eV

The binding energy of the $Co2p_{3/2}$ peak (780.8 eV) resembles that of CoO (780.0 eV) and $Co(OH)_2$ (780.4 eV). Furthermore, the presence of strong satellite peaks also matches what is observed for Co(II) species.[8]

[7] https://xpssimplified.com/elements/manganese.php
[8] http://www.xpsfitting.com/search/label/Cobalt

- Figure S12 -

MIL-100(Fe,Ni)

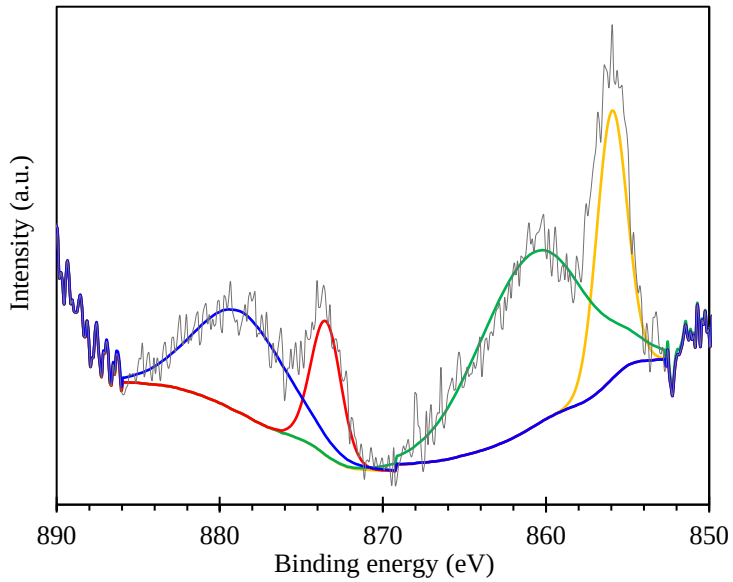

Ni2p region of the XPS spectrum

Identified oxidation state:

Ni^{2+}

Attribution of the deconvolution peaks:

$Ni2p_{3/2}$: 856.0 eV
$Ni2p_{3/2}$ sat.: 860.8 eV
$Ni2p_{1/2}$: 873.5 eV
$Ni2p_{1/2}$ sat.: 878.7 eV

Note: the shape of the main and satellite peaks of the spectrum resembles that of $Ni(OH)_2$, from which is was deduced that Ni is present in the +II oxidation state in the MOF. The binding energy of the $Ni2p_{3/2}$ peak (856.0 eV) also matches the one expected for Ni(II) in $Ni(OH)_2$ (855.6 eV).[9]

MIL-100(Fe,Cu)

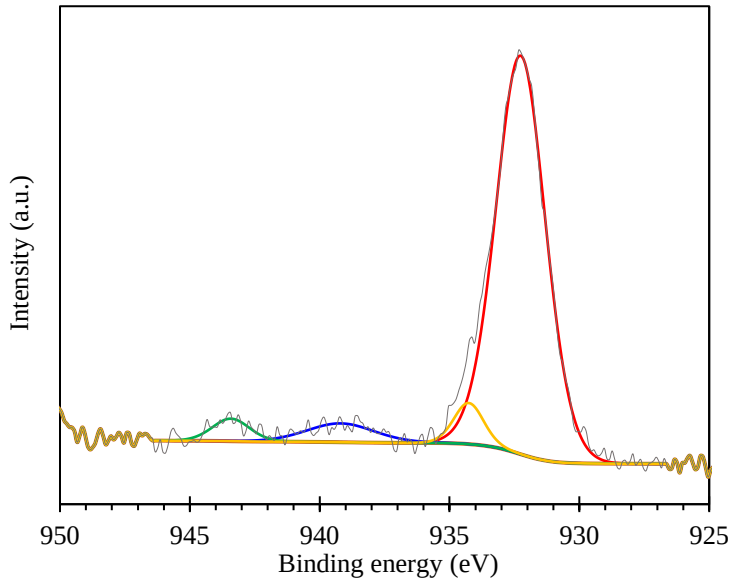

Cu2p region of the XPS spectrum

Identified oxidation state:

Mainly Cu^{+}, traces of Cu^{2+}

Attribution of the deconvolution peaks:

$Cu(I)2p_{3/2}$ sat.: 932.3 eV
$Cu(II)2p_{3/2}$: 934.3 eV
$Cu(II)2p_{3/2}$ sat.: 939.2 eV
$Cu(II)2p_{3/2}$ sat.: 943.4 eV

Note : the observed $Cu2p_{3/2}$ satellite peaks were attributed to traces of Cu^{2+}, as Cu(II) species feature important $Cu2p_{3/2}$ satellites. However, Cu(I) species also feature small $Cu2p_{3/2}$ satellites at similar binding energies.[10,11]

[9] https://xpssimplified.com/elements/nickel.php
[10] http://www.xpsfitting.com/search/label/Copper
[11] https://xpssimplified.com/elements/copper.php

- Figure S12 -

MIL-100(Fe,Zn)

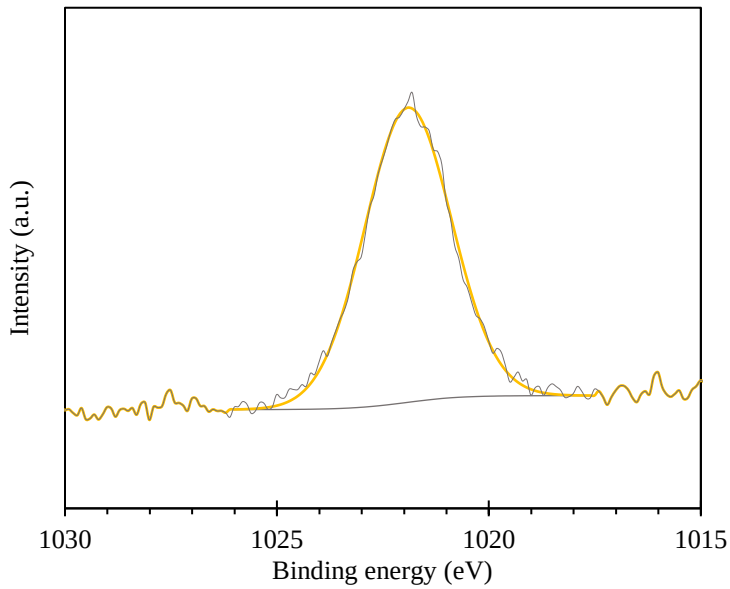

Zn2p region of the XPS spectrum

Identified oxidation state:

Zn^{2+}

Position of the peak:

Zn2p: 1021.9 eV

Note: Zn^{2+} can be difficult to distinguish from metallic Zn, however it is highly unlikely that Zn is reduced in the MOF.[12,13]

MIL-100(Fe,Y)

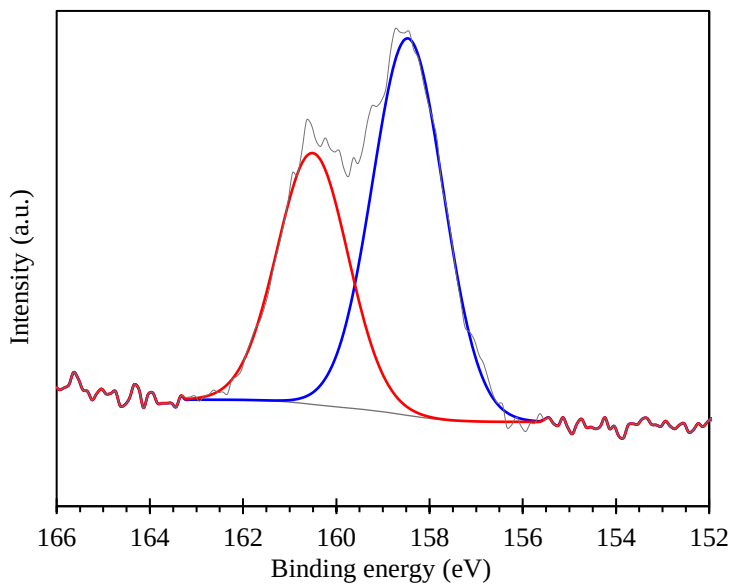

Y3d region of the XPS spectrum

Identified oxidation state:

Y^{3+}

Attribution of the deconvolution peaks:

$Y3d_{5/2}$: 158.5 eV
$Y3d_{3/2}$: 160.5 eV

Note: The chemical shift of the $Y3d_{5/2}$ component is significantly different from that of the metallic state (165 eV), the oxide (156.4 eV) and even from the carbonate (157.7 eV).[14]

[12] http://www.xpsfitting.com/search/label/Zinc
[13] https://xpssimplified.com/elements/zinc.php
[14] https://xpssimplified.com/elements/yttrium.php

- Figure S12 -

MIL-100(Fe,Cd)

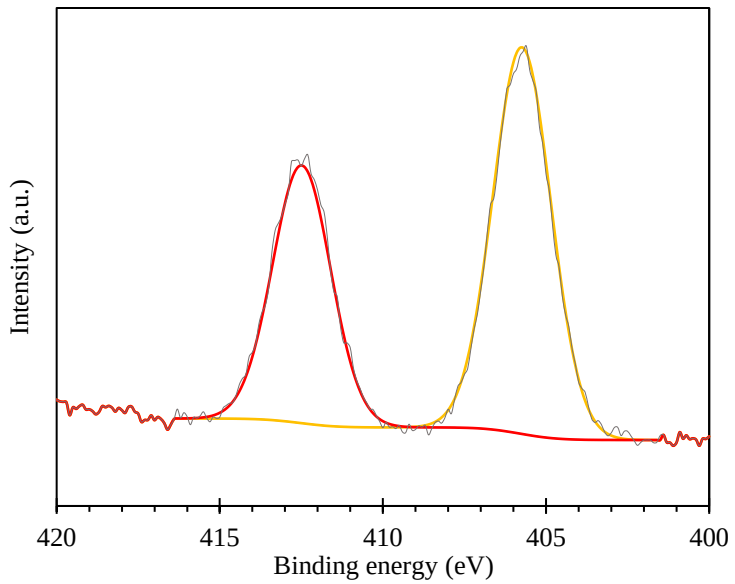

Cd3d region of the XPS spectrum

Identified oxidation state:

Cd^{2+}

Attribution of the deconvolution peaks:

$Cd3d_{3/2}$: 405.7 eV
$Cd3d_{1/2}$: 412.5 eV

Note:

The binding energy of the $Cd3d_{3/2}$ peak (405.7 eV) matches well that of CdO (404.6 ± 1.1 eV).[15]

MIL-100(Fe,La)

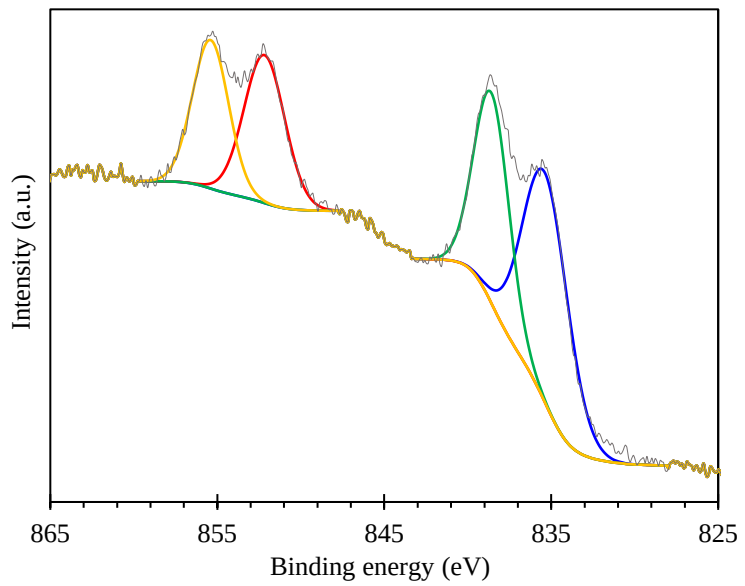

La3d region of the XPS spectrum

Identified oxidation state:

La^{3+}

Attribution of the deconvolution peaks:

$La3d_{5/2}$: 835.4 eV
$La3d_{5/2}$: 838.6 eV
$La3d_{3/2}$: 852.2 eV
$La3d_{3/2}$: 855.4 eV

Note:

The ΔE value between the $La3d_{5/2}$ multiplets = 3.2 eV. This value is close to the one expected for carbonate-like species [ΔE = 4.6 eV for La_2O_3, 3.9 eV for $La(OH)_3$ and 3.5 eV for $La_2(CO_3)_3$].[16]

[15] http://www.xpsfitting.com/search/label/Cadmium
[16] https://xpssimplified.com/elements/lanthanum.php

- Figure S12 -

MIL-100(Fe,Ce)

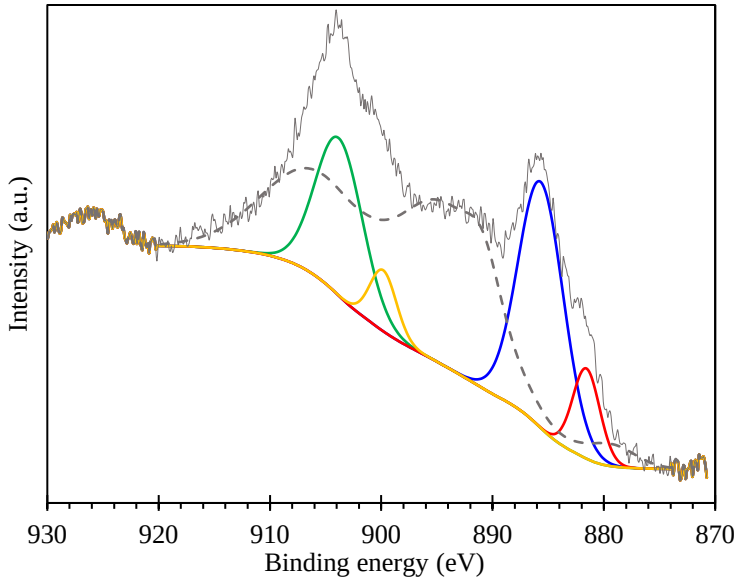

Ce3d region of the XPS spectrum

Identified oxidation states:

Ce^{3+}, Ce^{4+}

Dashed curve: Fe auger
(the shape of the Auger peak was taken from the XPS spectra of pure, undoped MIL-100(Fe))

Attribution of the deconvolution peaks:[17]

Ce(IV)$3d_{5/2}$: 881.6 eV
Ce(III)$3d_{5/2}$: 885.7 eV
Ce(IV)$3d_{3/2}$: 899.8 eV
Ce(III)$3d_{3/2}$: 903.8 eV

MIL-100(Fe,Pr)

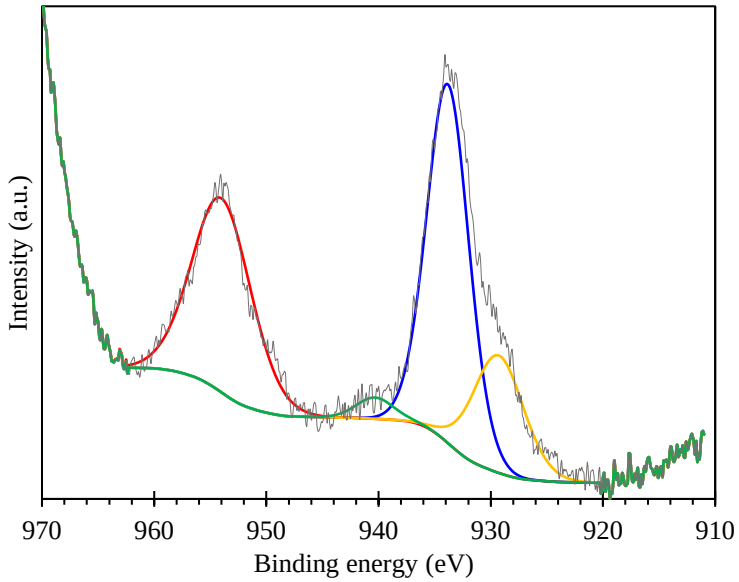

Pr3d region of the XPS spectrum

Identified oxidation state:

Pr^{3+}

Attribution of the deconvolution peaks:

Pr$3d_{5/2}$: 929.3 eV
Pr$3d_{5/2}$: 933.8 eV
Pr$3d_{3/2}$: 940.3 eV
Pr$3d_{3/2}$: 954.0 eV

Note:

Peaks characteristic of Pr(IV) close to 966 and 946eV are not found in the spectrum, which indicates that Pr(IV) is not present at the surface of the sample. Peaks characteristic of Pr(III) are usually found at binding energies of 933-934 eV, 953-954 eV and 929 eV, which is the case in the measured spectrum.[18]

[17] I. I. Udoh, H. Shi, F. Liu, E.-H. Han, *J. Electrochem. Soc.*, 166 (6), C185-C195, **2019**.
[18] E. Poggio-Fraccari, G. Baronetti, F. Mariño, *J. Electron. Spectrosc.*, 222, 1-4, **2018**.

- Figure S12 -

MIL-100(Fe,Sm)

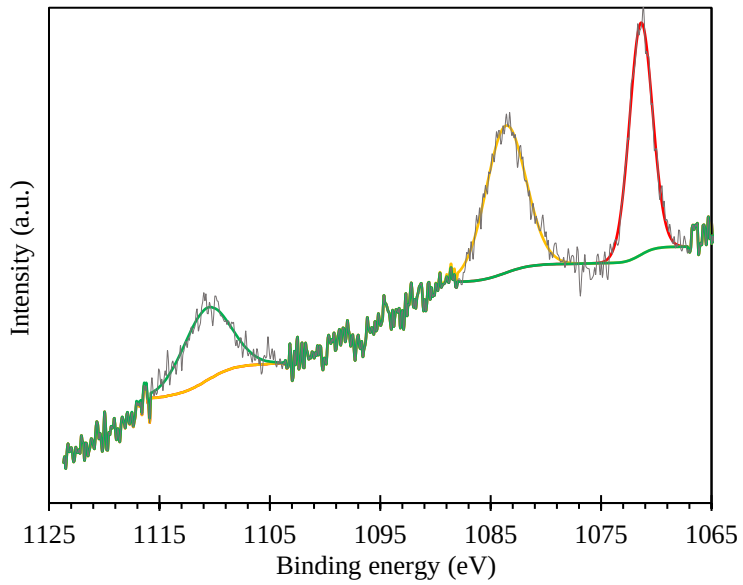

Sm3d region of the XPS spectrum

Identified oxidation state:

Sm^{3+}

Red curve: Na1s (1071.4 eV)

Attribution of the deconvolution peaks:

$Sm3d_{5/2}$: 1083.6 eV
$Sm3d_{3/2}$: 1110.8 eV

Note: Sm(II), if present, would show a component near 1100 eV. As no such peak is observed, it was concluded that Sm(II) is not present on the surface of the sample.[19]

MIL-100(Fe,Tb)

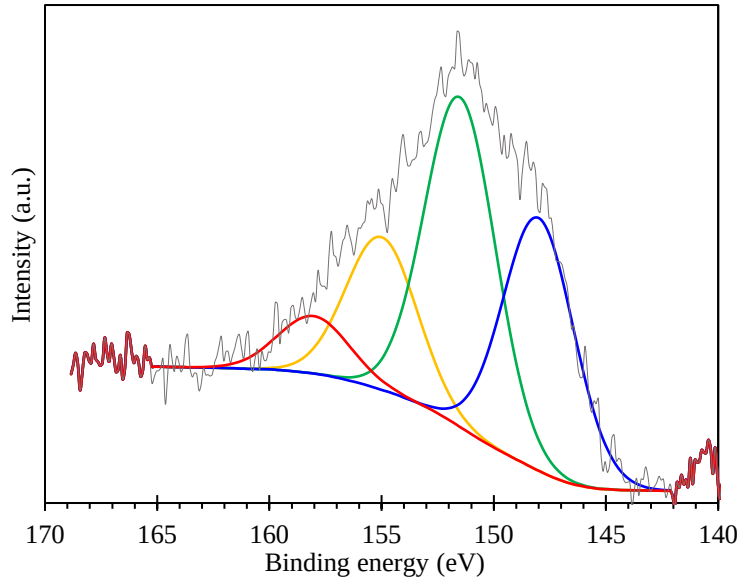

Tb4d region of the XPS spectrum

Identified oxidation state:

Tb^{3+}

Note: The components of the spectrum resemble that of Tb_2O_3,[20] however, they are shifted about 2 to 3 eV towards higher binding energies. Such shifted binding energies are similar to what is observed when comparing the Y3d region of Y_2O_3 and MIL-100(Fe,Y).

Binding energies:

148.0 eV, blue (146.0 eV for Tb_2O_3)
151.5 eV, green (148.6 eV for Tb_2O_3)
155.0 eV, yellow (151.6 eV for Tb_2O_3)
158.0 eV, red (155.3 eV for Tb_2O_3)

[19] A. Reisner, D. Kasinathan, S. Wirth, L. H. Tjeng, S. G. Altendorf, *EPL (Europhysics Letters)*, 117, 4, 1-6, **2017**.
[20] S.V. Belaya, V.V. Bakovets, A.I. Boronin, S.V. Koshcheev, M.N. Lobzareva, I.V. Korolkov, P.A. Stabnikov, *Inorg. Mater.*, 50 (4), 410-417, **2014**.

- Figure S12 -

Figure S13 A. PXRD patterns of the calcined MIL-100(Fe,M) samples.

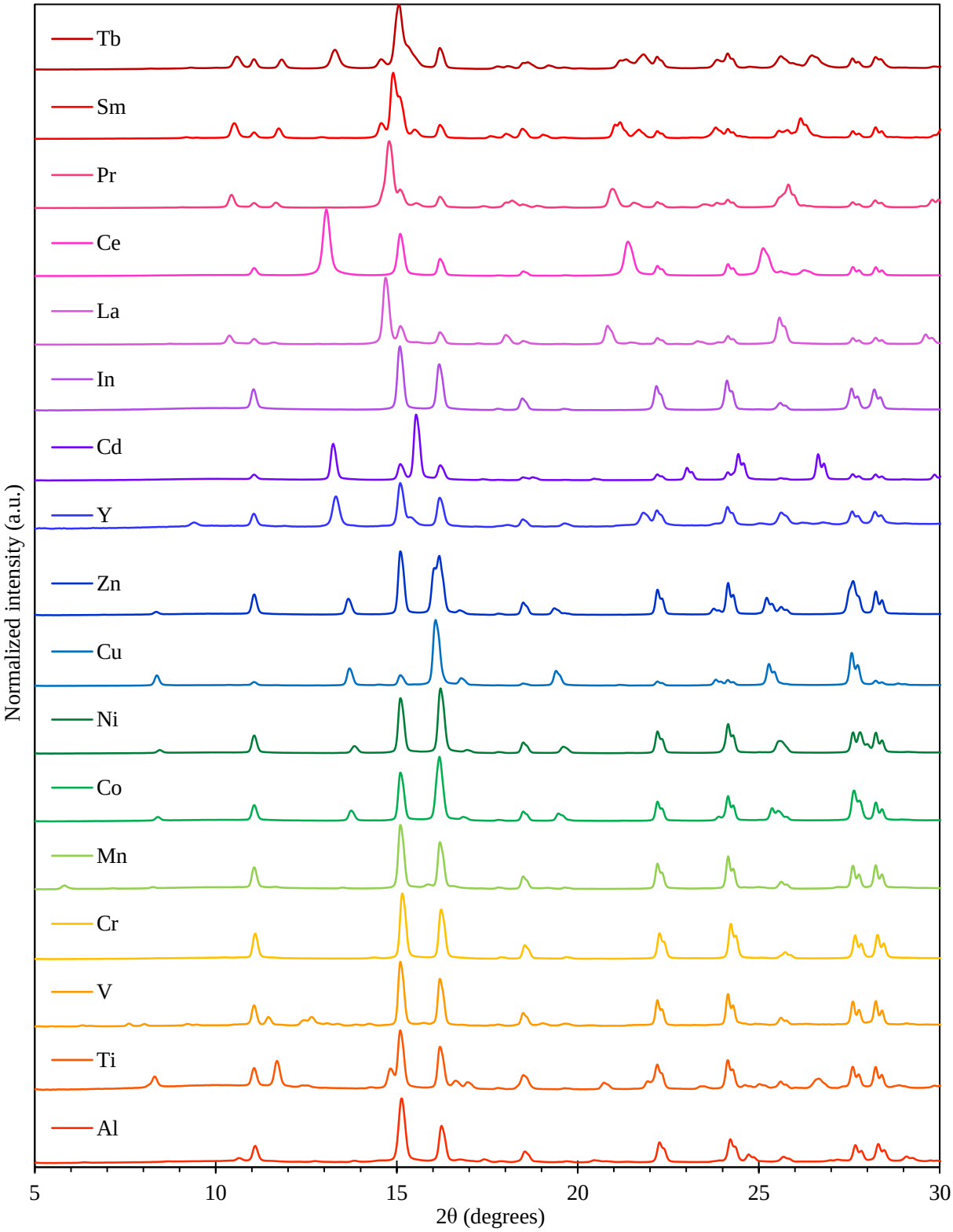

- Figure S13 -

Figure S13 B. PXRD patterns of the calcined MIL-100(Fe,Co) samples (indicated percentages correspond to mol%).

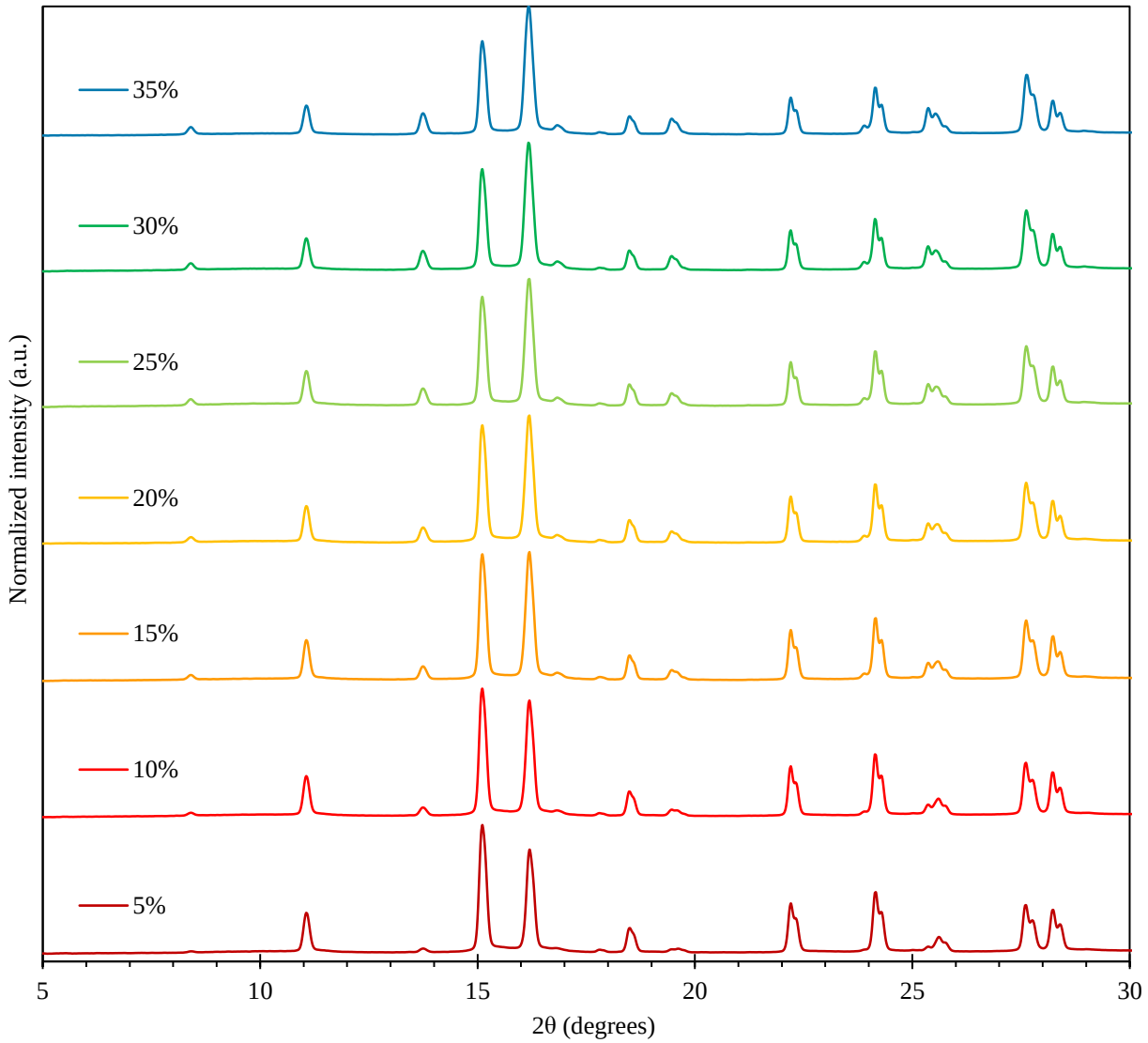

Figure S13 C. Rietveld refinement of the PXRD data of the calcined MIL-100(Fe,Co) samples. Identified phases in all powder patterns are Fe_2O_3 and $CoFe_2O_4$.

MIL-100(Fe,Co) 5%

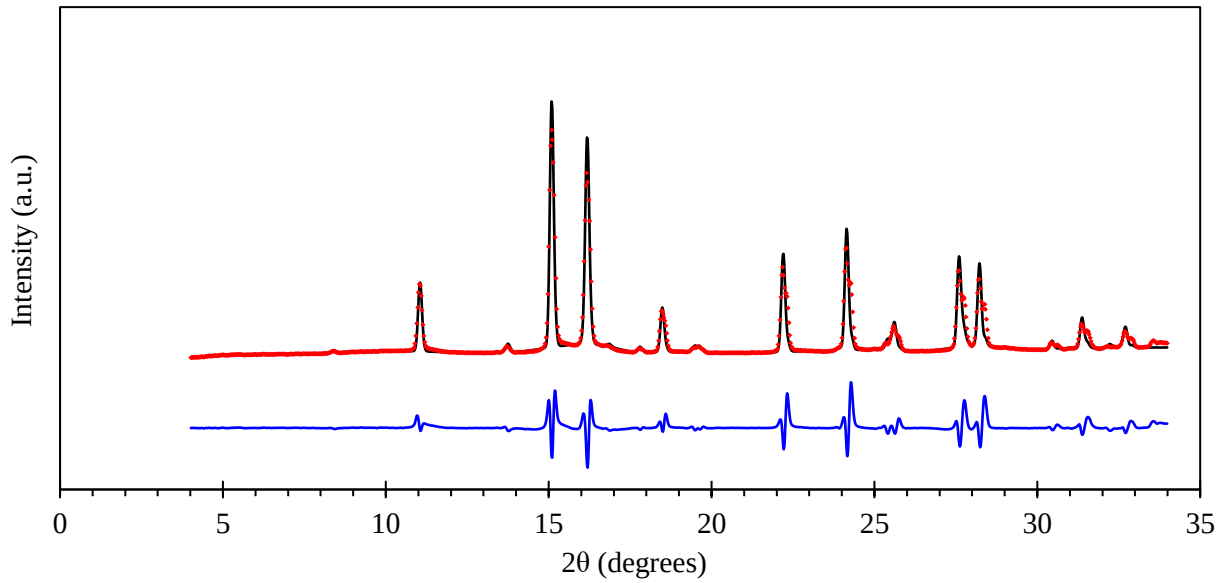

Mass fraction Fe_2O_3 : 90.84% Mass fraction $CoFe_2O_4$: 9.16%

MIL-100(Fe,Co) 10%

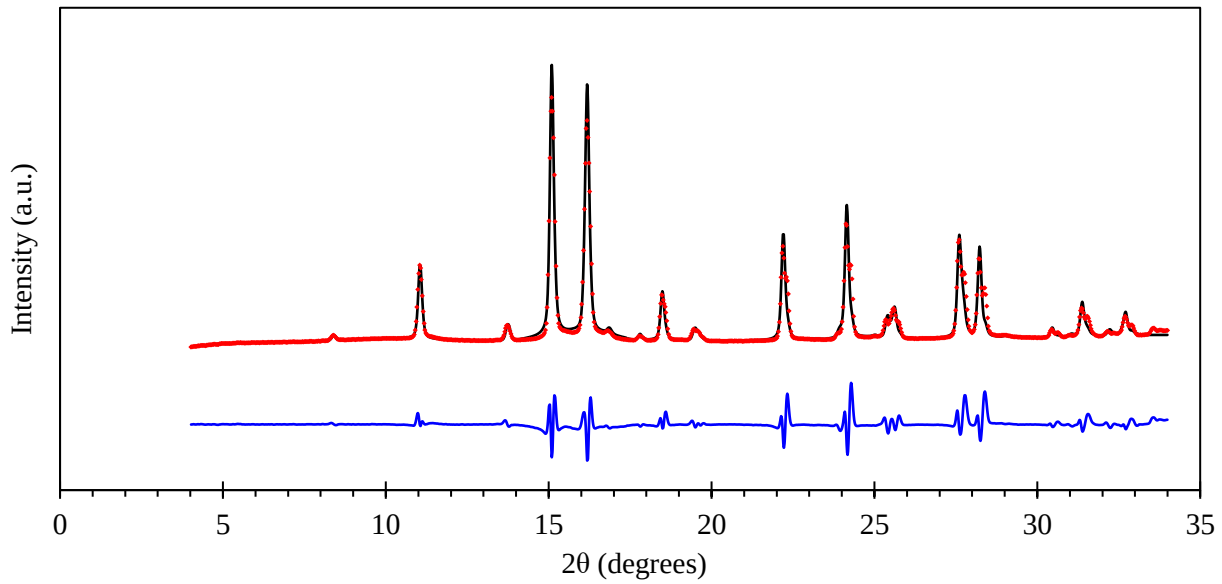

Mass fraction Fe_2O_3 : 89.48% Mass fraction $CoFe_2O_4$: 10.52%

- Figure S13 -

MIL-100(Fe,Co) 15%

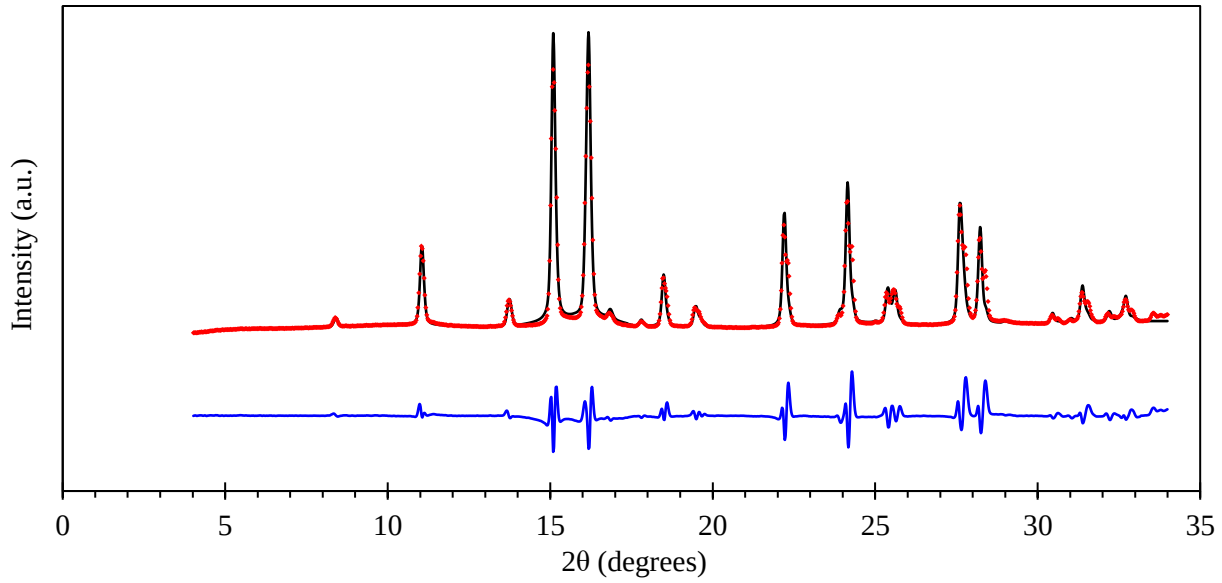

Mass fraction Fe_2O_3 : 83.07% Mass fraction $CoFe_2O_4$: 16.93%

MIL-100(Fe,Co) 20%

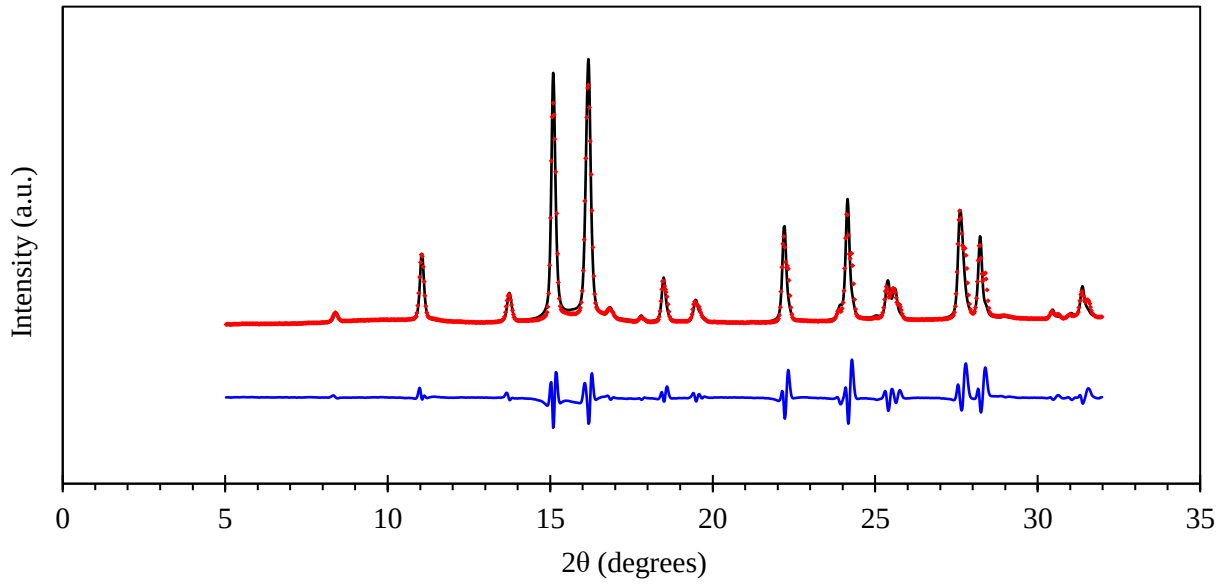

Mass fraction Fe_2O_3 : 78.50% Mass fraction $CoFe_2O_4$: 21.50%

- Figure S13 -

MIL-100(Fe,Co) 25%

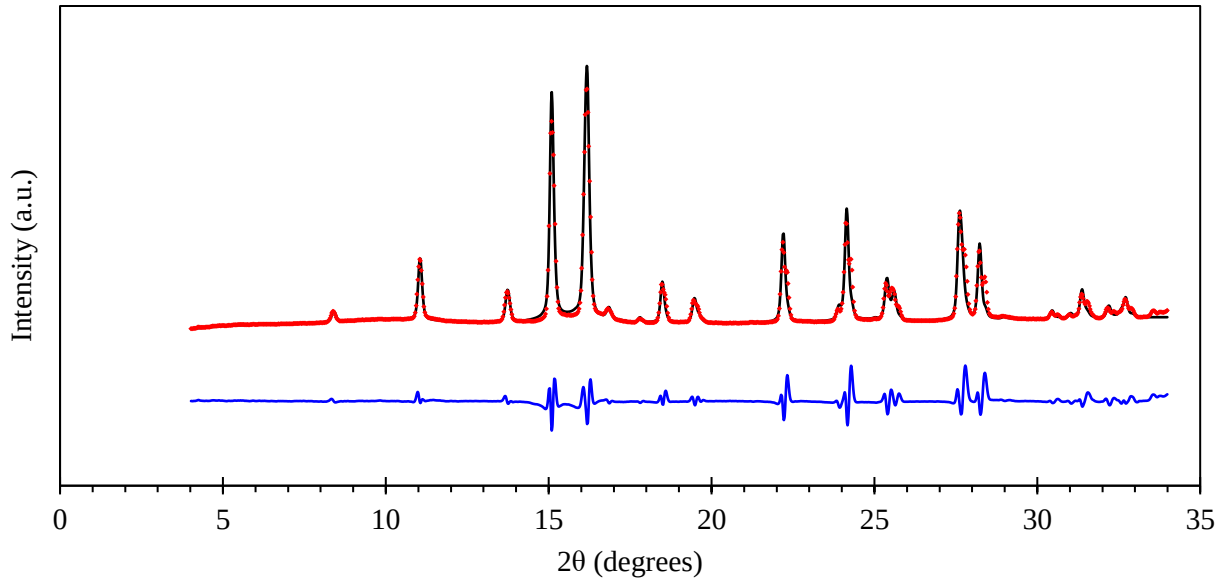

Mass fraction Fe_2O_3 : 75.00% Mass fraction $CoFe_2O_4$: 25.00%

MIL-100(Fe,Co) 30%

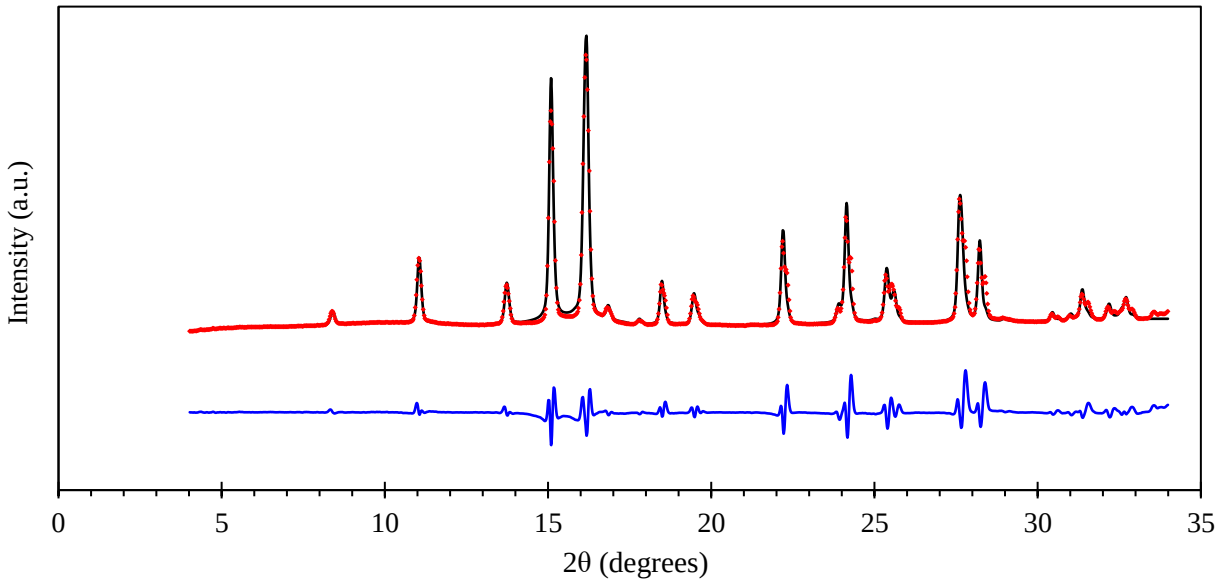

Mass fraction Fe_2O_3 : 71.25% Mass fraction $CoFe_2O_4$: 28.75%

- Figure S13 -

MIL-100(Fe,Co) 35%

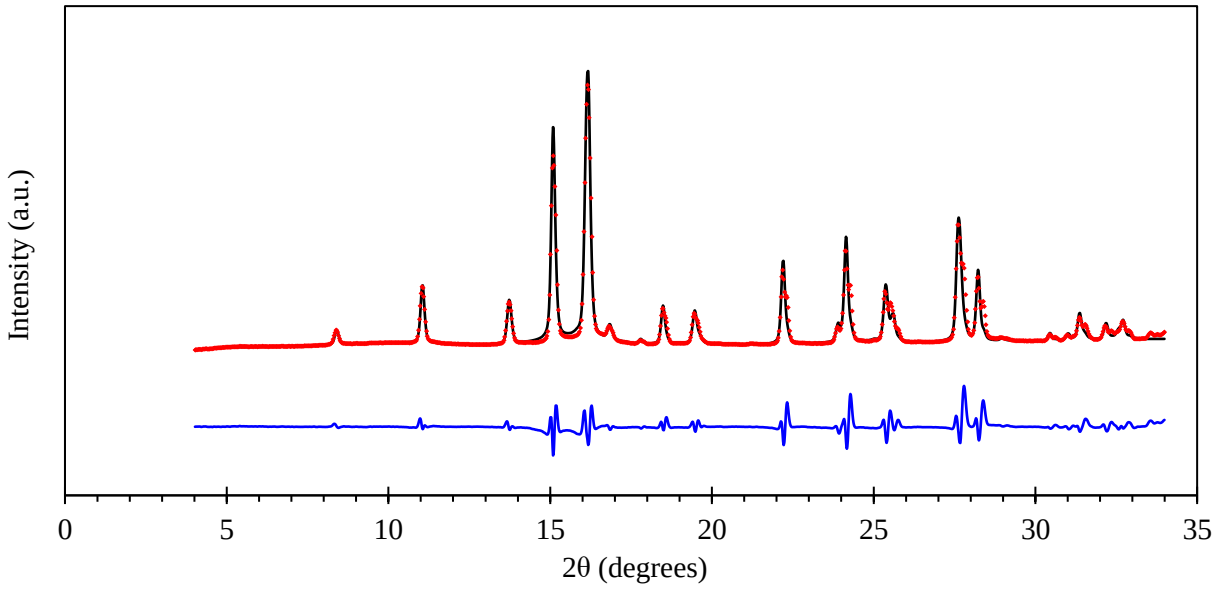

Mass fraction Fe_2O_3 : 67.00% Mass fraction $CoFe_2O_4$: 33.00%

- Figure S13 -

Figure S13 D. PXRD determination of the Co/M_{tot} ratio in the MIL-100(Fe,Co) samples versus the ratios determined by AAS and ICP.

The weight fractions obtained from PXRD are converted to Co/M_{tot} percentages by using the following equation:

$$M/M_{tot}=\frac{1\times\left(\frac{\%_{CoFe_2O_4}}{M_{CoFe_2O_4}}\right)}{2\times\left(\frac{\%_{Fe_2O_3}}{M_{Fe_2O_3}}\right)+2\times\left(\frac{\%_{CoFe_2O_4}}{M_{CoFe_2O_4}}\right)+1\times\left(\frac{\%_{CoFe_2O_4}}{M_{CoFe_2O_4}}\right)}$$

Where $\%_{Fe_2O_3}$ and $\%_{CoFe_2O_4}$ stand for the weight fractions of each phase obtained from Rietveld refinement. $M_{Fe_2O_3}$ and $M_{CoFe_2O_4}$ stand for the molar weight of each type of oxide. A more general equation for obtaining the M/M_{tot} content a mixture of an iron-only containing oxide phase, denoted as Fe_xO_a, and a second mixed-metal oxide, denoted as $Fe_yM_zO_b$ is the following:

$$M/M_{tot}=\frac{z\times\left(\frac{\%_{Fe_yM_zO_b}}{M_{Fe_yM_zO_b}}\right)}{x\times\left(\frac{\%_{Fe_xO_a}}{M_{Fe_xO_a}}\right)+y\times\left(\frac{\%_{Fe_yM_zO_b}}{M_{Fe_yM_zO_b}}\right)+z\times\left(\frac{\%_{Fe_yM_zO_b}}{M_{Fe_yM_zO_b}}\right)}$$

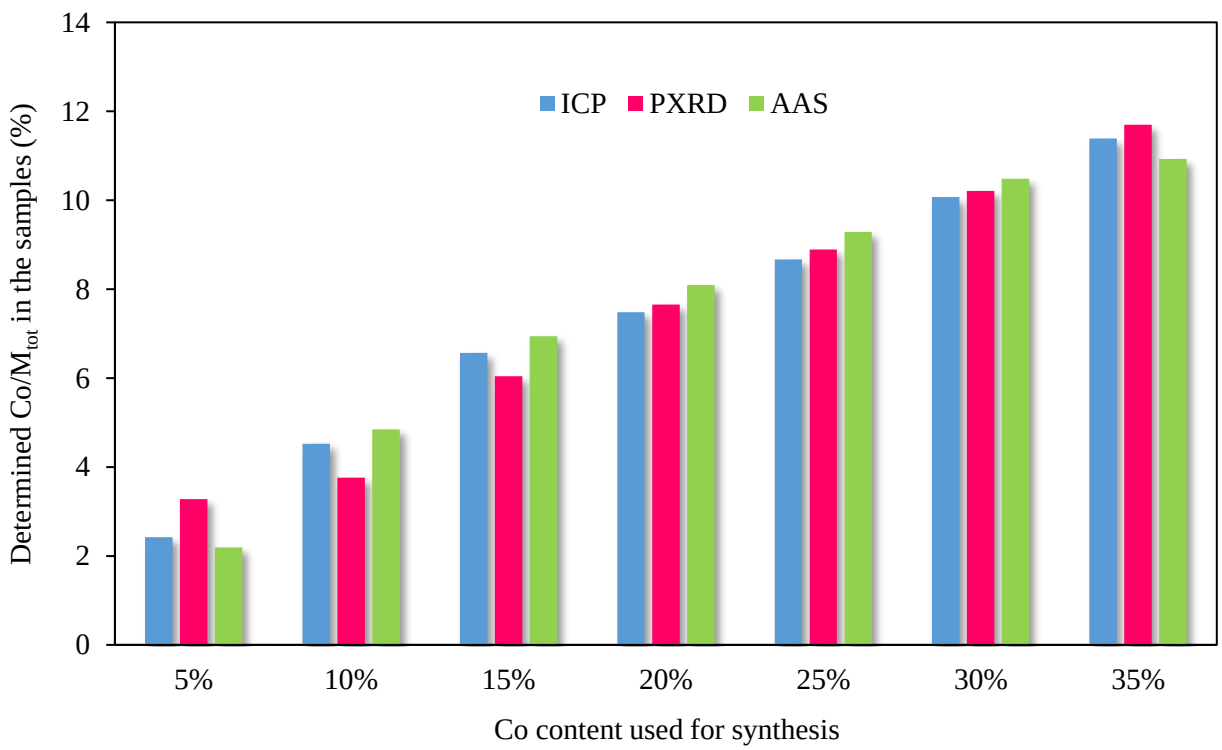

- Figure S13 -

Figure S13 E. Rietveld refinement of the oxide phases in MIL-100(Fe,M), M = Co, Ni, Zn, Cu and Cr and comparison of the quantification obtained by PXRD and ICP showing the limitations of the method. The samples were all synthesized using 20 mol% M/M_{tot} for the synthesis.

MIL-100(Fe,Cr)

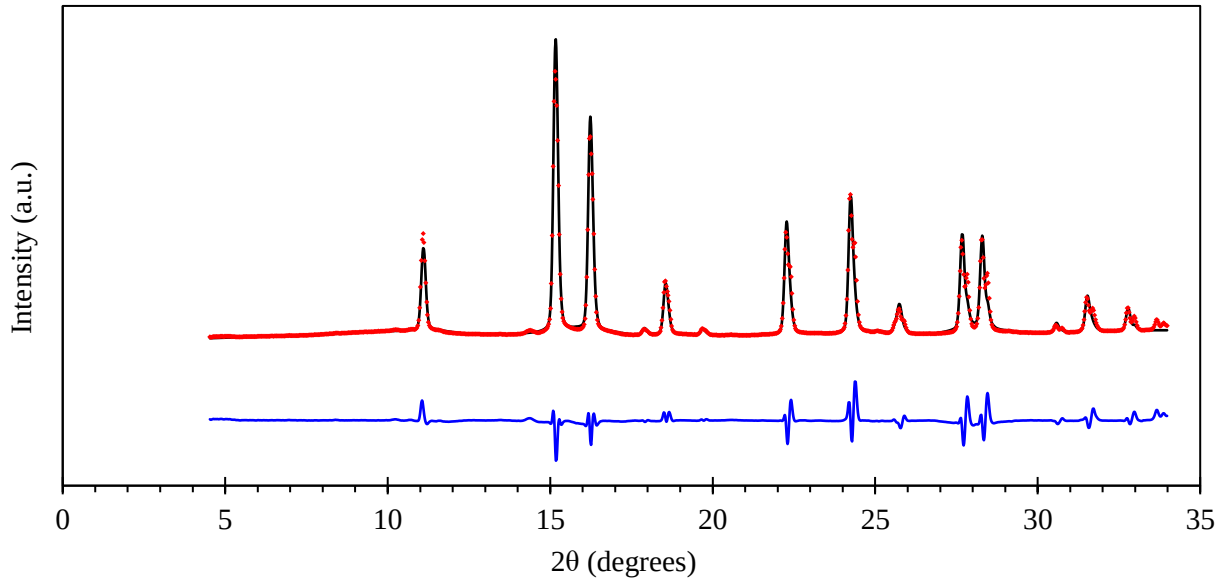

Mass fraction Fe_2O_3 : 67.98% Mass fraction Cr_2O_3 : 32.02%

MIL-100(Fe,Co)

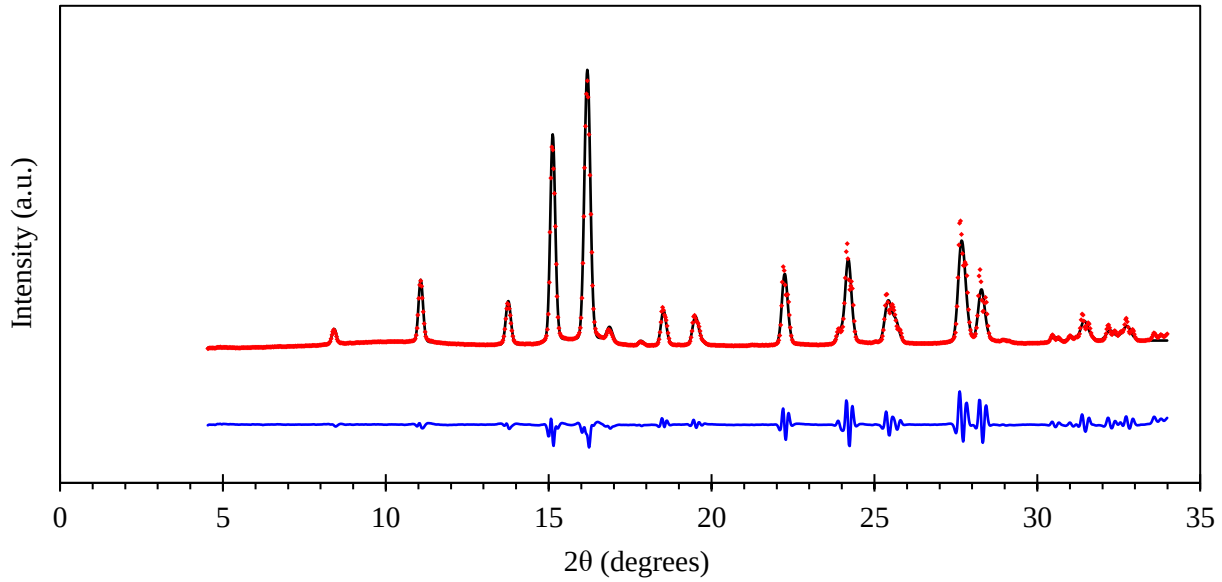

Mass fraction Fe_2O_3 : 68.70% Mass fraction $CoFe_2O_4$: 31.30%

- Figure S13 -

MIL-100(Fe,Ni)

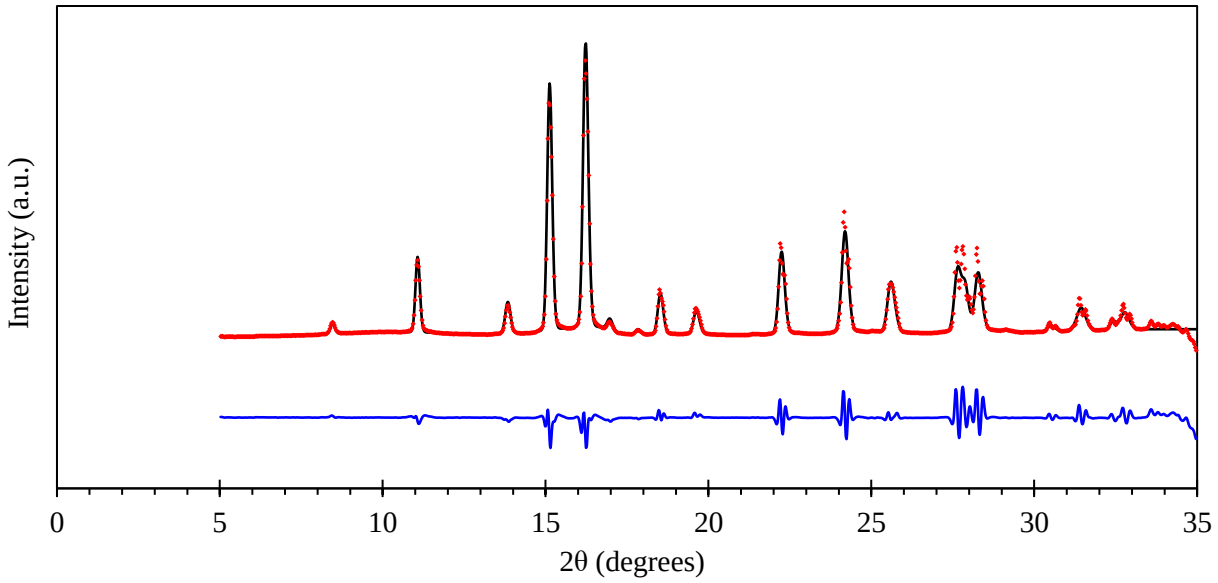

Mass fraction Fe_2O_3 : 78.43% Mass fraction $NiFe_2O_4$: 21.57%

MIL-100(Fe,Cu)

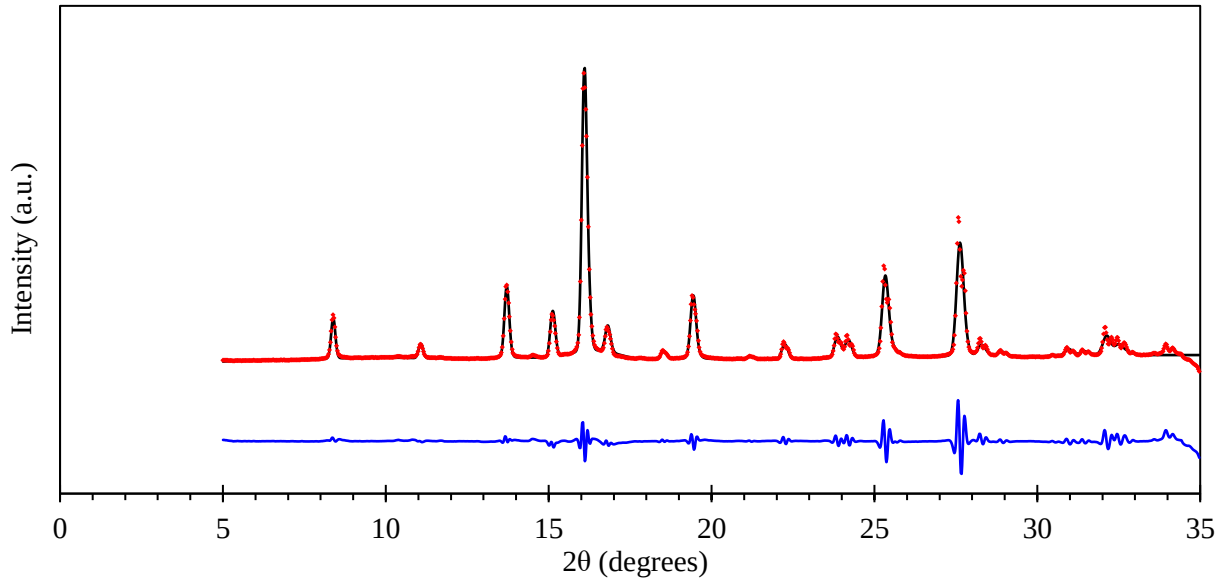

Mass fraction Fe_2O_3 : 18.00% Mass fraction $CuFe_2O_4$: 82.00%

- Figure S13 -

MIL-100(Fe,Zn)

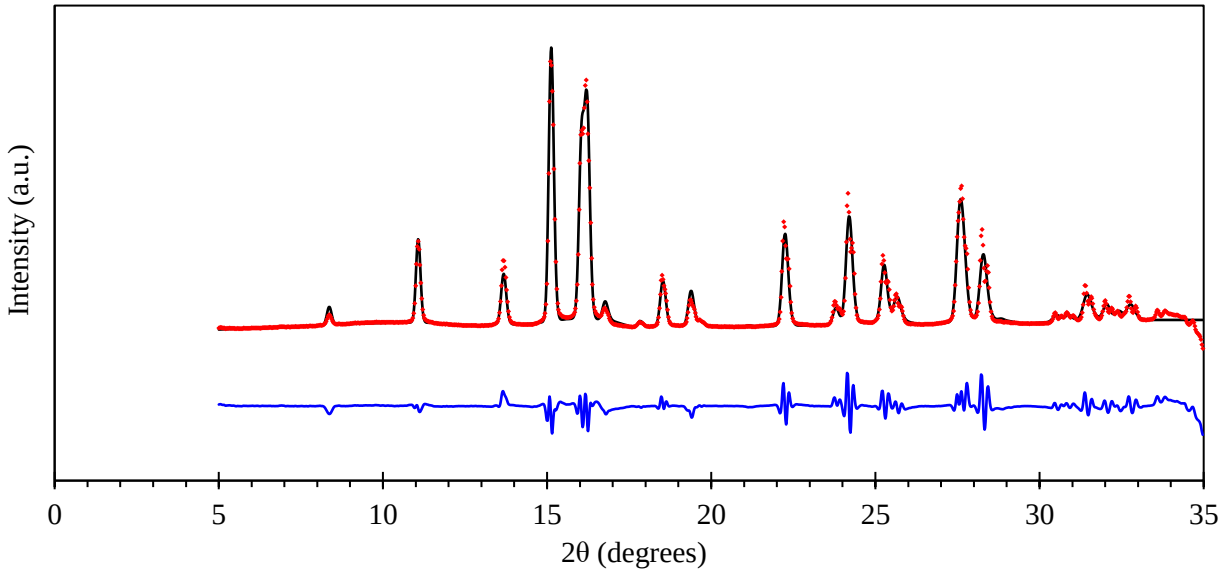

Mass fraction Fe_2O_3 : 70.27% Mass fraction $ZnFe_2O_4$: 29.73%

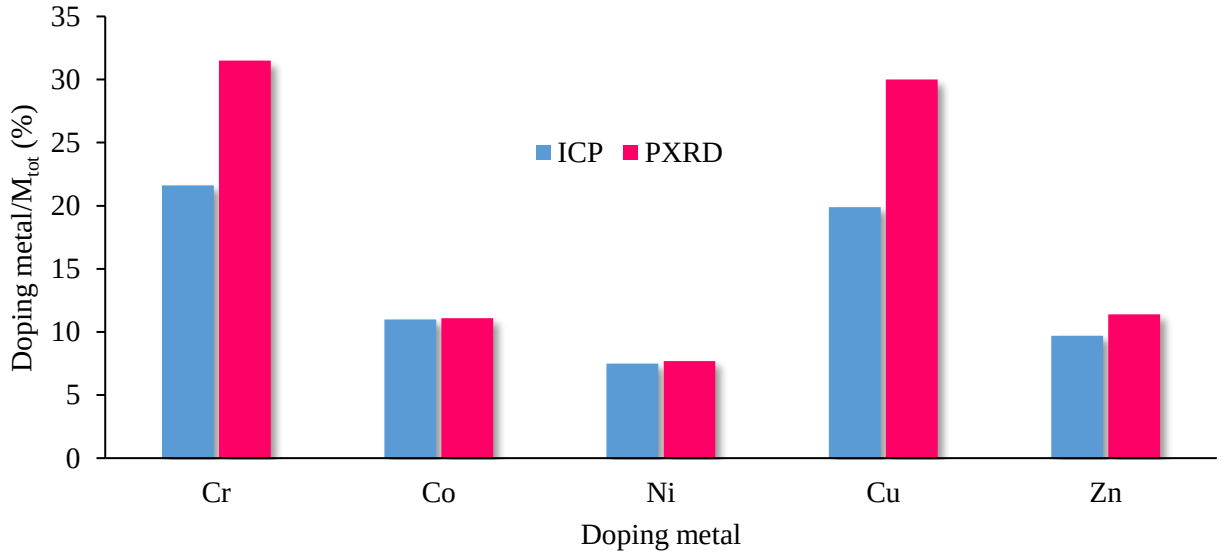

- Figure S13 -

Table S2 A. Quantities of reagents used for the synthesis of MIL-100(Fe,M) derivatives.

Doping metal	Metal salt used	Quantity of metal salt used (g)	Quantity of $FeSO_4$ used (g)
Al	$AlCl_3$	0.19	1.50
Ti	$TiCl_3$	0.21	1.50
V	VCl_3	0.21	1.50
Cr	$CrCl_3{\cdot}6H_2O$	0.34	1.50
Mn	$MnCl_2$	0.17	1.50
Co	$CoCl_2{\cdot}6H_2O$	0.32	1.50
Ni	$NiCl_2{\cdot}6H_2O$	0.33	1.50
Cu	$CuCl_2{\cdot}2H_2O$	0.23	1.50
Zn	$ZnCl_2$	0.19	1.50
Cd	$Cd(NO_3)_2{\cdot}4H_2O$	0.42	1.50
Y	$Y(NO_3)_3{\cdot}5H_2O$	0.61	1.50
La	$LaCl_3{\cdot}xH_2O$	0.51	1.50
Ce	$Ce(OAc)_3{\cdot}xH_2O$	0.50	1.50
Pr	$PrCl_3{\cdot}xH_2O$	0.50	1.50
Sm	$SmCl_3{\cdot}xH_2O$	0.50	1.50
Tb	$Tb(NO_3)_3{\cdot}5H_2O$	0.61	1.50

Table S2 B. pH measurements and colours of solutions and precipitates during the synthesis of the MIL-100(Fe,M) materials.

Doping metal	pH before addition of Na_3BTC	pH after addition of Na_3BTC	Colour of metals salt solution	Colour of immediate precipitate	Colour of precipitate after 10 min
Al	3.39	4.70	Light green	Yellow-white	Same (turns orange)
Ti	2.58	4.95	Blue-violet	Dark brown	Whitening
V	2.85	5.08	Orange-greenish yellow	Green greyish	Green greyish
Cr	3.59	4.85	Deep green emerald	none	Dark green
Mn	4.86	5.60	Light green	None	Yellow (slightly orange)
Co	4.33	5.83	Red	None	Orange
Ni	4.28	6.01	Green	None	Yellow
Cu	3.64	5.20	Light blue	Pale blue (turns grey quickly)	Brown
Zn	4.68	4.89	Light green	Yellow (canary)	Yellow (canary)
Cd	4.79	6.13	Light green	-	Light yellow
Y	4.83	5.87	Light green	White	Yellowing
La	4.04	5.91	Light green	White	Yellowing
Ce	4.5*	5.98	Yellow orange turbid	White	Yellowing
Pr	3.95	5.89	Light green	White	Yellowing
Sm	4.87	6.02	Yellow	White	Yellowing
Tb	4.79	5.87	Light green	White	Yellowing

* The pH of the Ce^{III}/Fe^{II} solution is unstable and increases fast, so it was prepared very quickly and Na_3BTC was added as fast as possible once the metal salts were dissolved